Explorations of Contorted Polycyclic Aromatics as Electronic Materials

Ying Wu (吴 颖)

Submitted in partial fulfillment of the
Requirements for the degree of
Doctor of Philosophy
in the Graduate School of Arts and Sciences

COLUMBIA UNIVERSITY

2015

ABSTRACT

Explorations of Contorted Polycyclic Aromatics as Electronic Materials

Ying Wu

This thesis describes the design, synthesis, characterization, and application of organic molecular materials made from strained polycyclic aromatic compounds. The strain in the molecular subunits induces non-planar structures. We coined the term "contorted aromatics" to describe these molecules. Contorted polycyclic aromatic hydrocarbons (PAHs) are not only structurally intriguing, but also promising small active molecules for organic electronic devices. This thesis explores the contorted PAHs in two directions, (1) making c-PAHs with high enantiomeric purity and (2) studying c-PAHs with expanded size, for desirable physical, chemical, and electronic properties. The synthesis and chiral resolution of trichloro c-hexabenzocorones (c-HBCs) stereoisomers in Chapter 2 enables the study of conversion barrier in expanded aromatic systems with adjacent cove-units. We also rationalized the formation of thermodynamic stereoisomers and kinetically trapped stereoisomers with density functional theory (DFT) calculations. The organic film effect transistors (OFETs) fabricating from racemic trichloro c-HBC are photo-responsive, suggesting enantiopure OFETs may have potential application in detecting polarized light. Chapter 3 describes the expeditious synthesis of a supersized contorted aromatic molecule, c-octabenzocircumbiphenyl (c-OBCB). Spectroscopic and cyclic voltammetry characterizations show that c-OBCB has a smaller band-gap relative to its analog c-HBCs as designed. The expanded contorted shape results in strong association of c-OBCB with shape-complementary $PC_{70}BM$ fullerenes, as demonstrated by NMR

and fluorescence spectroscopies. Chapter 4 studies c-OBCB as an active component in OFETs and solar cells. The tetradodecyloxy-substituted c-OBCB self-assembles to form the active layer in OFETs. Transistor characteristics show that c-OBCBs transport holes readily in thin films. Bulk hetero-junction (BHJ) solar cells of c-OBCB: $PC_{70}BM$ fullerene improved solar power conversion efficiency to 2.88%. External quantum efficiency (EQE) spectra reveal that the red-shift in absorbance is responsible for the higher PCE for c-OBCB compared to the smaller c-HBC series, which charts a clear path to improving the properties of these materials in OPVs by further red-shifting the absorbance. Chapter 5 describes the selective dispersion of single-walled carbon nanotubes (SWCNTs) using c-OBCB. Our dispersion of SWCNTs with c-OBCB selectively disperses semiconducting SWCNTs in toluene with high purity, enabling direct film process with a simple filtration method. We fabricate SWCNTs network transistors using the sorted semiconducting SWCNTs. Our method demonstrates the use of small molecules for facile sorting of semiconducting SWCNTs in high purity (97%) and subsequent direct transistor fabrication from the dispersion.

Table of Contents

Acknowledgements

The past five years of my graduate studies at Columbia University have been exciting and fulfilling. I would like to express my gratitude to those who provided me with supports over the years.

First and foremost, I would like to thank my advisor, Professor Colin Nuckolls. I am sincerely indebted to him for recruiting me to his research group, where I received academic training, and matured through both independent thinking and collaborative work with the opportunities he provided. I admire Colin's knowledge, enthusiasm and insights in the field of organic materials. And I deeply appreciate him passing on the knowledge to me, which broadened my horizons and laid the foundation of my graduate research. I am grateful for all of his guidance and suggestions that helped my projects to succeed. I also thank Colin for being patient and encouraging during my hard times.

I would like to thank the members of my graduate committee, Professor James Leighton and Professor Jonathan Owen, for making sure I am on the right track towards the doctoral degree over the years. I would also like to thank Professor Luis Campos and Professor Shengxiong Xiao for taking the time to serve on my defense committee, special thanks to Xiao for his previous work on the contorted aromatics and helpful discussions.

I would like to express my gratitude to Dr. Michael Steigerwald. He mentored me on the DFT calculations and provided insightful advice on my projects. I could not have gone so far without his supports.

During my studies at Columbia, I have had the privilege to collaborate with and learn from a number of great scientists. I would like to thank Professor Lynn Loo at Princeton University and Dr. Jia Gao in her research group for collaborating on the project of

sorting SWCNTs with c-OBCB. I would also like to thank Dr. Seok Ju Kang, Yu Zhong and Qizhi Xu for device fabrication and measurement, Dr. Brandon Fowler for the HPLC and mass facilities, Professor Nina Berova for allowing me to conduct CD measurement, Dr. Steffen Jockusch for the photoluminescence measurements, and Dr. Daniel Paley for his help on crystallography.

I have had great pleasure of sharing my graduate experience with former and current members in the Nuckolls group. I am deeply indebted to Dr. Christine Schenck-Leo and Professor Sujun Wei for their mentorship when I started out in the lab. I would like to extend my gratitude to Dr. Delphine Bouilly, Jaeeun Yu, Dr. Chien-yang Chiu, Professor Rebekka Klausen, Dr. Bharat Kumar, Dr. Fay Ng, Mellisa Ball, Nate Schuster, Tim Su, Margarita Milton, Qishui Chen and Dr. Alexandra Velian. They are wonderful coworkers, and I appreciate their help and discussions.

Last but not least, I would like to thank my family for their unconditional love and support. My father is an educator and I owed much of my childhood education to him. My mother, a successful businesswoman, has always been inspiring me to become a mentally strong woman. Although they are far away during these years, their love and support have continued to nourish me. I would also like to thank my in-laws for their love and understanding over the years. I met my husband, Dr. Zhang Wang, in 2011 when we were both graduate students in this department. I am truly thankful for his endless love.

Chapter 1: Introduction[1]

This thesis describes the design, synthesis, characterization, and application of organic molecular materials made from strained polycyclic aromatic compounds. The polycyclic aromatics can be viewed as graphene fragments. Graphene is a two-dimensional, atomic-scale, hexagonal lattice made of carbon atoms. Graphene has many extraordinary properties, including a high strength-to-weight ratio, efficient heat and electrical conductivity, and near transparency.[2] There are three types of graphene edges: armchair, zigzag and cove. The flat hexabenzocoronene (HBC) **1** can be seen as the smallest armchair-edge, nano-size graphene fragment (Figure 1). While **1**, like graphene, is flat, the strain in the cove-edge compound **2** severely distorts the molecule away from planarity. The Nuckolls group coined the term "contorted aromatics" to describe this class of molecules.

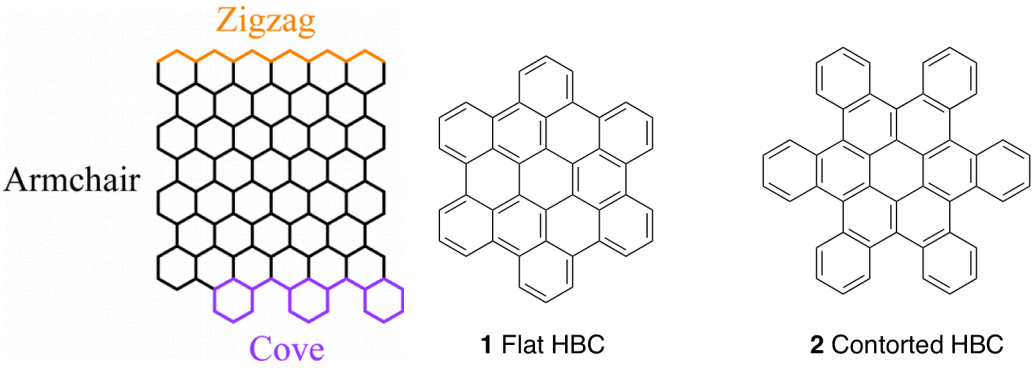

Figure 1. Structures of three graphene edges, flat HBC and contorted HBC.

1.1 Graphene fragments: flat vs. contorted

The contorted aromatics have several advantages over their planar analogs. The intermolecular arrangement in crystals and polycrystalline films are distinct relative to flat aromatics, resulting in their improved charge transport properties in devices.[3] The

weaker intermolecular π-π stacking due to the structural contortion decreases aggregation and increases solubility; thus, these contorted materials can be easily integrated into electronic devices through solution-based processing.[3-8] In addition, these non-planar structures provide doubly concave surfaces that complement the convex surfaces of fullerenes. This mode of self-assembly makes them useful in creating atomically defined p-n junctions in organic photovoltaics.[3-5,9,10] Finally, we developed novel synthetic routes to the contorted aromatics that allow for attaching functionality, which is driven by the goal of improving performances in electronic devices.[5,11,12]

1.2 Previously studied contorted-hexabenzocorone and its derivatives

The first generation of contorted aromatics is the contorted-HBC (c-HBC). As introduced above, c-HBC can be seen as the smallest cove-edge, nano-size graphene fragment. The steric congestion within their cove edges results in highly non-planar structures. On the other hand, c-HBC fuses from three pentacenes, which are well-known electronic materials.[7,13] Therefore c-HBC combines the structural elements of linear acenes and a disk-shaped core.

Figure 2 shows the structure of the c-HBC **2** deduced from single-crystal X-ray diffraction. The structure adopts the conformation where the exterior benzo-groups fold alternatively above or below the π-plane. The steric congestion in the cove position forces the contorted configuration. Figure 2A, 2B demonstrate that the majority of the bending is concentrated in carbons (circled in red) that act as pivot points. The contorted structure has unique consequences for both supramolecular structure and electronic characteristics that will be detailed below.

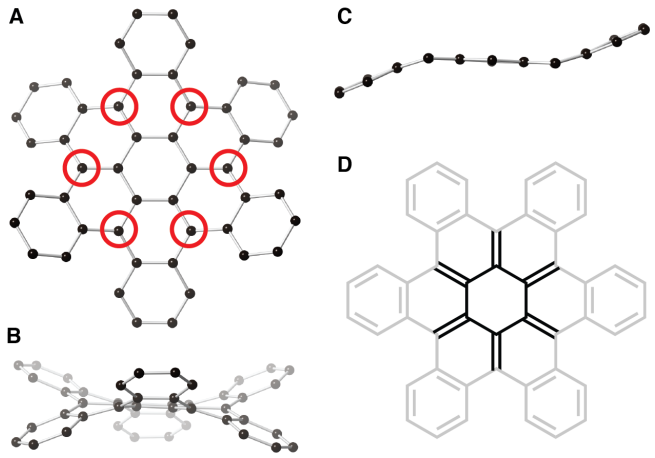

Figure 2. Crystal structure of the unsubstituted c-HBC **2**. The crystals were grown from 1,2,4-trichlorobenzene. Hydrogens are removed to clarify the view. (a) Face-on view with the pivot points marked (red circles). (b) Side-on view. (c) Side-on view of one of the acene segments extracted from the crystal structure. The other atoms of the HBC are hidden from view. (d) Radialene resonance form. Reproduced from ref. 1, 7 and 14.[1 7,14]

The contortion in the crystal structure also elucidated a strong contribution from the radialene resonance that exists in the core. Figure 2D shows a depiction of this arrangement with its double bonds radiating away from the central six-membered ring. This radialene resonance is born from the contortion that inhibits full conjugation throughout the system. Spectroscopic measurements and density functional theory (DFT) support the existence of two π-systems attributed to a relatively lower energy radialene-core and higher energy out-of-plane phenyl rings.[14] Calculations support that the c-HBC core's up-down conformation is the lowest energy conformer by a substantial margin.[14] This is also true for many substituted c-HBCs. However, the shape shifting does exist in some of the c-HBC derivatives, which we will discuss later.

1.2.1 c-HBC derivatives for field effect transistors and solar cells

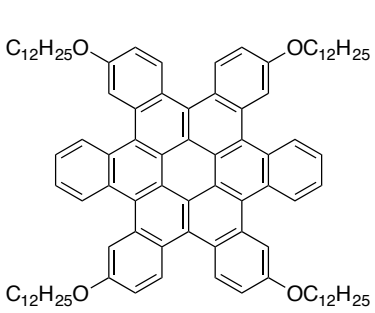

2a tetradodecyloxyl c-HBC

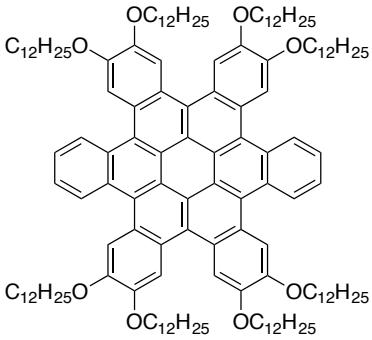

2b Octododecyloxy lc-HBC

Figure 3. Structures of substituted c-HBCs.

The studies in the Nuckolls group have demonstrated that contorted-HBC is a promising p-type hole-transporting material. The synthesis developed by Xiao *et al.* enabled the derivation for tetradodecyloxy-substituted c-HBC **2a** and octadodecyloxy-substituted c-HBC **2b** (Figure 3).[15] The tetradodecyloxy substituted c-HBC **2a** self-assembles into a hexagonally ordered columnar liquid-crystalline phase. This macroscopic-scale columnar array forms the active layer in organic field effect transistor (OFET) devices, which shows good characteristics relative to other similar materials, with a mobility of 0.02 $cm^2 V^{-1} s^{-1}$ and an on/off current ratio of greater than 10^6.[7] The self-assembly changes when the substitution is octadodecyloxy for c-HBC. The octadodecyloxy substituted c-HBC **2b** forms macroscopically long fibers (~250 nm in diameter) that can be controlled by the solvent, temperature and concentration. By using an elastomeric stamp to pick and place the fibers between Au/Cr electrodes, individual fibers could be made into devices, where the c-HBC **2b** exhibits p-type semiconducting characteristics.[8]

The field effect transistors (FET) made from tetradodecyloxy-substituted c-HBC **2a** is photo-responsive when the FET is constructed with single-walled carbon nanotubes as point contacts.[16] In a 1-10 nm nanotube gap cut by lithography, c-HBC **2a** self-assembles into columnar arrays in monolayers. SWCNTs as point contacts can measure the photoconductivity of the 1D liquid crystalline columns because the size of these columnar nanostructures perfectly matches the diameter of SWNT electrodes. The photocurrent originates from photoexcitations that are restricted in the hexaradialene core by the insulating alkoxyphenyl cladding.[14]

The contorted p-type semiconductive HBCs are complementary in both size and shape with n-type convex fullerene. c-HBC and C_{60} fullerene forms co-crystals from solution or physical vapor deposition. The ball-and-socket arrangement (Figure 4) is essential for device performances. We tested two devices utilizing contorted HBC and its cousin, a completely planar HBC derivative. Both molecules share similar electronic and physical properties, with the notable difference being their three-dimensional shapes. We found devices made from contorted HBC were more efficient relative to the non-contorted derivative by about two orders of magnitude in power conversion efficiency (PCE).[3] Notably, under UV-LED irradiation, contorted-HBC device out-performed flat-HBC by more than two orders of magnitude (average efficiencies of 3.36 % versus 0.03 %). We were able to conclude that the c-HBCs form a shape complementary complex with n-type acceptors like fullerenes, yielding donor/acceptor interface that results in enhanced electronic properties.[3]

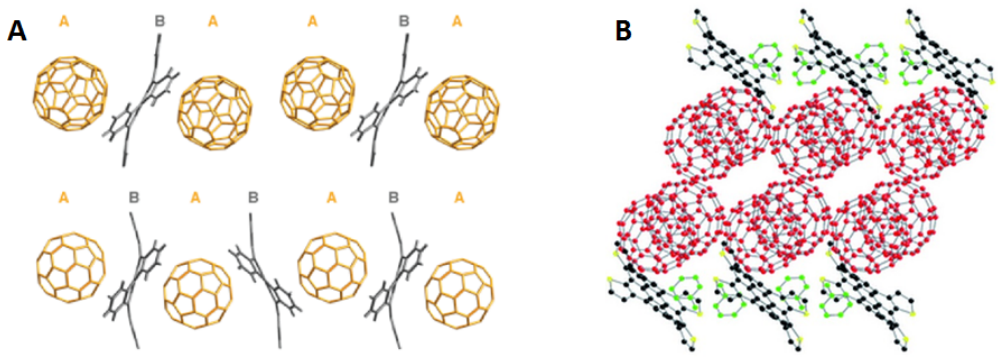

Figure 4. Co-crystals of c-HBC/C_{60} fullerene and c-DBTTC /C_{60} fullerene. Reproduced from ref. 3 and 4.[3,4]

Before these studies, it had been generally accepted that large, planar molecules exhibited good charge transportation properties due to their ability to pack co-facially.[17,18] The outstanding charge transport characteristics of OFET and solar cell devices fabricating from contorted-HBCs revised this conventional wisdom. The synthesis and application of contorted-HBC laid the foundation for understanding the class of contorted aromatics.

We have continued to explore the contorted aromatics by designing new molecules, developing synthetic routes, studying their physical organic properties, and testing them in a wide range of electronic applications. The first modern synthesis of c-HBCs by Xiao *et al.* applied the two-step Barton-Kellogg olefination and photo-cyclization as key steps.[12] Subsequently, Plunkket et al. developed the expeditious one-step Barton-Kellogg approach that uses Scholl reaction as the cyclization step.[11] In addition, Suzuki reaction was employed as the key step to form the key intermediate bis-olefin.[4,19] Chapter 2 will describe the background of previous syntheses for c-HBCs with more details.

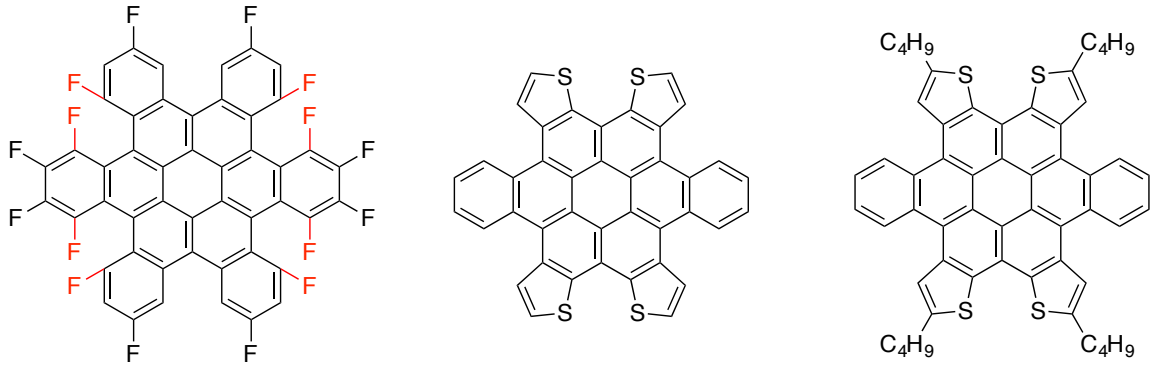

3 16-fluorinated c-HBC **4** c-DBTTC **4a** tetrabutyl c-DBTTC

Figure 5. Structures of fluorinated c-HBC and c-DBTTCs.

1.2.2 Fluorinated c-HBC

The fluorinated c-HBC **3** revealed intriguing structural information as well as shifting the optical absorbance and improving the molecular packing in the solid state relative to the parent c-HBCs (Figure 5).[19] As we discussed earlier, the lowest energy conformation for c-HBC and many substituted c-HBCs is the up-down conformation in which the six exterior benzo-groups fold alternatively above and below the π-plane. However, the crystal structure of fluorinated c-HBC **3** that was substituted with sixteen fluorines is unusual (Figure 6). Typically, the bis-olefin intermediate of **3** could be cyclized to c-HBC **3** with a Katz-modified Mallory photocyclizaton or under the Scholl conditions. The crystals grew from photocyclization product were the usual up-down conformation. But the Scholl cyclization product gave a different structural conformation: the central pentacene subunit containing eight fluorine atoms bents to one direction and the other four benzo-rings bent to the opposite direction with different dihedral angles, much like a saddle structure (Figure 6B, 6C). This less-energetically favorable conformation is kinetically trapped during the synthesis. As expected, the two

conformations of c-HBC **3** showed different NMR chemical shifts. Variable-temperature NMR experiments showed that the less-energetically favorable conformation, which was made from Scholl cyclization, was able to be converted quantitatively to the up-down conformation by heating above 100 °C in five minute intervals to eighty-five minutes.[19]

1.2.3 c-Dibenzotetrathiophenecoronene (c-DBTTC)

Given the widespread usage and efficacious electronic properties of thiophene oligomers and polymers, we expanded our research to incorporate these structures within the HBC molecules (Figure 5). The recent synthetic route based on Suzuki coupling and Katz-modified Mallory photocyclization made it possible to substitute four benzene groups with four thiophene groups, forming dibenzotetrathienocoronene (c-DBTTC).[4,10]

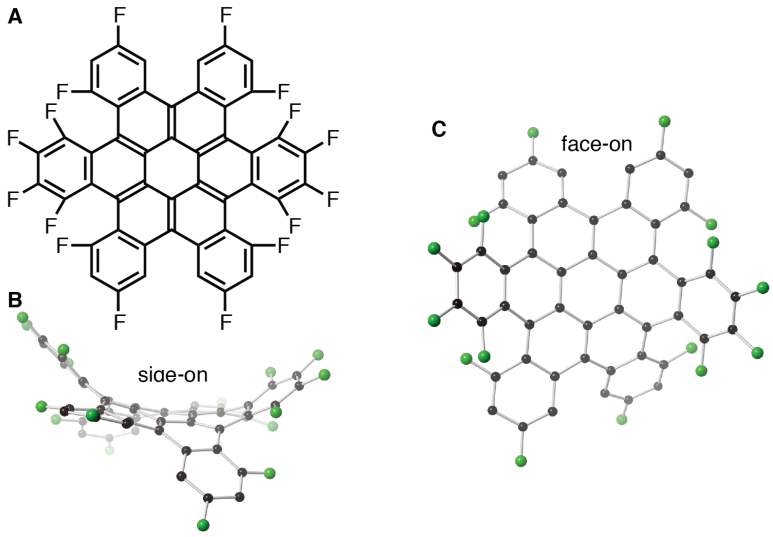

Figure 6. Unusual shape-shifting for fluorinated c-HBC **3** from single-crystal X-ray diffraction. Fluorine, green; hydrogens have been removed. Reproduced from ref. 18.

The structure can be viewed as two anthradithiophene units and one pentacene unit stack over the center benzene ring, with the coronene core preserved. Our synthetic pathway provides only the syn-regioisomer of the anthradithiophenes within the c-DBTTC

structure and was the first example of a completely regioselective anthradithiophene synthesis. The calculation and cyclic voltammetry experiment show that c-DBTTC is electron donating, similar to its parent c-HBC. Density functional theory (DFT) calculation showed that the molecular structure of c-DBTTC is flatter than c-HBC due to relaxed steric interactions in the periphery, allowing c-DBTTC to adopt more conformations which are energetically close.[4] This versatility allows the c-DBTTC structure to accommodate a wide-range of electron acceptors, such as small-size tetracyanoquinodimethane (TCNQ) and large-size fullerenes.[4,20-22] The first two of these predicted conformations are isoenergetic, with the circumferential rings adopting an up-down-up-down-up-down conformation (Figure 7A) and an up-down-down-up-down-down conformation. (Figure 7B). In Figure 7B, the pentacene subunit forms the body of the "butterfly" while two anthradithiophenes form its wings; therefore, we called this structure the "butterfly conformation." The third molecular conformation (Figure 7C) is predicted to be ~4 kcal/mol higher in energy and has not been observed experimentally. Here, the benzo groups adopt an up-down-down-twist-up-down (U-D-D-T-U-D) arrangement.[4]

Crystal structures revealed that c-DTBBC displays molecular flexibility and tunable supramolecular self-assembly properties in the solid state by shifting molecular conformations between the up-down and butterfly conformations. The packing of c-DBTTC crystals and co-crystals with electron acceptors is influenced by sulfur–sulfur interactions, the inherent molecular contortion of the three-dimensional c-DBTTC core, and the neighboring environment. The unsubstituted c-DBTTC **4** solely adopts the up-down conformation and packs into dense crystals containing columnar arrays with close

intra-columnar packing. This molecular packing is interesting because typically when electron-rich aromatics stack co-facially, the atoms are offset from each another.[23,24] In crystals of the tetrabutyl-DBTTC **4a**, with only solvent as a guest, we observe both the butterfly and up-down conformations. In co-crystals with electron acceptors, the tetrabutyl-DBTTC **4a** either adopts the butterfly conformation when the electron acceptor (such as TCNQ) is small enough to be completely enveloped or the up-down conformation when the electron acceptor is relatively large (two molecules of C_{60}).

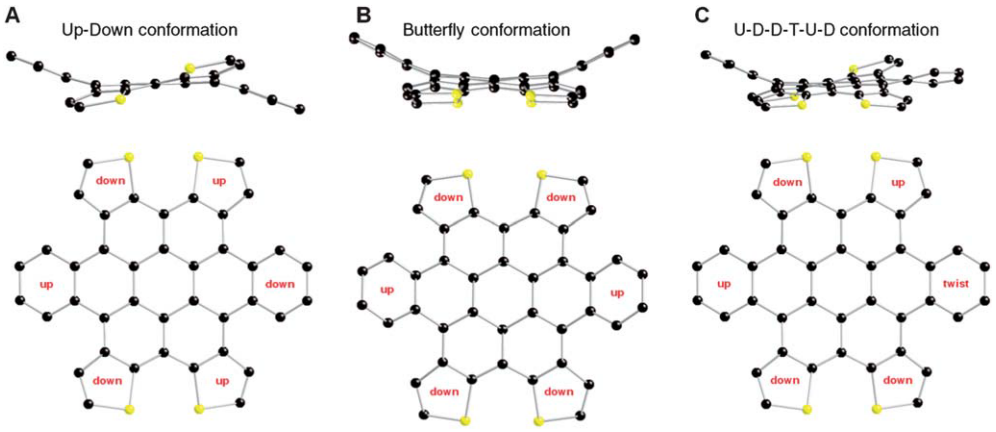

Figure 7. Side and top views of the DFT-optimized structures of c-DBTTC. Black: carbon; yellow: sulfur. Hydrogens are omitted for clarity. Reproduced from ref. 4.[4]

We grew micrometer-size c-DBTTC epitaxial crystals around the surface of macroscopic C_{60} rod-shape crystals. We can control the density of c-DBTTC by varying temperature and time (Figure 8). Raman mapping of the C_{60}-DBTTC co-crystals confirmed the center rod of the heterostructure is C_{60} and the attaching small molecules are c-DBTTC. The epitaxial growth of c-DBTTC on C_{60} rod provides a wide range of interfaces between the electron donor c-DBTTC and acceptor C_{60} for efficient electron transfer. In future studies, we can put electrodes on the C_{60}-DBTTC co-crystals and

measure the photo-induced electrical current.

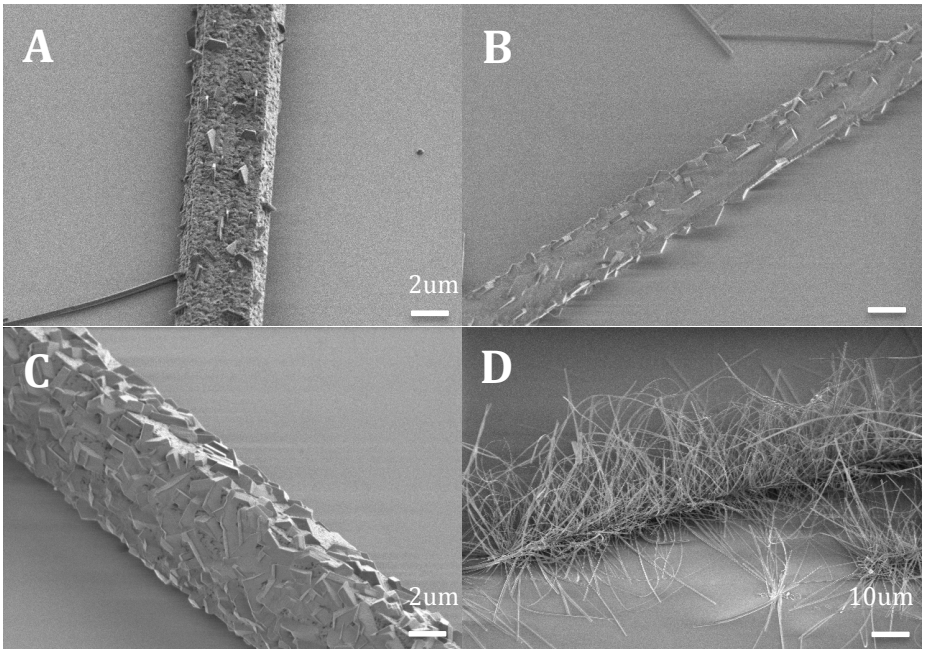

Figure 8. c-DBTTC epitaxial crystal growth on C_{60} crystalline-nanorods.

1.3 c-HBC based on three-fold symmetry: trichloro-substituted hexabenzocoronene

As we have introduced in section 1.2.2, two opposite fluorine atoms on the same cove units of HBCs (red ones in compound **3**, Figure 5) increase the steric hindrance to a degree that induces the molecule to be trapped in the butterfly conformation under the Scholl-condition synthesis. Previously, the dichloro-substituted c-HBC **5** and tetrachloro-substituted c-HBC **6** were prepared as intermediates for the subsequent intra-molecular Heck reaction to make the bowl-shape aromatics (Figure 9). But the tructures of these chlorine-substituted c-HBCs were not fully studied at the time. Wei et.al. reported a new synthesis for c-HBCs using a "three-fold symmetry" method.[25] The three-fold symmetry method breaks the intrinsic symmetrical plane in c-HBCs, which gives rise to the structural chirality of trichloro-substituted c-HBC **7**.

In this thesis, we introduced chlorines onto contorted-HBCs based on the three-fold symmetry method[25] and synthesized the chiral member for thorough chirality studies in the c-HBC family for the first time. The chlorinated c-HBCs **7** have four stable stereoisomers, or two sets of enantiomers. Although unsubstituted [4]-helicene flips up and down rapidly under room temperature,[26] we discovered that the chlorinated c-HBCs exhibit strong steric hindrance on the [4]-helicenes subunits, resulting isomers being stable at room temperature.

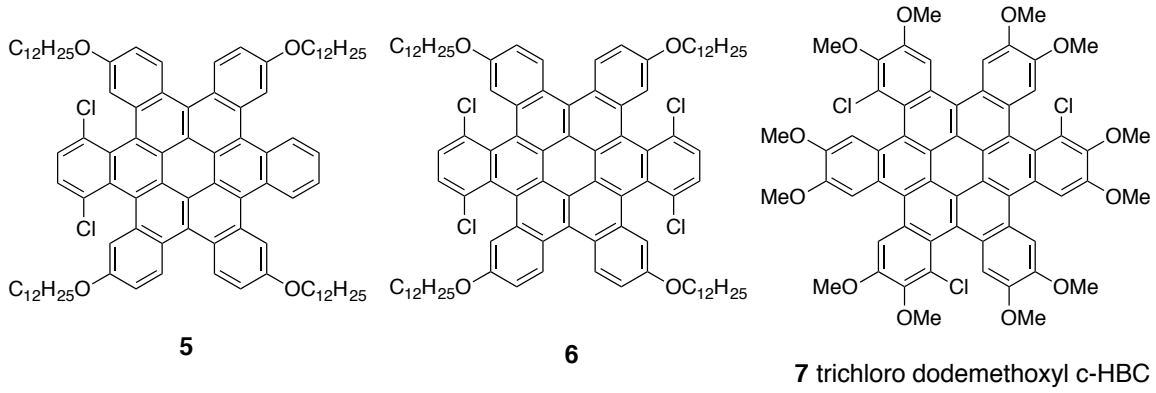

Figure 9. Structures of dichloro-substituted c-HBC **5**, tetrachloro-substituted c-HBC **6**, and trichloro-substituted c-HBC **7**.

Chapter 2 describes the design, synthesis, and characterization for the chiral trichloro-substituted c-HBCs (Figure 10). We isolated two products with identical mass and UV-Vis spectra, but the two NMR spectra in the aromatic region are distinct. One has three aromatic peaks (we named it "3-peak" or "up-down") while the other has nine peaks (we named it "9-peak" or "butterfly") in the aromatic region, and the ratio of the two (3-peak to 9-peak) in the combined raw product is about 1:3. From DFT calculations, we also found two stable conformers for the trichloro-HBCs. Obviously, from symmetry

difference, we identified the 3-peak NMR spectrum to be the up-down conformation and 9-peak spectrum to be the butterfly conformation.

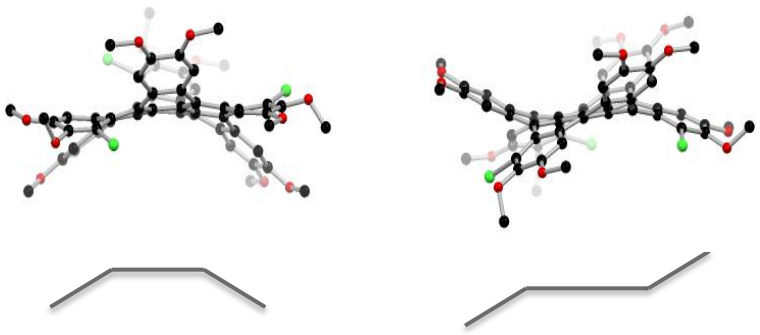

Butterfly or the 9-peak Up-down or the 3-peak

Figure 10. DFT-optimized structures of the 9-peak and 3-peak diastereomers. Black: carbon; red: oxygen; green: chlorine. Hydrogens are omitted for clarity.

The ground state energy of the butterfly conformation is higher than the up-down by 9 kcal/mol on the level of B3LYP and 6-31G**. The big difference of ground state energy and the fact that the higher energy conformation is the major product suggest the two conformers not interconvert after formation under the reaction condition and therefore must be formed kinetically. The two conformers do not interconvert up to 410K from the VT-NMR study (Chapter 2). In Chapter 2 we will discuss the mechanism of the 1:3 product ratio (up-down: butterfly) using DFT calculations.

Both the enantiomers of the 3-peak (up-down conformation) and those of the 9-peak (butterfly conformation) are resolved on high performance liquid chromatography (HPLC), respectively. The optical rotation and circular dichroism (CD) measurement confirmed the chirality of the enantiomers. We then carried out kinetic studies to evaluate

the racemization barrier of the antipodes of the two conformations. In Chapter 2 we will describe the kinetic experiments and discusses the racemization behaviors.

The organic field effect transistors (OFETs) fabricating from the racemic 9-peak compound showed promising photon-induced response. We envision that the enantiopure OFETs will only respond to the corresponding polarized light due to its intrinsic chirality, making it a detector for circular polarized light which has immense potential in circularly polarized ellipsometry-based tomograph,[27,28] optical communication of spin information[29] and quantum-based optical computing and information processing[30,31].

1.4 Expanding the core: contorted-Octobenzocircumbiphenyl (c-OBCB)

Previous studies showed that c-HBC and c-DBTTC shared similar optical and electronic properties. However, the optical absorption spectra of the HBC families thus far overlapped poorly with the solar spectrum, which is the primary limitation for using these materials in efficient solar cell devices.[3,9,10,32] In order to evoke meaningful electronic changes, we used the parent structure as a template and expanded the core. Thus, octabenzocircumbiphenyl (OBCB) **8** was designed. The effect turned out to be profound. The absorption spectrum was dramatically red-shifted, and this new core has more accessible HOMO/LUMO levels. Figure 11 shows the DFT-optimized structure of the lowest energy conformer of the c-OBCB. The c-OBCB structure is similar to the c-HBC as it adopts the contorted disc-shape. Eight benzo-groups alternate up or down around the exterior of the circumbiphenyl core. Additionally, the circumbiphenyl core of c-OBCB has two superimposed coronenes to form two 5-helicenes with the exterior benzo-groups, making the molecule chiral.[5]

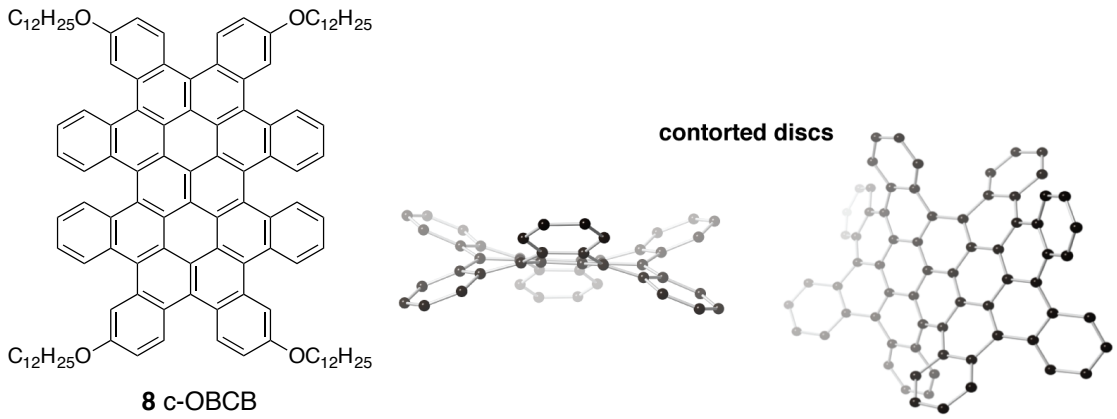

Figure 11. Structure of tetradodecyloxy c-OBCB. Side and top views of DFT-optimized structure of the c-OBCB skeleton.

The calculated band gap of OBCB is smaller than the calculated band gap of c-HBC by 0.34 eV, which indicates OBCB would red-shift and thus become a more efficient donor material. This is indeed the case as confirmed by experimental data. The absorbance peak of the UV-Vis spectrum of c-OBCB is red-shifted by 80 nm relative to c-HBC. The cyclic voltammetry shows HOMO, LUMO and band gap are -5.4 eV, -3.0 eV, and 2.4 eV, respectively (ferrocene was used as the standard reference). Both the absorbance spectrum and CV results are in consistence with our previous calculations. Therefore, c-OBCB is red-shifted as proposed, which would be a potentially more desirable donor material for solar cell.

Chapter 3 describes the development of the expeditious synthesis for c-OBCB, its optical and cyclic voltammetry (CV) characteristics, the semiconducting properties in OFETs, and the solar cell performance using the c-OBCB/C_{70} as active layer in bulk hetero-junction (BHJ) solar cells. Our studies charts a clear path to improve the properties

of these materials in organic photovoltaics (OPVs) by making molecules with further red-shifted absorbance and retaining their association with the acceptors.

Due to the unique three-dimensional shape of c-OBCB, we explored the interactions of c-OBCB and single-wall carbon nanotubes (SWCNTs). Chapter 4 describes the c-OBCB-controlled chirality-selective dispersion of SWCNTs. We found that c-OBCB selectively dispersed SWCNT, which we characterized to be high-purity semiconducting nanotubes. Conjugated polymers have been investigated extensively for sorting SWCNTs' post-growth.[33-35] Our successful sorting of semiconducting carbon nanotubes offers a new direction using aromatic molecule to sort new kinds of SWCNTs. We also demonstrated the fabrication of SWCNT network transistors directly from our dispersion of high-purity semiconducting carbon nanotubes.

1.5 References

(1) Part of this chapter is adapted from our published work: Ball, M.; Zhong, Y.; Wu, Y.; Schenck, C.; Ng, F.; Steigerwald, M.; Xiao, S.; Nuckolls, C. *Acc. Chem. Res.* **2015**, *48*, 267.

(2) Andronico, M. In *Laptop.com* 2014.

(3) Tremblay, N. J.; Gorodetsky, A. A.; Cox, M. P.; Schiros, T.; Kim, B.; Steiner, R.; Bullard, Z.; Sattler, A.; So, W. Y.; Itoh, Y.; Toney, M. F.; Ogasawara, H.; Ramirez, A. P.; Kymissis, I.; Steigerwald, M. L.; Nuckolls, C. *ChemPhysChem* **2010**, *11*, 799.

(4) Chiu, C. Y.; Kim, B.; Gorodetsky, A. A.; Sattler, W.; Wei, S. J.; Sattler, A.; Steigerwald, M.; Nuckolls, C. *Chem. Sci.* **2011**, *2*, 1480.

(5) Xiao, S. X.; Kang, S. J.; Wu, Y.; Ahn, S.; Kim, J. B.; Loo, Y. L.; Siegrist, T.; Steigerwald, M. L.; Li, H. X.; Nuckolls, C. *Chem. Sci.* **2013**, *4*, 2018.

(6) Xiao, S. X.; Kang, S. J.; Zhong, Y.; Zhang, S. G.; Scott, A. M.; Moscatelli, A.; Turro, N. J.; Steigerwald, M. L.; Li, H. X.; Nuckolls, C. *Angew. Chem. Int. Ed.* **2013**, *52*, 4558.

(7) Xiao, S. X.; Myers, M.; Miao, Q.; Sanaur, S.; Pang, K. L.; Steigerwald, M. L.; Nuckolls, C. *Angew. Chem. Int. Ed.* **2005**, *44*, 7390.

(8) Xiao, S. X.; Tang, J. Y.; Beetz, T.; Guo, X. F.; Tremblay, N.; Siegrist, T.; Zhu, Y. M.; Steigerwald, M.; Nuckolls, C. *J. Am. Chem. Soc.* **2006**, *128*, 10700.

(9) Kang, S. J.; Ahn, S.; Kim, J. B.; Schenck, C.; Hiszpanski, A. M.; Oh, S.; Schiros, T.; Loo, Y. L.; Nuckolls, C. *J. Am. Chem. Soc.* **2013**, *135*, 2207.

(10) Kang, S. J.; Kim, J. B.; Chiu, C.-Y.; Ahn, S.; Schiros, T.; Lee, S. S.; Yager, K. G.; Toney, M. F.; Loo, Y.-L.; Nuckolls, C. *Angew. Chem. Int. Ed.* **2012**, *51*, 8594.

(11) Plunkett, K. N.; Godula, K.; Nuckolls, C.; Tremblay, N.; Whalley, A. C.; Xiao, S. X. *Org. Lett.* **2009**, *11*, 2225.

(12) Xiao, S., PhD thesis, Columbia University, 2007.

(13) Katz, H. E.; Bao, Z.; Gilat, S. L. *Acc. Chem. Res.* **2001**, *34*, 359.

(14) Cohen, Y. S.; Xiao, S. X.; Steigerwald, M. L.; Nuckolls, C.; Kagan, C. R. *Nano Lett.* **2006**, *6*, 2838.

(15) Miao, S.; Bangcuyo, C. G.; Smith, M. D.; Bunz, U. H. F. *Angew. Chem. Int. Ed.* **2006**, *45*, 661.

(16) Guo, X. F.; Xiao, S. X.; Myers, M.; Miao, Q.; Steigerwald, M. L.; Nuckolls, C. *Proc. Natl. Acad. Sci. USA* **2009**, *106*, 691.

(17) Kazmaier, P. M.; Hoffmann, R. *J. Am. Chem. Soc.* **1994**, *116*, 9684.

(18) Schmaltz, B.; Weil, T.; Müllen, K. *Adv. Mater.* **2009**, *21*, 1067.

(19) Loo, Y. L.; Hiszpanski, A. M.; Kim, B.; Wei, S. J.; Chiu, C. Y.; Steigerwald, M. L.; Nuckolls, C. *Org. Lett.* **2010**, *12*, 4840.

(20) Gorodetsky, A. A.; Chiu, C. Y.; Schiros, T.; Palma, M.; Cox, M.; Jia, Z.; Sattler, W.; Kymissis, I.; Steigerwald, M.; Nuckolls, C. *Angew. Chem. Int. Ed.* **2010**, *49*, 7909.

(21) Kang, S. J.; Kim, J. B.; Chiu, C. Y.; Ahn, S.; Schiros, T.; Lee, S. S.; Yager, K. G.; Toney, M. F.; Loo, Y. L.; Nuckolls, C. *Angew. Chem. Int. Ed.* **2013**, *52*, 7063.

(22) Schiros, T.; Mannsfeld, S.; Chiu, C. Y.; Yager, K. G.; Ciston, J.; Gorodetsky, A. A.; Palma, M.; Bullard, Z.; Kramer, T.; Delongchamp, D.; Fischer, D.; Kymissis, I.; Toney, M. F.; Nuckolls, C. *Adv. Funct. Mater.* **2012**, *22*, 1167.

(23) Anthony, J. E. *Chem. Rev.* **2006**, *106*, 5028.

(24) Chebny, V. J.; Gwengo, C.; Gardinier, J. R.; Rathore, R. *Tetrahedron Lett.* **2008**, *49*, 4869.

(25) Zhang, Q.; Peng, H.; Zhang, G.; Lu, Q.; Chang, J.; Dong, Y.; Shi, X.; Wei, J. *J. Am. Chem. Soc.* **2014**, *136*, 5057.

(26) Shen, Y.; Chen, C.-F. *Chem. Rev.* **2012**, *112*, 1463.

(27) Yu, C.-J.; Lin, C.-E.; Yu, L.-P.; Chou, C. *Appl. Opt.* **2009**, *48*, 758.

(28) Jan, C.-M.; Lee, Y.-H.; Wu, K.-C.; Lee, C.-K. *Opt. Express* **2011**, *19*, 5431.

(29) Farshchi, R.; Ramsteiner, M.; Herfort, J.; Tahraoui, A.; Grahn, H. T. *Appl. Phys. Lett.* **2011**, *98*, 162508.

(30) Sherson, J. F.; Krauter, H.; Olsson, R. K.; Julsgaard, B.; Hammerer, K.; Cirac, I.; Polzik, E. S. *Nature* **2006**, *443*, 557.

(31) Wagenknecht, C.; Li, C.-M.; Reingruber, A.; Bao, X.-H.; Goebel, A.; Chen, Y.-A.; Zhang, Q.; Chen, K.; Pan, J.-W. *Nat. Photon.* **2010**, *4*, 549.

(32) Chu, C. W.; Shao, Y.; Shrotriya, V.; Yang, Y. *Appl. Phys. Lett.* **2005**, *86*.

(33) Lee, H. W.; Yoon, Y.; Park, S.; Oh, J. H.; Hong, S.; Liyanage, L. S.; Wang, H.; Morishita, S.; Patil, N.; Park, Y. J.; Park, J. J.; Spakowitz, A.; Galli, G.; Gygi, F.; Wong, P. H. S.; Tok, J. B. H.; Kim, J. M.; Bao, Z. *Nat. Commun.* **2011**, *2*, 541.

(34) Krupke, R.; Hennrich, F.; Löhneysen, H. v.; Kappes, M. M. *Science* **2003**, *301*, 344.

(35) Strano, M. S.; Dyke, C. A.; Usrey, M. L.; Barone, P. W.; Allen, M. J.; Shan, H.; Kittrell, C.; Hauge, R. H.; Tour, J. M.; Smalley, R. E. *Science* **2003**, *301*, 1519.

Chapter 2. Chiral trichloro-substituted c-HBC

2.1 Introduction

In this chapter, we will describe the design, synthesis, separation, chirality characterization, and OFET devices for the chiral trichloro c-HBCs. By introducing chlorines onto contorted-HBCs based on the three-fold symmetry,[1] we synthesized and resolved the chiral member in the c-HBC family for comprehensive chirality studies for the first time. The three-fold symmetry breaks the intrinsic symmetrical plane in c-HBCs and gives rise to the structural chirality of trichloro-substituted c-HBC.

The structures of trichloro c-HBC have two conformations. We name them "butterfly" and "up-down" conformers, similar to the fluorinated c-HBCs and c-DBTTCs.[2,3] In the up-down structure, six peripheral functionalized benzo-groups alternate up or down around the central core, much like the parent c-HBC and many other derivatives of c-HBC. The up-down structure has a three-fold symmetry in NMR spectrum, which shows three aromatic protons. But the trichloro-substitution breaks the symmetrical plane cutting across the pentacene-unit and perpendicular to the core in the parent up-down c-HBC (Figure 1). Therefore, the up-down trichloro c-HBC is chiral (C_3 symmetry) and has two enantiomers. On the other hand, the butterfly structure shifts away from the parent c-HBC's up-down structure. Our DFT calculations show that one pentacene-unit bends toward one direction and the other four benzo-goups fold to the opposite direction in the butterfly structure (Figure 2). The trichloro-substitution also breaks the symmetrical plane of the parent butterfly c-HBC (perpendicular to the butterfly's "abdomen"). As a result, the butterfly conformation of trichloro c-HBC is also chiral and has two

enantiomers. The nine protons of the butterfly trichloro c-HBC lose the three-fold symmetry in the NMR spectrum and therefore its NMR spectrum has nine distinct aromatic protons.

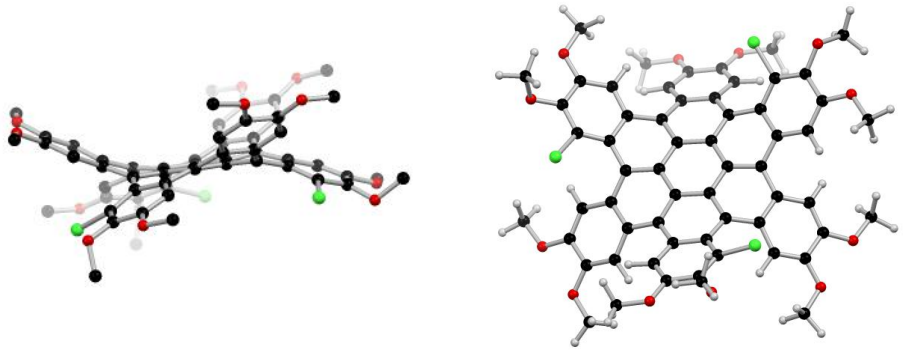

Up-down or the 3-peak Up-down top view

Figure 1. Side and top views of the up-down conformation from DFT optimization. Black: carbon; red: oxygen; green: chlorine. Hydrogens are omitted for clarity.

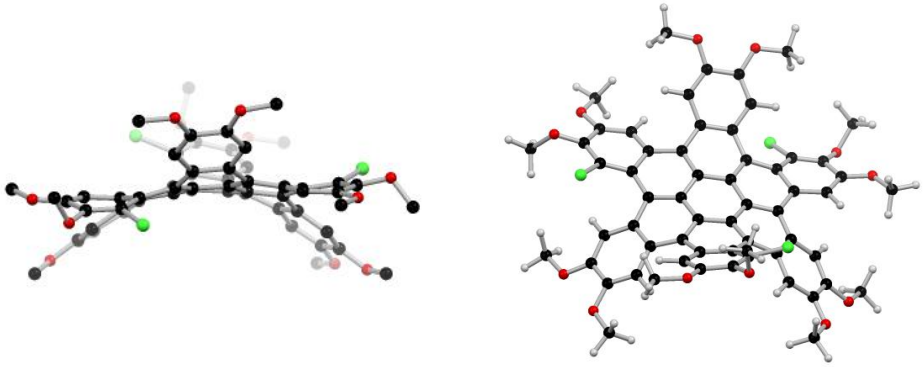

Butterfly or the 9-peak Butterfly top view

Figure 2. Side and top views of the butterfly conformation from DFT optimization. Black: carbon; red: oxygen; green: chlorine. Hydrogens are omitted for clarity.

We used experimental data and calculations to demonstrate that the butterfly

structure is the kinetically trapped product. The two conformations, up-down and butterfly, do not interconvert up to 412 K. We were able to resolve the two sets of enantiomers and quantified the conversion barrier of each set. Before we discuss the synthesis and properties of the trichloro c-HBCs, we will first review the background of previous synthetic routes for c-HBCs.

2.2 Background of previous synthetic routes for c-HBCs

Clar and coworkers were the first to synthesize the c-HBC.[4] However, their synthesis precluded an in-depth study of this motif, as it consists of seven steps that involve harsh conditions such as high temperature (440 °C) and low yields (≤ 2%).[4]

The first modern synthesis of c-HBCs by Xiao et al. uses the two-step Barton-Kellogg olefination and Katz-modified Mallory photocyclization as key steps (Figure 3).[5] Subsequently, Plunkket et al. developed the expeditious one-step Barton-Kellogg approach and also studied Scholl reaction in combination with photocyclization as the cyclization step.[6] Their route is shown in Figure 4. For most substituents, a combination of photo-cyclization and Scholl reaction is required for complete cyclization in the final step. But when R_5 and R_6 are both alkoxy chains, sole Scholl condition leads to fully cyclized product. In another study on fluorine-substituted c-HBCs, Loo et al. found that the solely photocyclized product and the product from the Scholl reaction in conjunction with photocyclization share different conformations.[3] The photocyclized product with sixteen fluorine substitutions forms the usual up-down conformation, while the use of Scholl reaction to close the half-cyclized byproduct from photoreaction kinetically traps the butterfly conformation. In the third approach to synthesize c-HBCs, Suzuki reaction

was employed as the key step to form the key-intermediate, bis-olefin.[2,3] This approach is not only less labor-intensive, but also provides the facile incorporation of thiophene units regioselectively to form c-DBTTCs.

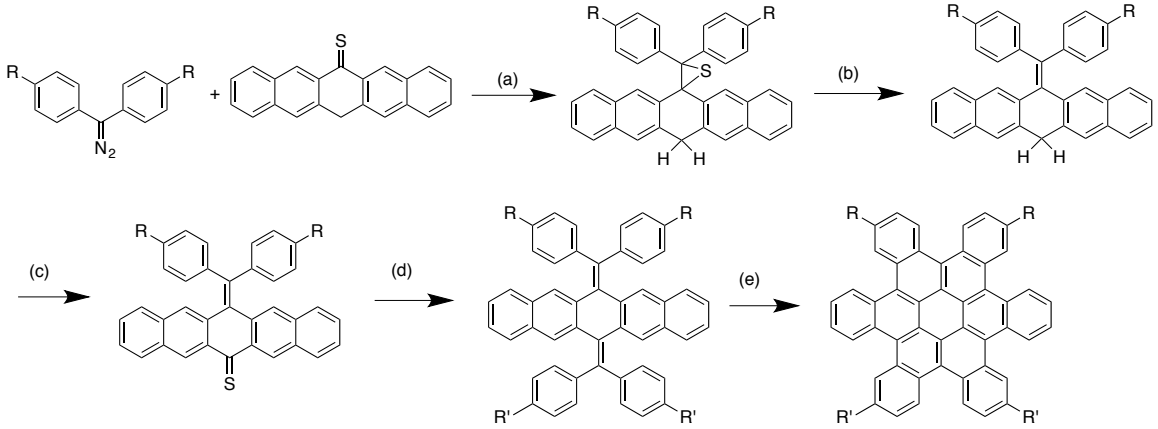

Figure 3. Synthesis 1.0 for c-HBC using a 2-step Barton-Kellogg olefination and Katz-modified Mallory photocyclization as key steps. (a) dichloromethane/absence of light. (b) PPh_3, xylenes, reflux. (c) i: $KMnO_4$/ acetone; ii: Lawesson's reagent (d) i: dichloromethane, ii: PPh_3. (e) *hv,* I_2, propylene oxide, benzene. Reproduced from Ref. 3.

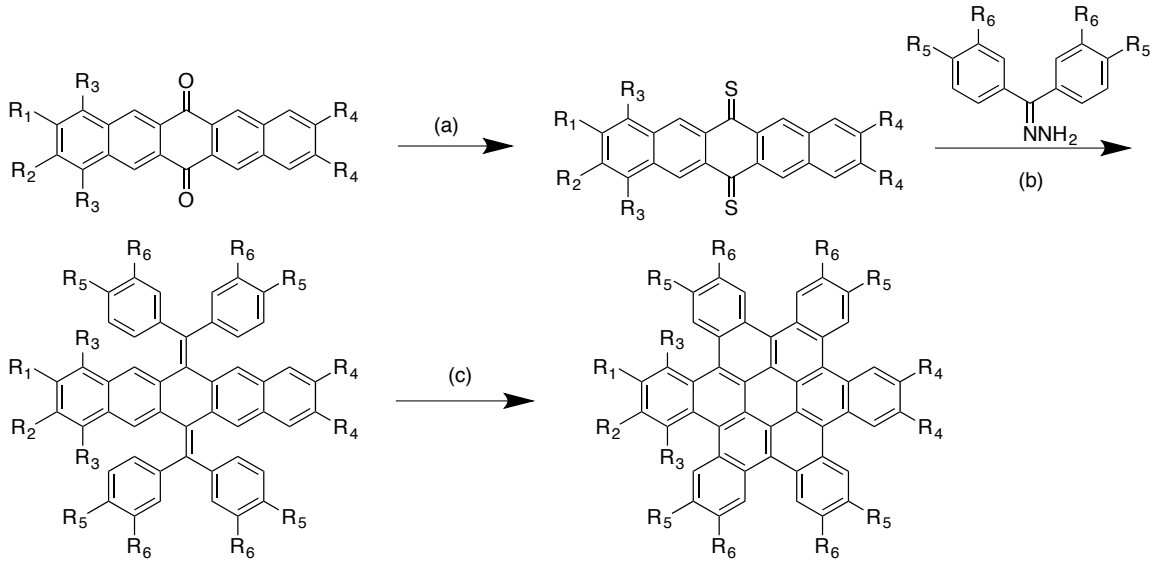

Figure 4. Synthesis 2.0 for c-HBC. (a) Lawesson's reagent. (b) i: reaction *in situ* with MnO_2; ii: PPh_3. (c) for most substituents, a combination of photocyclization (*hv,* I_2, propylene oxide, and benzene) and Scholl reaction ($FeCl_3$, nitromethane and dichloromethane) is required for complete cyclization. But when R_5 and R_6 are both alkoxy chains, sole Scholl condition leads to fully cyclized product.

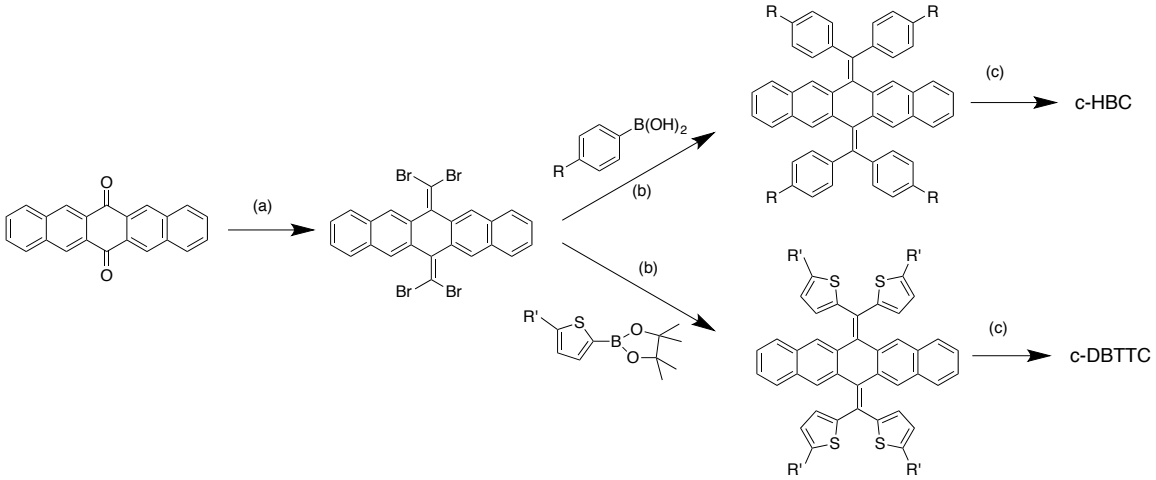

Figure 5. Synthesis 3.0 for c-HBC and the thiophene derivative c-DBTTC. (a) CBr_4, PPh_3 and toluene. (b) Na_2CO_3, $Pd(PPh_3)_4$, THF/H_2O, 70 ^{0}C. (c) *hv,* I_2, propylene oxide and benzene.

2.3 Synthesis of trichloro c-HBC based on the three-fold symmetry

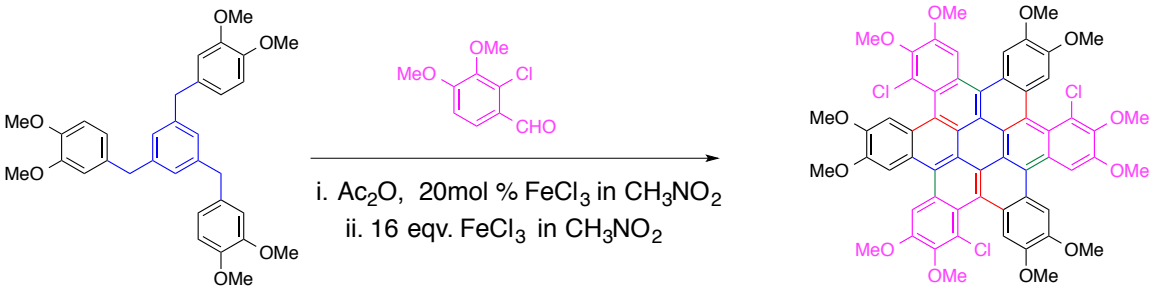

Figure 6. Synthesis of trichloro-substituted c-HBC based on three-fold symmetry.

The synthesis of tricholoro c-HBC **7** was adapted from Wei's method.[1] When

purifying the final product from the reaction mixture, prep-TLC gave a yellow to orange compound that matches the expected mass of the product by MALDI mass spectroscopy, This (crude) product showed twelve aromatic peaks on ^{1}H-NMR spectrum (Figure 7). After carefully adjusting the solvent ratios, we were able to further separate the mixture into two compounds. One has nine aromatic peaks and the other has three aromatic peaks on ^{1}H-NMR spectra, and the ratio of aromatic protons and methoxy protons matches well.

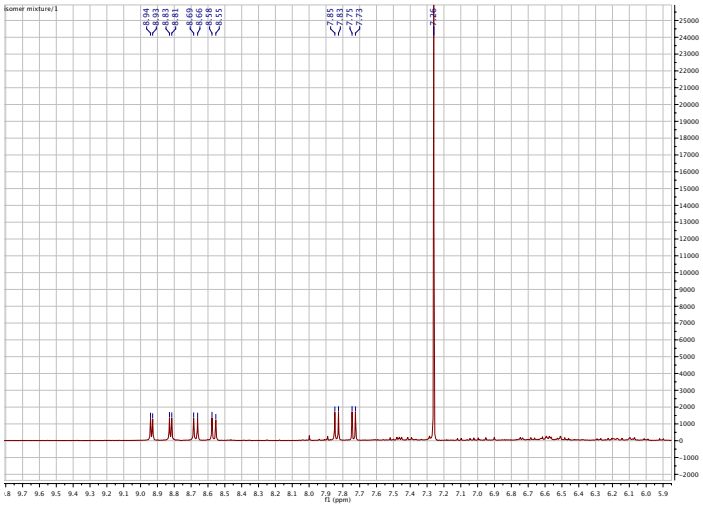

Figure 7. Zoomed-in aromatic region for 1: 3 mixture of the 3-peak: the 9-peak.

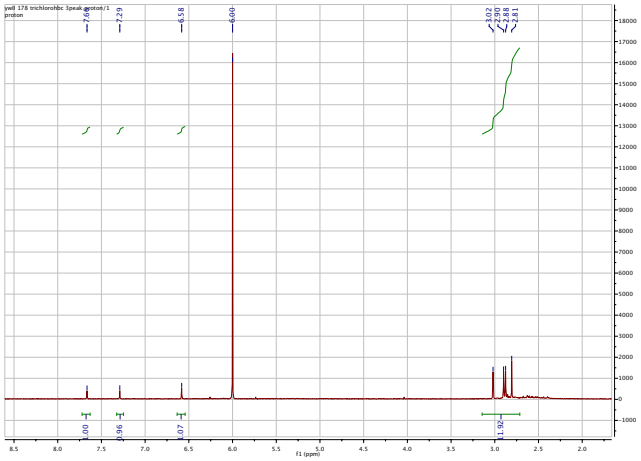

Figure 8. Zoomed-in aromatic region for the 3-peak compound.

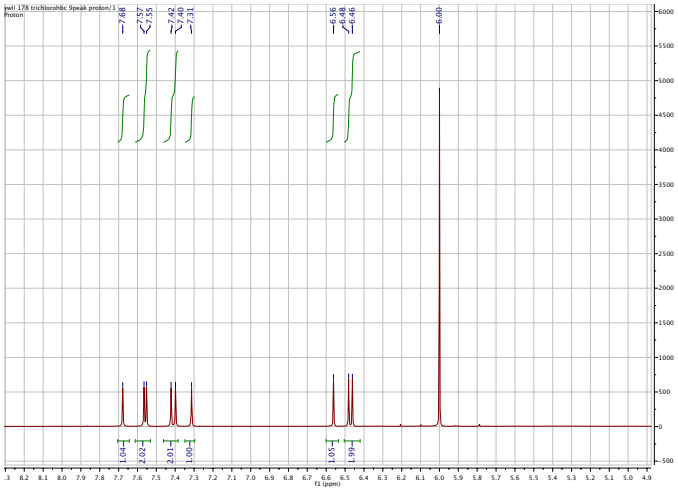

Figure 9. Zoomed-in aromatic region of the 9-peak compound.

(See the full spectra in supporting information at the end of this chapter.) Both of the two compounds have the expected mass of trichloro c-HBC and the isotopic distribution of chlorines is also in a good match. The product ratio of the 9-peak compound and the 3-peak compound is about 3:1 according to the integration ratio in NMR spectra.

2.4 Mechanistic study with DFT calculations

According to our previous knowledge on the c-HBC family, we hypothesize that the two compounds both with correct mass originate from the two conformations of trichloro-HBCs, the butterfly conformation and the up-down conformation. Indeed, we found two stable geometries for the trichloro-HBC using DFT calculation, namely, the butterfly and the up-down for the optimized structures (Figure 1 and Figure 2). From their symmetry differences, we identified the 3-peak NMR spectrum (Figure 8) to be the up-down conformation and 9-peak spectrum to be the butterfly conformation (Figure 9). Therefore, this Scholl-type reaction gives two conformations. The overall yield of their sum is 51%.

The ground state energy of the butterfly (9-peak) conformer is higher than that of the up-down conformer (3-peak) by 9.6 kcal/mol, on the level of B3LYP and 6-31G**. The big difference of ground state energy and the fact that the higher energy conformer is the major product suggest the two conformers not interconvert after formation under the reaction condition and therefore must be formed kinetically. Indeed, the two conformers did not interconvert up to 412 K from the VT-NMR study (Figures 10 and 11).

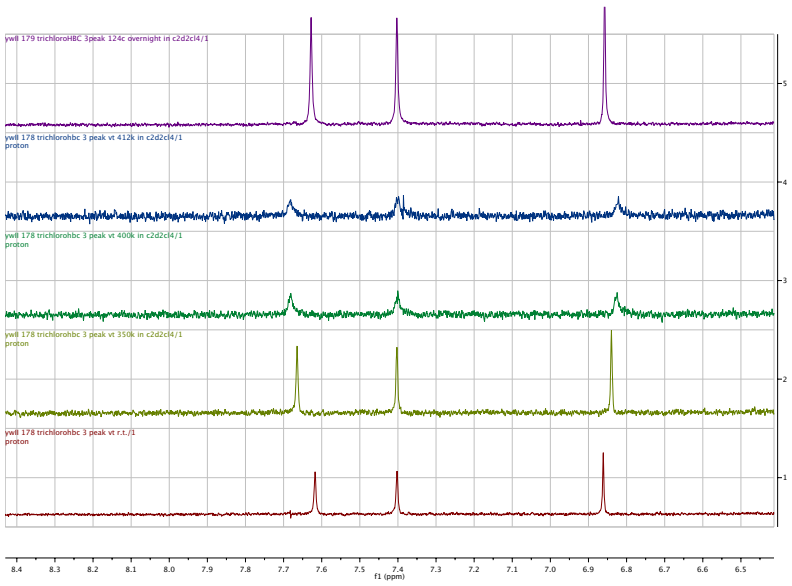

Figure 10. VT NMR spectra of the 3-peak heating from R.T. to 412 K, holding 10 minutes at each temperature (solvent 1,1,2,2-tetrachloroethane-d_2). The top trace shows the NMR spectrum remained the same as the R.T. spectrum after heating the sample in a 124 °C oil bath overnight.

The ratio of the two conformers in the mixture is about 1:3 for up-down: butterfly according to the ratio of the integrals in NMR spectrum. We rationalize the formation of the two isomers and their ratio with the assistance of DFT calculation. The reaction, forming twelve covalent bonds in one pot, starts from two stages of three-fold Friedel-

Crafts reaction with catalytic iron(III) chloride, followed by "partial" aromatization to form the uncyclized key intermediate (Figures 12 and 13). The excess iron(III) chloride then transfers the key intermediate **A** to trichloro c-HBC in a Scholl-type reaction.

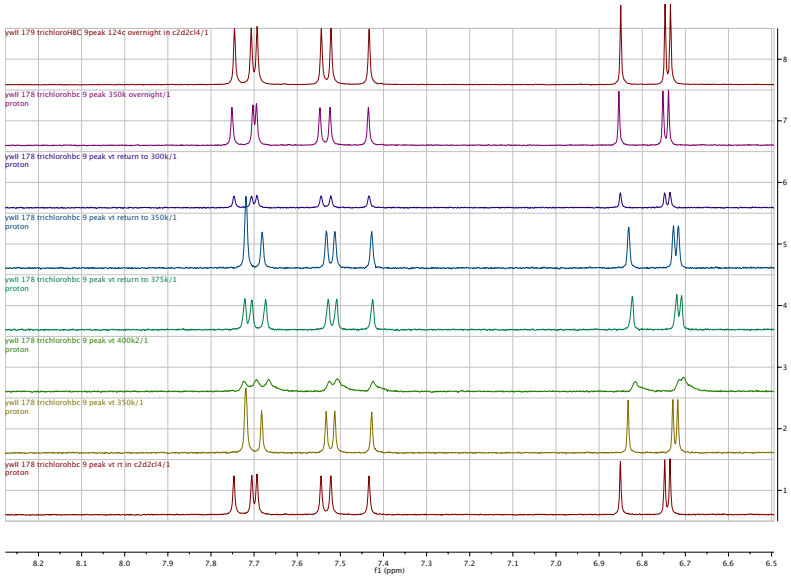

Figure 11. VT NMR spectra of the 9-peak heating from R.T. to 400 K, holding 10 minutes at each temperature (solvent 1,1,2,2-tetrachloroethane-d_2). The traces at elevated temperatures are different than the R.T. trace. However, this is more likely due to the temperature effect on NMR spectra rather than conformational changes. Because the spectrum returns to the R.T. spectrum as temperature is decreased to 300K. The top two traces show the NMR spectra remained the same as the R.T. spectrum after heating the samples in a 75 °C and 124 °C oil bath overnight.

Scholl reactions are known to form kinetically trapped products as we have discussed in the heavily fluorinated c-HBCs.[3] Because the two conformations in the product **7** cannot interconvert after formation as demonstrated by our VT NMR study, the orientation of the chlorine atoms when forming the key intermediate **A** determines the

chirality of its own [4]-helicene subunit in the Scholl reaction. Thus the chlorines being on one side of the plane or on different sides will form the up-down or butterfly conformers, respectively. We calculated the total energy of the two conformers of key intermediates **A** with DFT. The geometry optimization was done by opening up the rings step by step on the butterfly or on the up-down structures, respectively. The total energy

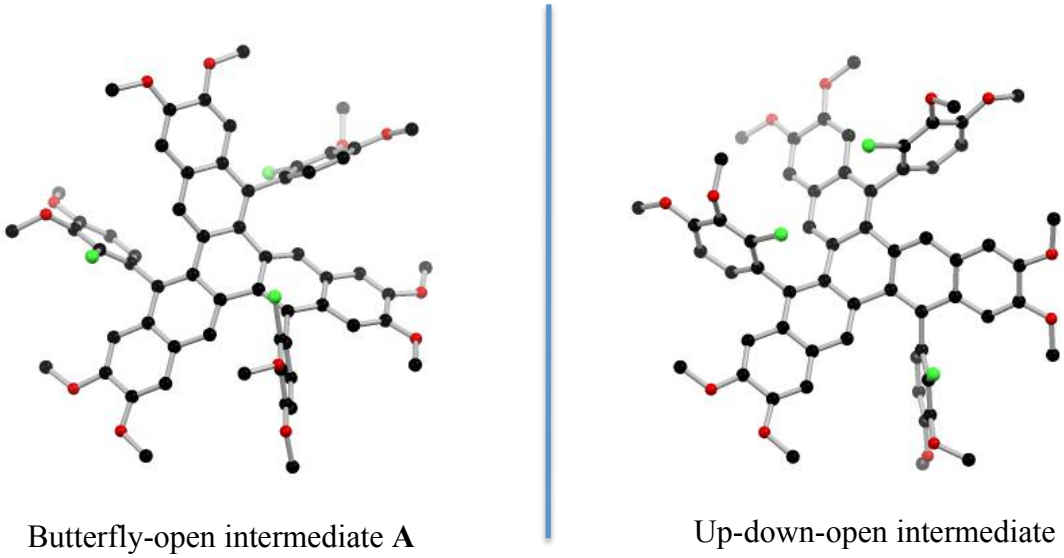

Butterfly-open intermediate **A** Up-down-open intermediate **A**

Figure 12. DFT optimized structures of the butterfly-open intermediate and up-down-open intermediate **A**.

difference of the key intermediates **A** of the 9-peak and the 3-peak is small, only 0.03 kcal/mol (Figure 12 and Table S1). This small energy difference indicates that the chlorine atoms choose their orientations above or below the plane randomly. Thus the Scholl cyclization will lead to products in which the chlorine atoms are above or below the plane accordingly. So we rationalize that the ratio of the 3-peak and 9-peak is due to statistics, which is 1:3 for up-down to butterfly.

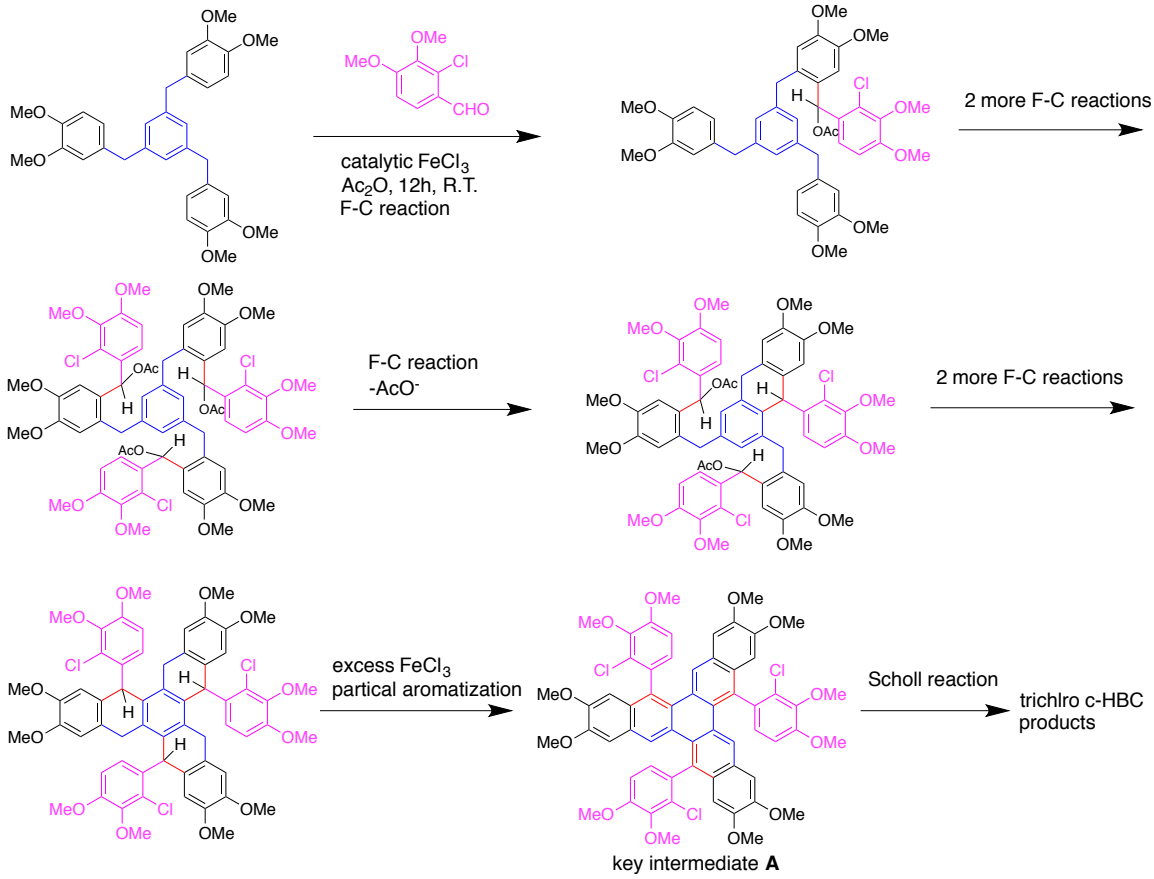

Figure 13. Mechanistic steps in the one-pot reaction.

2.5 Separation of diastereomers with HPLC

The 9-peak and 3-peak conformers were then subjected to chiral HPLC for resolution. The 9-peak conformer is resolved on the cholester column (a reverse-phase chiral column) with 15% THF and 85% hexanes (1mL/min). The 3-peak is resolved on the 1-B3 column with 10% THF and 90% hexanes (1mL/min). We are also able to resolve the enantiomers of the 9-peak conformer on the preparative scale using cholester column. The chirality of the diastereomers is confirmed by optical rotation measurement and circular dichroism spectra. The optical rotation of 9-peak-I is -10°±2°, and that of 9-peak-II is +10°±2° (23.4 °C, c = 0.1, $CHCl_3$). Similarly, the optical rotation of 3-peak-I is

-11°±2°, and that of 3-peak-II is +11°±2° (24.0 °C, c = 0.1, $CHCl_3$). Figure 14 shows the circular dichroism (CD) spectra and UV-Vis spectra of the 9-peak and 3-peak conformers. The vibrational modes at the peaks of 268 nm, 280 nm and 322 nm in CD specta arise from the helicene units.[7] The intense peak in the UV-Vis spectrum at 400 nm is suppressed in the CD spectra, because the 400 nm peak belongs to the vibration of the radialene core of trichloro c-HBC whose vibrational mode is roughly symmetrical.[8]

2.6 Chiral structures of diastereomers

We have separated four diastereomers for trichloro c-HBCs using HPLC, and confirmed the chirality by using polarimetry and CD measurement. The number of the diastereomers can be explained by the 3-D structural information of trichloro c-HBCs. Half of the six cove-units in the trichloro c-HBCs are chlorinated [4]-helicene with steric hindrance that induces chirality. Helicenes are well known for their structural chirality, which results from the helicity itself. By convention a left-handed helix is *minus* and labeled **M**, a right-handed helix is *plus* and labeled **P**. The chirality increases as the size of helicene increases, the chirality can also be tuned with substitution on side-chains or on the helicene skeleton. [9,10,11] We consider the trichloro-HBCs as the fusion of three chloro-[4]-helicene in the central ring, making six [4]-helicene bays. Three chlorinated [4]-helicenes are locked in either P or M configuration due to steric hindrance, whereas the three non-chlorinated [4]-heliecenes have much more flexibility and can rest in any configuration that buffers the steric hindrance of the adjacent chlorinated 4-helicenes. Three-P or three-M chloro-[4]-helicene would make the two enantiomers of the up-down or the 3-peak. Two-P-and-one-M or two-M-and-one-P would make the two enantiomers of the butterfly or the 9-peak.

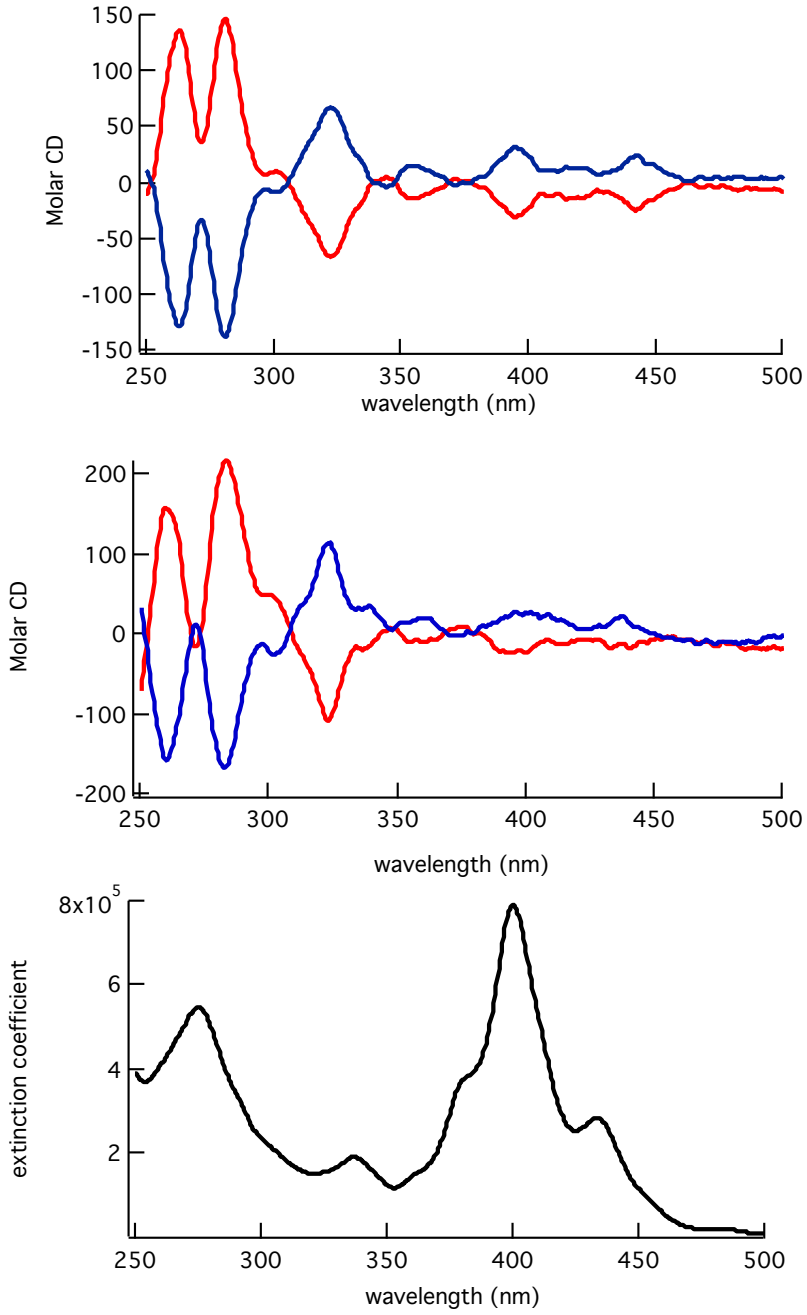

Figure 14. CD spectra of the 9-peak (top) and 3-peak (middle). UV-Vis of the trichloro c-HBC (bottom).

Although there were studies revealing the conversion barrier for individual helicenes or aza-helicenes,[12-15] there is no preceding example for quantifying the conversion of

fused helicene-units in one molecule. Despite the wide investigation of many novel organic materials containing helicene-units for application in OFET and renewable energies, etc., the conversion barrier in expanded aromatic systems with adjacent helicene-units remained intriguing.[16,17] The structural conformations in these materials affect the self-assembly in the film, the annealing process and, consequently, the device performance. Therefore, it is important to understand how the conversion of the helicene units behaves in an expanded aromatic system and how stable the overall conformation is. The chiral nature of the trichloro c-HBCs has provided us an excellent handle to study the conversion barrier. In the next section, we heated our enantiopure samples and used HPLC to quantify the racemization energy barrier of the 9-peak and 3-peak, respectively.

2.7 Kinetic studies

The (+)-9-peak-II from HPLC separation was heated in an oil bath in DMF at 120 °C. Aliquots are taken at different temperatures and cooled in -78 °C bath immediately. DMF was removed and aliquot samples are subjected to HPLC for analysis on cholester column with the condition described in section 2.5. The same experiments were carried out at 130 °C, 135 °C and 140 °C. The plots and linear fitting data are displayed in Figure 15 A-D, and HPLC traces are included in Supporting Information at the end of this chapter. We then plot ln(ee%) against time, the linear fit of which gives the rate constant according to the first-order kinetics (value *b* in the inset). The rate constants *k* at each temperature were converted to the proper units, and ln(*k*/T) was linearly fitted against 1/T using Eyring equation below.

$\ln(k/T) = \Delta S^{\neq}/R - \ln(h/k_B) - \Delta H^{\neq}/(RT)$, where R is the gas constant, h is the Planck's

constant and k_B is the Boltzman constant.

According to the Eyring equation, we calculated $\Delta S^{\neq}=27.9 \pm 4.7$ cal·K^{-1}·mol^{-1}, $\Delta H^{\neq}=41.4 \pm 1.9$ kcal·mol^{-1}.

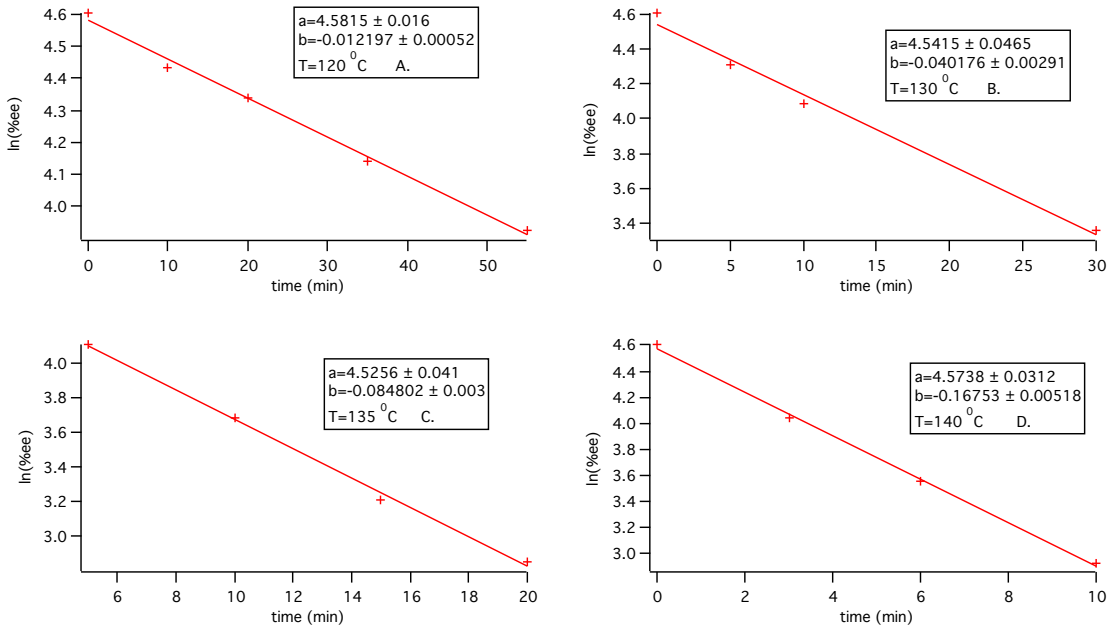

Figure 15 A-D. Linear fit of plots ln(%ee) vs. time at 120 °C (A), 130 °C (B), 135 °C (C) and 140 °C (D). Value *b* is the slope of the linear fit, which is the rate constant to be used in the following Eyring equation.

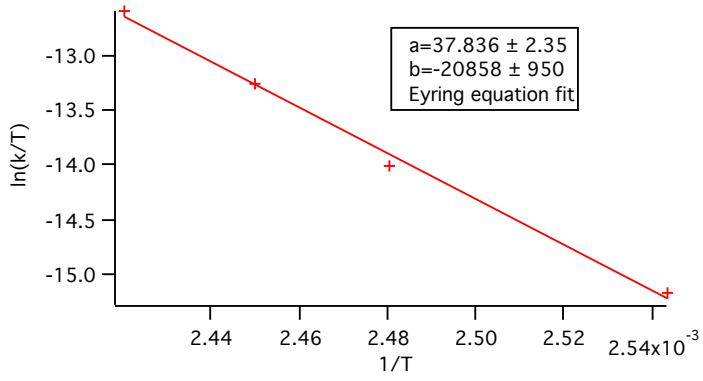

Figure 16. Eyring equation fitting for the 9-peak compound.

We applied similar method to calculate the racemization energy barrier of the (+)3-peak(II) compound, besides each sample was heated in DMF in a J-Young tube after freeze-pump-thaw. The samples heating at 125 ^{o}C, 130 ^{o}C, 135 ^{o}C and 140 ^{o}C were then subjected to HPLC on 1B-3 column with the condition described in section 2.5. Eyring analysis revealed $\Delta S^{\neq}$=30.1± 12.2 cal·K^{-1}·mol^{-1}, $\Delta H^{\neq}$=42.9± 4.9 kcal·mol^{-1}. (Figures 17 A-D and Figure 18)

The values of $\Delta S^{\neq}$ and $\Delta H^{\neq}$ are basically the same for both 9-peak and 3-peak conformers with experimental errors, suggesting the two conformers may share the same racemization mechanism. Although for the 9-peak compound, we can propose the whole molecule can be converted to its antipode when only one single chloro-[4]-helicene "racemizes", this is not the case for the 3-peak conformer. If we suppose the 3-peak

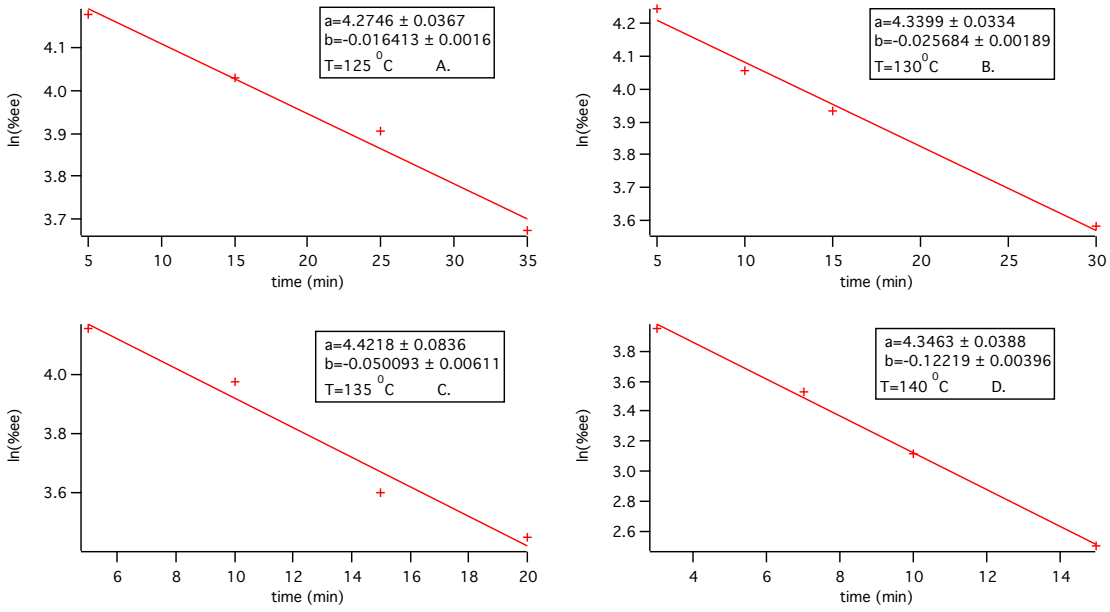

Figure 17 A-D. Linear fit of plots ln(ee%) vs. time at 125 °C (A), 130 °C (B), 135 °C (C) and 140 °C (D). Value *b* is the slope of the linear fit, which is the rate constant to be used in the following Eyring equation.

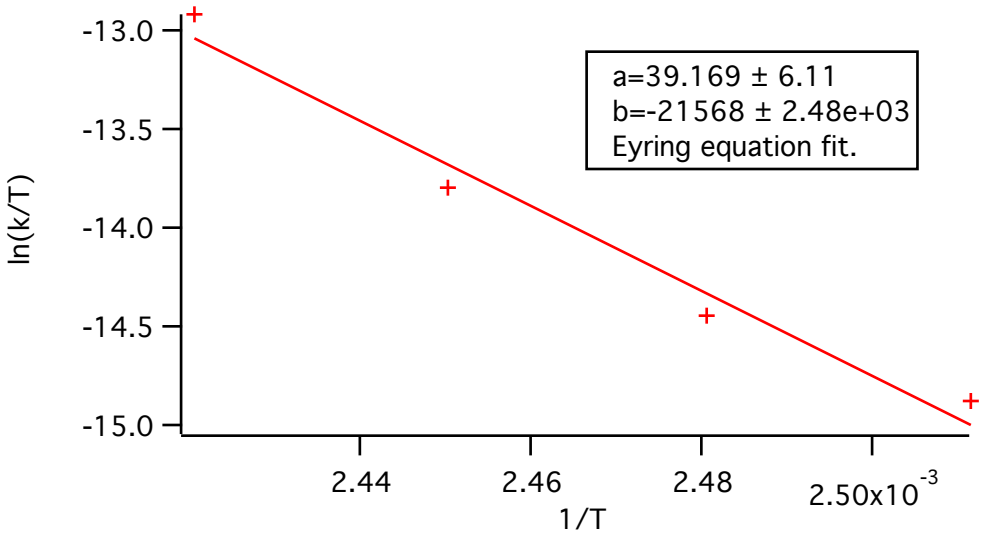

Figure 18. Eyring equation fitting for the 3-peak compound.

undergoes single chloro-[4]-helicene racemization, it should go through the 9-peak conformation as an intermediate during its own racemization. We have two experimental evidences that this is false. First, we did not observe any 9-peak compound in either VT NMR spectra or the HPLC traces. Subsequently, VT NMR experiment also reveals that the 9-peak conformer is stable enough at the elevated temperatures we ran the kinetic study, which precludes the possibility of converting from (+)-3-peak to 9-peak and then to (-)-3-peak.

The racemization mechanism of the 9-peak and 3-peak should therefore involve concerted flipping of three chloro-[4]-helicene rather than a single one. The large value of $\Delta S^{\neq}$ (30 cal·K^{-1}·mol^{-}1) suggests the transition states during racemization differ in a great deal from the ground-state diasteromers,[18,19] matching the concerted flipping mechanism because its transition-state and ground-state conformations are distinct. The value of $\Delta H^{\neq}$ for both 9-peak and 3-peak is much larger than sole [4]-helicene

derivatives,[12-15] resulting stable enantiomers whose half-life are over 25 years at room temperature.

2.8 Light-responsive OFET characteristics

Based on previous investigation on the c-HBC family, we understood that c-HBC derivatives can be fabricated into OFETs through solution processing.[2,20-23] (Chapter 1) Moreover, tetra(dodecyloxy) c-HBCs self-assemble into columnar arrays in a carbon nanotube gap cut by lithography, resulting in a filed effect transistor that is light responsive.[20] The photocurrent originates from photoexcitations that are restricted in the radialene core by the insulating alkoxyphenyl cladding.[24]

We fabricated bottom-contact OFETs using the racemic 9-peak compound. Gold electrodes were thermo-evaporated on a silicon/ silicon dioxide substrate covered with a patterned mask. The chip with electrodes was then treated with pentafluorothiopheneol for an hour and trichloro(octadecyl)silane for 20 minutes. 5mg/mL solution of racemic 9-peak c-HBC in chloroform was spun cast onto the substrate with pre-treated gold electrodes. We then measured the transfer characteristics in dark and under light illumination. We chose the 405 nm laser (10 mW) as the light source because the absorption spectra reveal that π–π transition radialene core which is responsible for the photocurrent[24] shows around 400 nm. Figure 19 displays the transfer characteristics of the OFET with the light on and off.[25] Notably, the off drain-current increases from 10 pA to 2 nA under illumination.

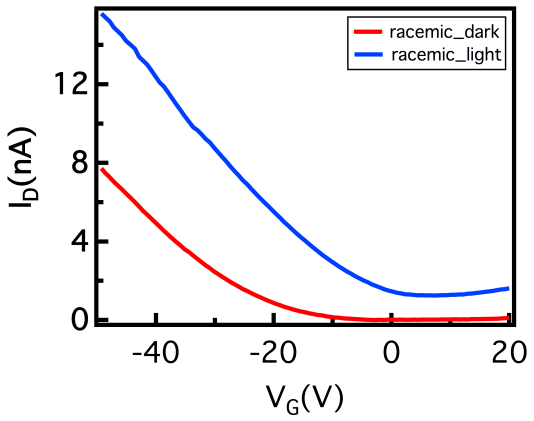

Figure 19. Transfer characteristics with the 405 nm laser illumination on and off.

With the successful separation of the 9-peak enantiomers, we envision that the enantio-pure OFETs will respond to their corresponding polarized light,[26] which have potential applications in ellipsometry-based tomography,[27] optical communication of spin information,[28] and quantum-based optical computing and information processing.[29]

2.9 Experimental procedures

2.9.1 Synthesis

General. Reagents employed were either commercially available or prepared according to a known procedure as noted below. Anhydrous and oxygen-free CH_2Cl_2, diethyl ether and THF were obtained from a Schlenk manifold with purification columns packed with activated alumina and supported copper catalyst (Glass Contour, Irvine, CA). Unless otherwise noted, all reactions were run in oven-dried glassware, and monitored by TLC using silica gel 60 F_{254} precoated plates (EM Science) when necessary. Column chromatography was performed on a CombiFlash® Sg100c system using RediSepTM normal phase silica columns (ISCO, Inc., Lincoln, NE). ^{1}H NMR (400 MHz), and ^{13}C

NMR (100 MHz) spectra were recorded on Bruker DRX-300 and Bruker DRX-400 spectrometers at room temperature unless otherwise noted. HRMS were recorded on JEOL JMS-HX110A/110A Tandem mass spectrometer if not otherwise noted. Analytical HPLC were recorded on Agilent. Prep-scale HPLC were recorded on Waters. All HPLC columns are purchased from Comsmosil. Full ^{1}H NMR and ^{13}C NMR spectra are contained in the supporting information at the end of this chapter.

Synthesis of 1,3,5-tri(3,4-dimethoxybenzyl)benzene (OMe-TBB)

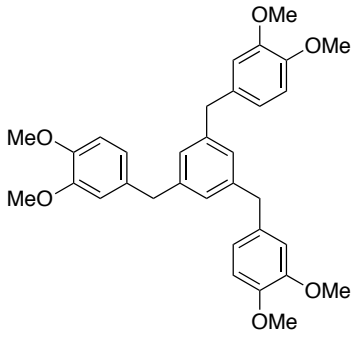

1,3,5-tri(3,4-dimethoxybenzyl)benzene (TBB) was prepared according to Wei's paper[1] from commercially available reagents.

Synthesis of 1,3,5-tri(3,4-didodecyloxybenzyl)benzene (12-TBB)

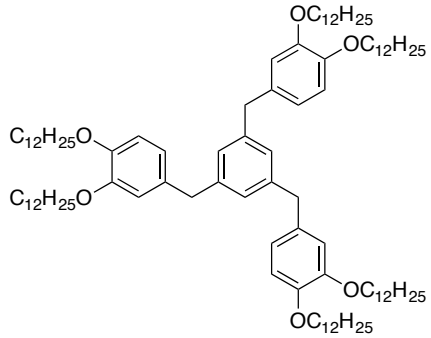

The dodecyloxy-substituted 12-TBB are obtained by removing the methoxy groups in OMe-TBB using BBr_3, followed by adding 1-Bromododecane, Na_2CO_3 and heating at 80 ^{0}C in DMF overnight. The spectroscopic data matched the reported ones in Wei's paper.[1]

Synthesis of trichlor c-HBC

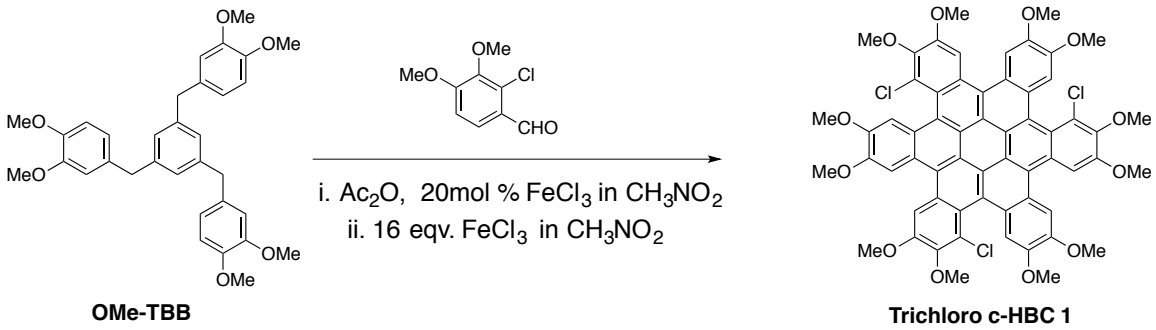

To a stirring solution of 2-chloro3,4-dimethoxybenzaldehyde (63mg, 0.31 mmol) and Ac_2O (0.1 mL, 0.95 mmol) in 60 mL DCM at room temperature was added a solution of $FeCl_3$ (5 mg, 0.02 mmol) in nitromethane (0.3 mL), followed by dropwise addition of Ome-TBB (50 mg, 0.095 mmol) in DCM (20 mL). The resulting mixture was stirred at r.t. overnight and then degassed with N_2 for 15 min before a second portion of excessive $FeCl_3$ (246 mg, 1.52 mmol, 15.6 equiv) solution in nitromethane (5 mL) was added dropwise under nitrogen atmosphere and stirred for 12 h. Then, cold Methanol (25 mL) was added with stirring to quench the reaction and the mixture was poured into cold water (120 mL). The organic layer was separated, washed with water, dried by anhydrous Na_2SO_4 and rotary evaporated under vacuo. The residue was purified by Prep-TLC (silica gel, Hexanes:DCM:EA = 45:5:50 v/v, loading ~30 mg crude product each plate) to give **1** in two adjacent yellow bands on the Prep-plate. The overall yield of their sum is 51%. ^{1}H NMR of **1-9-peak** (400 MHz, chloroform-d) δ (ppm): 8.94 (s, 1H), 8.83 (s, 1H), 8.81 (s, 1H), 8.68 (s, 1H), 8.66 (s, 1H), 8.58 (s, 1H), 7.82 (s, 1H), 7.74 (s, 1H), 7.72 (s, 1H), 4.28-4.07 (m, 36 H) ^{13}C NMR **1-9-peak (**100 MHz, chloroform-d) δ (ppm): 152.13, 152.12, 152.04, 148.55, 148.27, 147.29, 147.23, 147.09, 147.04, 145.97, 145.91, 145.84, 128.40, 128.34, 128.11, 127.66, 127.55, 127.29, 126.02, 125.23, 125.13, 124.85, 124.52, 124.51, 124.41, 124.27, 123.27, 123.12, 122.95, 122.90, 122.78, 122.18, 122.04, 121.20,

120.96, 120.91, 120.77, 119.96, 111.76, 110.68, 110.60, 109.37, 109.33, 108.95, 108.88, 108.86, 108.74, 107.80, 61.12, 61.06, 61.02, 60.39, 56.45, 56.34, 56.33, 56.13, 56.02, 55.97, 55.90, 53.41.MS (MALDI-TOF) (CHCA): m/z found for $C_{60}H_{45}O_{12}Cl_3$ [M+2] 1064.34 ^{1}H NMR of **1-3-peak** (400 MHz, chloroform-d) δ (ppm): 8.92 (s, 3H), 8.55 (s, 3H), 7.84 (s, 3H), 4.28 (s, 9H), 4.16 (s, 9H), 4.14 (s, 9H), 4.07 (s, 9H). ^{13}C NMR **1-3-peak (**100 MHz, chloroform-d) δ (ppm): 152.21, 148.29, 147.36, 145.77, 128.66, 127.19, 126.25, 125.15, 122.79, 122.59, 122.34, 121.79, 120.19, 111.78, 109.45, 107.68, 61.06, 56.48, 56.01, 55.97. (MALDI-TOF) (CHCA): m/z found for $C_{60}H_{45}O_{12}Cl_3$ [M+2] 1064.36.

2.9.2 Theoretical methods of DFT calculations:

The DFT calculations were done with Jaguar (versions 5.0, 6.0 and 6.5) [Schrodinger, L.L.C., Portland, OR, 1991-2005.] Except where specified, complete geometric relaxation was performed. Thermochemistry calculations were performed with hybrid functional of Becke, B3LYP, basis 6-31G**.

The total below lists the total energy differences of two conformations of trichloro c-HBC, that of the open forms of them. (**9peak minus 3peak**) Open_1 denotes opening one ring in the trichloro c-HBC (9-peak or 3-peak conformation), open_2 denotes opening two rings in the trichloro c-HBC, and open denotes opening three rings in the trichloro c-HBC which we named as intermediate **A** in the main text.

	Total energy differences
trichloro c-HBC	9.6 kcal/mol
Open_1	11.7 kcal/mol
Open_2	9.5 kcal/mol
Open_3 (intermediate **A**)	-0.03 kcal/mol

Table S1. Total energy differences

Optimized geometries of molecules

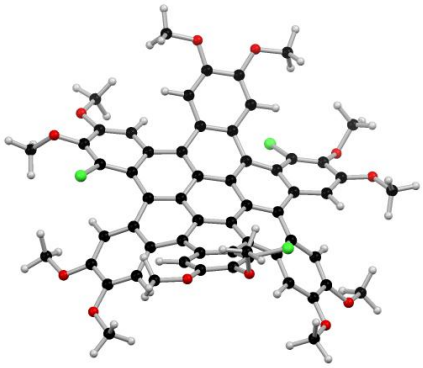

1-9-peak (butterfly)

total energy: -4596.72092992774 hartrees

angstroms

atom	x	y	z
C1	0.0804698121	-0.0543092444	0.0375683433
C2	0.0871956223	-0.0552664086	1.4570227615

C3	1.3280062351	0.0824995414	2.1438525183
C4	2.4936780809	0.3065304972	1.3573248073
C5	2.4649924060	0.3132383975	-0.0222494950
C6	1.2324562265	0.0909021516	-0.7018357999
C7	1.3321515183	0.1548239326	3.5982135571
C8	0.1332596971	0.5387943518	4.2295309785
C9	-1.0973805564	0.5630673613	3.4883633266
C10	-1.1514564715	0.0214720270	2.1936817077
C11	-2.2476952828	1.2145631014	4.0455061234
C12	-3.3761294730	1.4212357367	3.2383422876
C13	-3.5728230474	0.5166897616	2.1218225617
C14	-2.4706986856	-0.2658617834	1.6528005456
C15	-2.7816121564	-1.3487421430	0.7799406135
C16	-4.0572505168	-1.5614907746	0.2699868816
C17	-5.1148449888	-0.7127175445	0.6867798736
C18	-4.8742253935	0.2754928926	1.6215777251
C19	0.0941965690	0.8262336439	5.6372328775

C20	-1.1132560249	1.3479820938	6.2351070397
C21	-2.2279699402	1.6911535438	5.3985712885
C22	-3.3285619215	2.4171563934	5.9023312596
C23	-4.1893013076	3.0459540036	4.9128159278
C24	-4.2462451297	2.5177974483	3.5932301940
C25	-4.8493334511	4.2732187709	5.1730691481
C26	-5.5876734652	4.9302457059	4.2127203614
C27	-5.6792109423	4.3776798057	2.9010960519
C28	-5.0134105424	3.2044842722	2.6132913477
C29	-1.1557868583	1.6349003331	7.6095942746
C30	-2.2529565412	2.4218701949	8.1300120022
C31	-3.4165851288	2.6440047628	7.3281923886
C32	1.2480064019	0.6655639889	6.4288994029
C33	1.0416183310	0.5179905801	7.8604054471
C34	-0.1599100745	0.9938672544	8.4508604113
C35	-4.5883783948	3.0579203609	8.0492932736
C36	-4.5334921977	3.5539823363	9.3416976083

C37	-3.2686422641	3.6348807584	9.9906022536
C38	-2.1774544343	3.0209531720	9.4164704888
C39	2.5162730091	0.4455423927	5.7678831890
C40	2.5208565720	-0.0072864745	4.4108868425
C41	-0.4253249403	0.6527936709	9.8066066398
C42	0.4556470314	-0.0881642360	10.5654422057
C43	1.6679336100	-0.5487513796	9.9763061772
C44	1.9223467166	-0.2628559763	8.6530459127
C45	3.8074434457	0.6587699493	6.3562500744
C46	4.9714243313	0.1483577913	5.8064846193
C47	4.8783664546	-0.6200448361	4.6118896625
C48	3.6920593947	-0.6391731710	3.9111904803
O49	-6.3974806462	5.1156202849	2.0115256447
H50	-4.9991356884	2.8403470829	1.5966638413
H51	-5.6986046818	0.8367714044	2.0364995170
O52	-6.3358185909	-1.0070810297	0.1554201661
O53	-4.2913519187	-2.5701117184	-0.6189810953

Cl54	-1.6119035824	-2.6177621200	0.4337543193
O55	1.3017589801	0.1025383806	-2.0589173788
O56	3.5306468469	0.5639214613	-0.8315090462
O57	-3.2758816285	4.2786996451	11.1910386598
H58	-1.2279547725	3.0136512488	9.9310839344
H59	-1.3813160620	0.9152258962	10.2314792223
O60	0.2516954842	-0.4798410090	11.8531226399
O61	2.4614415907	-1.2957631128	10.7906871770
H62	2.7972835972	-0.6884816135	8.1864718072
O63	6.1983080871	0.4449002387	6.3296111433
O64	6.0336433561	-1.2339225814	4.2319368221
O65	-6.2301756924	6.1171046563	4.3877196450
H66	-4.7316229081	4.7272250370	6.1451498316
O67	-5.6699667621	3.8682086583	10.0331772237
Cl68	-6.2052537193	2.7653678796	7.4191044786
H69	3.6324405194	-1.1668598835	2.9721423788
Cl70	4.0204540316	1.7589527444	7.7129174088

H71	3.4178090970	0.5533536090	1.8549248018
H72	-0.8691473645	-0.1142109969	-0.4729672688
C73	-2.0421550676	4.4133672153	11.8828787078
H74	-2.2632934013	4.9923280463	12.7805035773
H75	-1.6341868152	3.4374565435	12.1743712849
H76	-1.2971373727	4.9456539726	11.2785588298
C77	-5.9712446676	5.2645458000	10.1189604783
H78	-6.9011805120	5.3394369230	10.6857921713
H79	-5.1784801608	5.8090055333	10.6407776717
H80	-6.1213258590	5.6951427652	9.1208904545
C81	-6.1838687669	6.7146541712	5.6733427591
H82	-6.7842920724	7.6229415388	5.6026485775
H83	-6.6102062473	6.0538822437	6.4388615805
H84	-5.1580959449	6.9819633756	5.9591025965
C85	-6.4675215377	4.6601821025	0.6717046927
H86	-7.0824310894	5.3871982171	0.1390429122
H87	-5.4747059087	4.6141478386	0.2058757513

H88	-6.9382790848	3.6700363767	0.6041982686
C89	-7.4556309650	-0.2531792798	0.5981037557
H90	-8.3138692960	-0.6408110576	0.0475039219
H91	-7.6275909822	-0.3769381048	1.6746010138
H92	-7.3345127565	0.8145866944	0.3760294402
C93	-5.0098997010	-3.7021513216	-0.1088729031
H94	-5.0922456915	-4.4040666092	-0.9406537270
H95	-4.4570740341	-4.1745412979	0.7107486537
H96	-6.0094597980	-3.4153773845	0.2294613601
C97	0.1066292552	-0.1518075199	-2.7838517201
H98	0.3943265065	-0.1721996707	-3.8358798090
H99	-0.3350050444	-1.1161183127	-2.5048247619
H100	-0.6365381023	0.6407740496	-2.6287758606
C101	4.7627752505	0.9134124242	-0.2265407864
H102	5.4571240925	1.1029990085	-1.0464706328
H103	4.6718084241	1.8171633614	0.3894544476
H104	5.1553743902	0.0978689305	0.3957982573

C105	6.0029144868	-2.0557855984	3.0737850274
H106	7.0008517379	-2.4871951542	2.9853440557
H107	5.2634215919	-2.8604668349	3.1701923228
H108	5.7810059401	-1.4733957217	2.1709055571
C109	6.7910167519	-0.5789024133	7.1343626897
H110	7.7500895213	-0.1815043297	7.4719567049
H111	6.1660935174	-0.8020464623	8.0082262056
H112	6.9556513198	-1.4919583043	6.5543525503
C113	3.6972262610	-1.7595960493	10.2718525133
H114	4.1914108817	-2.2783671072	11.0948294280
H115	3.5505474653	-2.4611674153	9.4403032965
H116	4.3274584480	-0.9271585709	9.9335970042
C117	-0.9728181481	-0.1287014184	12.4732750712
H118	-0.9282662122	-0.5431710646	13.4815983416
H119	-1.0975618844	0.9607706168	12.5366592556

H120	-1.8346920472	-0.5541743003	11.9436728064

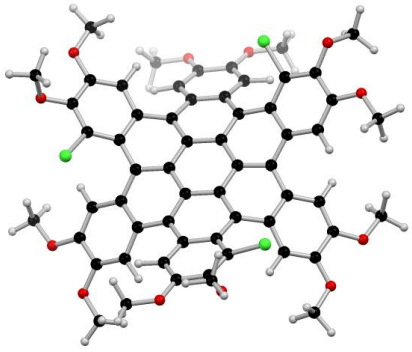

1-3-peak (up-down)

total energy: -4596.73618100742 hartrees

angstroms

atom	x	y	z
C1	-0.0718522150	0.1210024932	-0.1150761020
C2	-0.1184065173	0.0302192371	1.3095765878
C3	1.1394264196	-0.0780625866	1.9855650447
C4	2.3349342361	-0.1922386273	1.2369797211
C5	2.3270087413	-0.2031705585	-0.1428261237
C6	1.1049554404	-0.0264606009	-0.8403034803
C7	1.2007135242	0.1107665443	3.4252364807
C8	0.1121232471	0.7504210479	4.0432545569
C9	-1.1697219636	0.7542041263	3.3921652085

C10	-1.3207960993	0.1822474711	2.1147908401
C11	-2.3147058212	1.2832777125	4.0773267304
C12	-2.1689192891	1.8716344413	5.3820955753
C13	-0.8904365894	1.8573830305	6.0349315323
C14	0.2580984624	1.3263456563	5.3507986440
C15	-3.2901792545	2.3934934902	6.0528326824
C16	-3.2367705073	2.4366662444	7.4953775867
C17	-1.9795148696	2.3560851352	8.1598785986
C18	-0.7697237876	2.2809543322	7.3706185553
C19	-4.4235549994	2.3920044525	8.2721321516
C20	-4.3975311051	2.2959415131	9.6449551936
C21	-3.1401602826	2.1868643801	10.3119265044
C22	-1.9734327631	2.2131848880	9.5758857499
C23	1.5124029457	1.3059852592	5.9866423531
C24	1.7080446071	2.2068872122	7.1102675815
C25	0.5582313092	2.6301673888	7.8507710646
C26	-3.5961552394	1.1556843486	3.5155960596

C27	-4.6389166563	2.0411261965	4.0062501712
C28	-4.4524195086	2.7314273131	5.2465544324
C29	2.3091911253	-0.2908280054	4.2642174824
C30	2.4646051107	0.3149780157	5.5433294329
C31	0.7179455551	3.5108800838	8.9476791317
C32	1.9611416910	3.9738836299	9.3322733781
C33	3.1050534737	3.6400934128	8.5646632140
C34	2.9523640343	2.8147268479	7.4571879926
C35	-2.6359945246	-0.3028938525	1.7619135439
C36	-3.7748359975	0.1661172988	2.4766650149
C37	-5.3621157088	3.7943035804	5.5272804739
C38	-6.4775000594	4.0586205756	4.7405713001
C39	-6.6827088405	3.2998561352	3.5604569034
C40	-5.7561318468	2.3449143209	3.1920675737
C41	3.4609570567	-0.1843702309	6.4218792571
C42	4.2964395572	-1.2197357335	6.0675674117
C43	4.1380542896	-1.8366118118	4.7907369229

C44	3.1700130542	-1.3722968572	3.9245159376
C45	-2.8057129248	-1.3624990339	0.8324596393
C46	-4.0338830151	-1.9395766499	0.5958320344
C47	-5.1719849344	-1.4873166355	1.3284410760
C48	-5.0288999883	-0.4627632350	2.2405676049
Cl49	4.3559945959	2.7318697791	6.3974809631
O50	4.3342923943	4.1229942380	8.9086113420
O51	2.1956953242	4.8124278965	10.3819270054
H52	-0.1640176864	3.8755867973	9.4506423012
H53	-1.9312633008	-1.7535391096	0.3339685234
O54	-4.2702575016	-2.9645669021	-0.2671019755
O55	-6.3268142921	-2.1634033816	1.0780149557
H56	-5.8743317229	-0.1757366291	2.8480890522
H57	3.5334658736	0.2403019435	7.4128107781
O58	5.2625675130	-1.7591214944	6.8570500142
O59	4.9625631484	-2.8945105596	4.5578675517
H60	3.0016169947	-1.8966561495	2.9957813262

H61	-5.8411392959	1.8634500778	2.2301903033
O62	-7.7843679213	3.6455246086	2.8349713563
O63	-7.3636537855	5.0344131412	5.0943194830
Cl64	-5.0417788770	4.9866449417	6.7835383385
H65	3.2761075738	-0.1892632008	1.7642981613
O66	3.4334087849	-0.2926788345	-0.9332993684
O67	1.1191912786	0.1517697811	-2.1949954054
Cl68	-1.4615432243	0.6422561723	-1.0593954282
H69	-5.3744091078	2.3943972584	7.7607617612
O70	-5.4891532470	2.2511048644	10.4534562141
O71	-3.2178260009	2.0218037625	11.6606722457
H72	-1.0298818494	2.0497352768	10.0760299002
C73	-6.7657127893	2.4159450407	9.8520058976
H74	-7.4837596974	2.4217535036	10.6732551278
H75	-6.8309107491	3.3616411661	9.3006143213
H76	-7.0026137793	1.5872142598	9.1725670965
C77	-2.0125035603	1.8375819882	12.3813913298

H78	-2.3021495137	1.7211573763	13.4268747003
H79	-1.4744908925	0.9395107441	12.0516196994
H80	-1.3462706298	2.7058685263	12.2860063687
C81	1.0829515816	5.2632166591	11.1406771751
H82	1.4936378847	5.9043185583	11.9220001511
H83	0.3807985214	5.8413796041	10.5272420463
H84	0.5466827767	4.4254272071	11.6041297493
C85	4.5613985685	5.5158206240	8.6523761247
H86	5.5852026482	5.7155415272	8.9739438111
H87	4.4689351934	5.7329572259	7.5824324518
H88	3.8690067374	6.1404401373	9.2235507169
C89	5.4823871143	-1.1700313669	8.1308422319
H90	6.3201499963	-1.7133703736	8.5701777835
H91	5.7398016099	-0.1074980558	8.0437499536
H92	4.6041634091	-1.2746159032	8.7808190838
C93	4.7872983030	-3.6256200850	3.3575354766
H94	5.5232097854	-4.4307551072	3.3856855397

H95	3.7800021744	-4.0565009514	3.2884626668
H96	4.9685581055	-3.0021383254	2.4714312344
C97	4.7044356263	-0.3417276206	-0.3010354824
H98	5.4372493283	-0.4021410840	-1.1068040581
H99	4.8928305633	0.5596627199	0.2945723553
H100	4.8015442579	-1.2240187957	0.3449406287
C101	1.2934785235	-1.0411814855	-2.9650788360
H102	1.2746018988	-0.7311432472	-4.0115587183
H103	2.2515988299	-1.5207625975	-2.7426600590
H104	0.4740192123	-1.7478118788	-2.7826220263
C105	-3.1795471903	-3.4496808331	-1.0337104202
H106	-3.5913884386	-4.2238093199	-1.6829474437
H107	-2.7346001088	-2.6561009919	-1.6469789995
H108	-2.4014996513	-3.8896050787	-0.3962468624
C109	-7.4767876635	-1.8195628262	1.8307933288
H110	-8.2721555557	-2.4808924948	1.4836890559
H111	-7.3198019607	-1.9737965805	2.9061350718

H112	-7.7754653528	-0.7760448869	1.6615872176
C113	-8.0023874069	2.9872924803	1.5954576615
H114	-8.9281972788	3.4028384540	1.1951156165
H115	-7.1843697533	3.1725872155	0.8882538557
H116	-8.1196742248	1.9046005245	1.7307647850
C117	-7.3212120951	6.2353065398	4.3111162630
H118	-8.0735895950	6.8993827229	4.7405529132
H119	-6.3361607418	6.7098391724	4.3823212875
H120	-7.5651736092	6.0325438264	3.2645172753

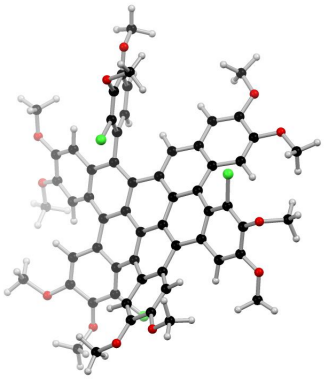

1_9peak_open_1

total energy: -4597.900976795831 hartrees

angstroms

atom	x	y	z
C1	0.0111120066	0.5066431928	0.0036699182
C2	-0.0770702105	0.4766935511	1.4221837990

C3	1.1074481476	0.7492828348	2.1586358364
C4	2.1144063659	1.5143630094	1.4912507144
C5	2.1185882783	1.6961535643	0.1173274027
C6	1.1018939062	1.0547039151	-0.6420736424
C7	-1.2997217544	0.1576244620	2.1511914058
C8	-1.2308110063	-0.0939154748	3.5470946969
C9	0.0546691286	-0.1124042937	4.2117572952
C10	1.2236968209	0.1919195287	3.4900564207
C11	-2.4198880689	-0.4035390421	4.3052341947
C12	-3.6004556603	-0.6966689674	3.6083224360
C13	-3.6883867023	-0.4314573190	2.2027136310
C14	-2.5944333796	0.1678862766	1.5170313964
C15	-2.8822396279	0.8077839273	0.2718893892
C16	-4.1045244649	0.6931295778	-0.3506037561
C17	-5.1087523799	-0.1473374564	0.2247462427
C18	-4.8991004679	-0.6623614974	1.4799686022
C19	0.1621271889	-0.4172119622	5.6231615396

C20	-1.0327947500	-0.4638884593	6.4277850957
C21	-2.3175595036	-0.3725917625	5.7827016811
C22	-3.4274190768	-0.1862212487	6.5855364932
C23	-5.9611558663	-0.2821354075	4.3372720644
C24	-4.8749469026	-1.1647407421	4.2485042159
C25	-0.9424788538	-0.5370801007	7.8467048948
C26	-2.0895068507	-0.1476473509	8.6355902225
C27	-3.3424745735	-0.0128126523	7.9806565254
C28	-5.0803738207	-2.4724803228	4.7219026276
C29	-6.2994218019	-2.8773240842	5.2829681458
C30	-7.3605313080	-1.9500203288	5.3761325430
C31	-7.1837917238	-0.6494612173	4.8973442322
C32	2.4854525570	-0.2983707576	4.0074542108
C33	2.5829272852	-0.6724893883	5.3720500834
C34	1.4283057075	-0.4969625848	6.2317083163
C35	1.5239370845	-0.5459137502	7.6777783713
C36	0.3551593970	-0.8116939377	8.4442599135

C37	-4.5008633849	0.3805824708	8.7101615400
C38	-4.4243049793	0.7082574287	10.0408949128
C39	-3.1440227713	0.6800027374	10.6861284198
C40	-2.0256741584	0.2668815196	9.9963343952
C41	0.5903103959	-1.3280835751	9.7601702513
C42	1.8192565829	-1.2157248544	10.3949808845
C43	2.8854343768	-0.5775295538	9.7032044819
C44	2.7492997531	-0.3140316508	8.3566832650
C45	3.7506366464	-1.3688917648	5.7966337468
C46	4.7888654774	-1.6583751703	4.9380077904
C47	4.7026034585	-1.2510963924	3.5749301505
C48	3.5669717584	-0.6082650397	3.1377544425
O49	-4.4763405077	1.3310239167	-1.4940323972
C50	-3.6063673122	2.3152393266	-2.0248479217
O51	-6.2328906244	-0.3089124791	-0.5218089080
C52	-7.2733376853	-1.1108577032	0.0165269298
Cl53	-3.8005937778	-3.6625750667	4.6153786957

O54	-6.4858156426	-4.1730808569	5.6699843788
C55	-6.4334419684	-4.4014083727	7.0848508268
O56	-8.5063355736	-2.4274863072	5.9389867276
C57	-9.6171582870	-1.5490278472	6.0397955975
O58	-3.1548999480	1.1045162177	11.9792329289
C59	-1.9350213999	1.0733652846	12.7019275606
O60	-5.4605269943	1.1069815366	10.8272069435
C61	-6.7414216518	1.1994584998	10.2285393583
Cl62	-0.6013108016	-2.3405843573	10.5699468035
O63	2.0442407096	-1.7928645611	11.6138910506
C64	2.0499398876	-0.8986025003	12.7301745784
O65	4.0060880015	-0.3485676267	10.4456121590
C66	5.1033904969	0.2940244739	9.8130520387
O67	5.9050988034	-2.3676326617	5.2607153916
C68	5.9879777361	-2.9292930905	6.5590191885
O69	5.7617779284	-1.6029444151	2.7957189965
C70	5.7338090935	-1.2286014122	1.4288993030

Cl71	3.3223802186	2.4066396193	2.4046474163
O72	3.0171583698	2.5252326135	-0.4924777618
C73	4.1013023291	1.8856148661	-1.1731013513
O74	1.2799226204	1.0946720748	-1.9942069212
C75	0.3440522967	0.4103501109	-2.8133729284
H76	-5.4417563994	0.4423398046	8.1758575851
H77	-7.9868001687	0.0758608824	4.9491127500
H78	3.5801792171	0.0896513600	7.7987938523
H79	3.7853355894	-1.7639159310	6.7992251678
H80	3.4679706362	-0.3876843519	2.0867506833
H81	-1.0683413936	0.3035078244	10.4918243558
H82	-0.7838652186	0.0699374122	-0.5785922380
H83	-2.1440803392	1.4643925641	-0.1591438700
H84	-5.6838049176	-1.2287447052	1.9564860125
H85	5.8638657727	0.4189295966	10.5850592832
H86	5.5137903131	-0.3153346974	8.9980485113
H87	4.8208869785	1.2768337679	9.4156188704

H88	2.2222370531	-1.5176286952	13.6127853869
H89	2.8491696473	-0.1569723750	12.6397182366
H90	1.0830035427	-0.3894769140	12.8303317388
H91	-2.1767918821	1.4101926571	13.7111739058
H92	-1.5201125038	0.0585670555	12.7438240782
H93	-1.1889816871	1.7504087105	12.2654222347
H94	-7.4195870875	1.5282203274	11.0177517293
H95	-6.7531937327	1.9325076544	9.4110627325
H96	-7.0779431849	0.2285734797	9.8412898738
H97	-10.4158126933	-2.1286473200	6.5047403668
H98	-9.3899930689	-0.6775856105	6.6674755336
H99	-9.9492033071	-1.2029677167	5.0528951390
H100	-6.5542461763	-5.4775115231	7.2212161686
H101	-5.4666381681	-4.0891589392	7.4954153676
H102	-7.2439553703	-3.8739513409	7.5975566068
H103	-8.0629350489	-1.1218147564	-0.7363554094
H104	-6.9347992184	-2.1374708440	0.2052581993

H105	-7.6662780008	-0.6886291986	0.9503677914
H106	-4.1316467116	2.7543550757	-2.8743101142
H107	-3.3833590524	3.0980845181	-1.2887988212
H108	-2.6618194177	1.8787788087	-2.3752719047
H109	0.7083421152	0.5135698639	-3.8364294085
H110	0.2811355923	-0.6535234677	-2.5529409387
H111	-0.6565399119	0.8543477344	-2.7423297281
H112	4.7104791990	2.6888741443	-1.5917834726
H113	4.7108704070	1.2996215535	-0.4743986753
H114	3.7377826267	1.2416057823	-1.9789538443
H115	6.6803212472	-1.5685024248	1.0053796350
H116	4.9053111184	-1.7097221762	0.8927139650
H117	5.6521890025	-0.1401019906	1.3134154481
H118	6.9300926388	-3.4788074077	6.5887579787
H119	5.9984204677	-2.1548184305	7.3376835857
H120	5.1579554347	-3.6194273210	6.7567844764
H121	-4.4021111979	-0.0638909776	6.1468194879

H122	-5.8344391131	0.7297052689	3.9675530998

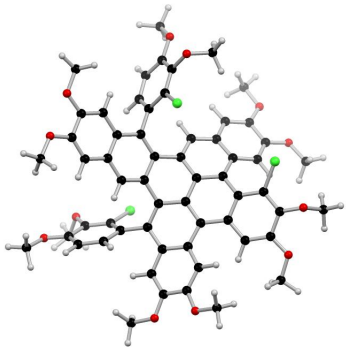

1_9peak_open_2

total energy: -4599.100136840010 hartrees

angstroms

atom	x	y	z
C1	0.0633670945	0.4706378496	0.1074931334
C2	0.0976943229	0.5600139152	1.5263794762
C3	1.2726105343	0.1928946968	2.1992423496
C4	2.4111720500	-0.2299537688	1.5316181623
C5	2.4194818551	-0.2641675930	0.0980567851
C6	1.2339335082	0.0483047109	-0.5943427178
C7	3.7275275716	-0.5101542517	-0.5466799972
C8	4.9271970822	-0.2147151116	0.2050573242
C9	4.8970579694	-0.1898215170	1.6517814924

C10	3.6462216958	-0.5032384882	2.2904949016
C11	6.0840899826	-0.0545769918	2.4107348044
C12	5.9779480091	-0.1961529471	3.8481995335
C13	4.8411361848	-0.8780446918	4.3796546263
C14	3.6576036440	-1.0265349457	3.5826231162
C15	-1.1335765098	0.8769410987	-0.5571518597
C16	-2.2162272831	1.3572177630	0.1403676003
C17	-2.1723161968	1.4433942161	1.5754097821
C18	-1.0381606338	1.0463423134	2.2371742865
C19	6.1655655791	-0.1011313658	-0.4621572393
C20	7.2915413798	0.4287152786	0.2902869393
C21	7.3305503226	0.2354728478	1.7031400088
C22	4.8763619091	-1.3032474279	5.7408864145
C23	5.8675173224	-0.9003544499	6.6033097395
C24	6.8533059507	0.0211040750	6.1359396162
C25	6.9110265460	0.3284734660	4.7929450246
C26	8.3927208994	1.1259171189	-0.2936691225

C27	9.5933683793	1.3145128005	0.3733782289
C28	9.7219722465	0.7703604455	1.6772366550
C29	8.6028793242	0.2971720514	2.3354682288
C30	3.8726582095	-0.9487517370	-1.8461222888
C31	0.5104924529	-1.1539209850	-2.6639814374
C32	1.0938673240	-0.0224609429	-2.0852305833
C33	5.1359270335	-1.1082262660	-2.4570471610
C34	6.3080575511	-0.6789215670	-1.7785670665
C35	1.4580231873	1.0247951665	-2.9506439551
C36	1.2845722206	0.9346262988	-4.3364824640
C37	0.7135700461	-0.2351532535	-4.8862755810
C38	0.3229287186	-1.2763806681	-4.0419735645
C39	5.2335786975	-1.7295753784	-3.7332470826
C40	6.4543599753	-1.9819262545	-4.3109717852
C41	7.6451416078	-1.6297977463	-3.5970646820
C42	7.5598647498	-1.0027041284	-2.3740938163
C43	2.4544667122	-1.6789386096	4.1941686726

C44	1.9147614786	-2.8896474503	3.7146485813
C45	0.7697167869	-3.4707974214	4.2746341430
C46	0.1437335828	-2.8451379592	5.3740142834
C47	0.6833344464	-1.6669481554	5.8912844744
C48	1.8160161447	-1.1074890660	5.3019454091
O49	-0.9687673679	-3.4719004392	5.8523232904
C50	-1.6714509995	-2.8586191999	6.9227686271
O51	0.2273688667	-4.5949408428	3.7201059086
C52	0.4044643185	-5.8026898969	4.4685308180
Cl53	2.6701654741	-3.7391658278	2.3811848439
O54	5.9720462885	-1.2538424910	7.9134257504
C55	5.0109671253	-2.1586579088	8.4315061455
O56	7.6644500469	0.5310347882	7.1036413928
C57	8.5722561804	1.5568610060	6.7436414386
O58	10.9828927721	0.8210640250	2.1979543688
C59	11.2021338816	0.2584592528	3.4807691468
O60	10.6003220521	2.0684887426	-0.1618141616

C61	11.6818368578	1.3335164681	-0.7410849801
O62	-3.3006669050	1.9363358559	2.1548315642
C63	-3.2988449261	2.0975723939	3.5626147950
O64	-3.3793728785	1.7898576956	-0.4159517099
C65	-3.4739890019	1.7958158188	-1.8317929933
Cl66	2.1554650654	2.4958297867	-2.3062790396
O67	1.5990965439	1.9883704491	-5.1468321188
C68	2.8404840515	1.8608679043	-5.8526108037
Cl69	8.2243356925	1.9553010331	-1.8364976297
O70	8.8036553113	-1.9825042925	-4.2206192076
C71	10.0276869932	-1.6311313843	-3.5982583293
O72	6.6569301562	-2.5792559341	-5.5170678823
C73	5.5139323771	-2.9877593232	-6.2481058991
O74	0.5864918589	-0.2357363057	-6.2442064773
C75	-0.0245433197	-1.3618845428	-6.8549633718
H76	1.2888615436	0.2965604851	3.2739963593
H77	2.2096898423	-0.1791917072	5.7023181551

H78	9.0579661267	1.8683127274	7.6696911783
H79	9.3365700072	1.1950874244	6.0432148601
H80	8.0573139319	2.4160794679	6.2952018482
H81	5.2884156897	-2.3267134136	9.4733996176
H82	3.9966736276	-1.7408917987	8.3888089695
H83	-0.0608149112	-6.5938544190	3.8777006936
H84	1.4693304395	-6.0278820406	4.5992674661
H85	-0.0859191681	-5.7391077468	5.4446910879
H86	8.7059985533	-0.0715443140	3.3421952096
H87	7.6436874915	1.0451345689	4.4586417530
H88	4.0743141082	-1.9281449833	6.1048964765
H89	12.2732117760	0.3460495404	3.6692038984
H90	10.6554947595	0.8061009582	4.2588367931
H91	10.9108358694	-0.7989137654	3.5160851508
H92	5.0244107524	-3.1144062874	7.8919057911
H93	-1.0535780992	-2.7878209019	7.8272410122
H94	-2.5304405632	-3.5003181236	7.1236635184

H95	-2.0246704712	-1.8562496793	6.6501188514
H96	3.6752619353	1.7261869327	-5.1555533726
H97	0.2232072365	-1.1707310436	6.7373495253
H98	-0.9788754011	1.1020140821	3.3178247780
H99	-2.5052015279	2.7826283793	3.8887600826
H100	-3.1746088034	1.1369428987	4.0799323809
H101	-4.2709382233	2.5220892905	3.8186215767
H102	12.3814612915	2.0773590703	-1.1273797502
H103	12.1830544302	0.7116455880	0.0068437915
H104	11.3309404327	0.7057055289	-1.5697895226
H105	8.4695138837	-0.7856602769	-1.8366011230
H106	10.1073047030	-0.5458809511	-3.4548207004
H107	10.8152586239	-1.9670200313	-4.2749302542
H108	10.1479381342	-2.1316065619	-2.6283698620
H109	5.8901614131	-3.4379468221	-7.1682542709
H110	4.9247039736	-3.7308799279	-5.6947721654
H111	4.8677643507	-2.1358875802	-6.4981976453

H112	-0.1280928021	-2.1763705420	-4.4420842896
H113	4.3153895973	-2.0206983840	-4.2299802408
H114	-1.0525836562	-1.5055500909	-6.4991698091
H115	0.5476114468	-2.2816845209	-6.6766482709
H116	-0.0407278062	-1.1500632664	-7.9250875060
H117	2.8058127794	1.0241582203	-6.5582244298
H118	2.9738117908	2.7950060647	-6.4013585706
H119	-1.1744957040	0.8257490187	-1.6347853883
H120	-3.3866664842	0.7834113402	-2.2467563816
H121	-4.4613437889	2.1979731195	-2.0639734181
H122	-2.7040713019	2.4338359781	-2.2837047405
H123	3.0102641724	-1.2485185969	-2.4185464430
H124	0.2093040617	-1.9684282179	-2.0124233900

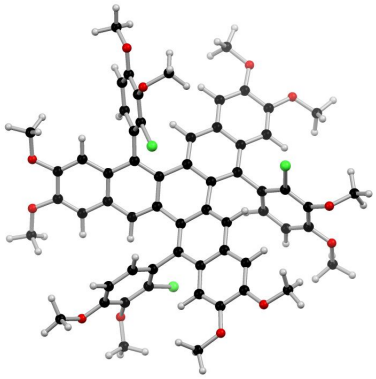

1_9peak_open_3

total energy: -4600.304231015938 hartrees

angstroms

atom	x	y	z
C1	-0.0845249579	-0.6607700180	0.0774577621
C2	-0.0434107489	-0.4974426181	1.4618776712
C3	1.1536259824	-0.3227340635	2.1623089411
C4	2.3336179460	-0.2925251579	1.3946879174
C5	2.3296198076	-0.4602613009	0.0052267319
C6	1.0993155887	-0.6496639135	-0.6599369445
C7	1.1073570442	-0.1081152709	3.6492415328
C8	0.7981884286	-1.1410288656	4.5523048576
C9	0.5309843386	-0.8374287718	5.9293539644
C10	0.6589758587	0.4765462491	6.3528687928
C11	1.0218154931	1.5209719666	5.4854126905
C12	1.2248111476	1.2412432620	4.1043516782
C13	-0.0906208220	-1.8684333059	6.7946493131
C14	-0.7968904361	-2.9337133145	6.1161049308
C15	-0.2880439906	-3.3984336573	4.7993339073

C16	0.6639410171	-2.5485624994	4.1343720696
C17	-0.5206986666	-4.6825669182	4.2629074522
C18	0.2259583140	-5.1576545558	3.1377813702
C19	1.2610154892	-4.3472399975	2.5968757368
C20	1.4531844275	-3.0602030050	3.1223358407
C21	0.1787766392	0.1502299430	9.7727642110
C22	0.7191312552	-0.9008535223	9.0216668865
C23	-0.1724134611	-1.7785185205	8.1964906368
C24	-1.1321768457	-2.5594510847	8.9166216175
C25	-2.0507602556	-3.3559572298	8.1761996399
C26	-1.8366946155	-3.5452339517	6.7985408717
C27	1.1070937119	2.8637278612	5.9578175541
C28	1.3698549129	3.9029015391	5.1015201921
C29	1.5574452403	3.6306616009	3.7025120634
C30	1.4818584956	2.3410815066	3.2322448380
C31	2.1013836076	-1.1348333815	9.1680487894
C32	2.9018286135	-0.3613592436	10.0184841992

C33	2.3167042099	0.6940368421	10.7498207013
C34	0.9507507531	0.9474817641	10.6172564045
C35	-3.1100769484	-4.0328027596	8.8455229074
C36	-3.2360392314	-3.9783808669	10.2111150520
C37	-2.2627307075	-3.2481176229	10.9750232032
C38	-1.2499426442	-2.5663820931	10.3400206133
C39	2.0640973708	-4.8298058191	1.5243944981
C40	1.8440324910	-6.0687959467	0.9775559553
C41	0.7897110483	-6.8910647720	1.5062450018
C42	0.0171507876	-6.4440150769	2.5523778216
C43	-1.4770777405	-5.6785589985	4.8502242809
C44	-2.8136843398	-5.7982148187	4.4235294295
C45	-3.6904326074	-6.7448002669	4.9674308936
C46	-3.2130238742	-7.6310857418	5.9581095594
C47	-1.8810894710	-7.5538906120	6.3673400050
C48	-1.0372192787	-6.5913688219	5.8121890495
Cl49	-3.4479002240	-4.7109789994	3.2007007319

O50	2.5401124043	-6.6171648297	-0.0541372233
C51	3.5881880995	-5.8451330062	-0.6205934012
O52	0.6516251195	-8.0955511114	0.8865380637
C53	-0.3757396531	-8.9596485582	1.3409480623
O54	-5.0070462628	-6.7589540714	4.5999977214
C55	-5.4011117327	-7.8444776539	3.7540375790
O56	-4.1324310518	-8.5160739817	6.4420370927
C57	-3.7159583791	-9.4220159294	7.4541125140
O58	-4.2108830055	-4.5821569230	10.9448831978
C59	-5.2154842938	-5.2931749453	10.2405455069
O60	-2.4468758910	-3.3043941419	12.3227861226
C61	-1.5102539685	-2.6331728702	13.1487420763
Cl62	2.8833722984	-2.4460096776	8.3081870413
O63	4.2185756505	-0.6738428385	10.2041441794
C64	5.1501256957	0.1857125469	9.5360213202
O65	3.1687795911	1.3915535415	11.5546238353
C66	2.6263749275	2.4280069746	12.3586305748

O67	1.4641016405	5.2159840060	5.4483125530
C68	1.2542461542	5.5524945780	6.8087773954
O69	1.7962195436	4.7332081061	2.9409550865
C70	1.9797850254	4.5485214520	1.5474074731
Cl71	3.8930167469	-0.1054392152	2.1823892733
O72	3.5080862314	-0.5243996585	-0.6870714581
C73	3.8203681962	0.6301909071	-1.4725427323
O74	1.1851628128	-0.8143298432	-2.0115690676
C75	-0.0144807571	-1.0734979626	-2.7271203192
H76	2.8435772978	-4.1828692577	1.1395235708
H77	-0.7675028944	-7.0753558823	2.9436481140
H78	4.0106696589	-6.4542441735	-1.4212653046
H79	3.2145811350	-4.9015055757	-1.0382979454
H80	4.3689202957	-5.6220347207	0.1178394059
H81	-0.3174648168	-9.8509240173	0.7138865373
H82	-1.3671955824	-8.5010827973	1.2311753089
H83	-0.2303789654	-9.2436531362	2.3914410240

H84	-0.0071788158	-6.5309653209	6.1482536907
H85	-4.8378355566	-7.8305945733	2.8133363353
H86	-6.4606155512	-7.6915442650	3.5402358536
H87	-5.2643120444	-8.8071002238	4.2560204284
H88	-3.3721176371	-8.8932597876	8.3518538857
H89	-4.5951899840	-10.0186611659	7.7015938636
H90	-1.4945775138	-8.2271501712	7.1227550947
H91	-2.9161851933	-10.0852239214	7.1008030641
H92	-2.4960811033	-4.2285082154	6.2908615041
H93	-3.8039362405	-4.6111927679	8.2467327949
H94	-0.5282120889	-2.0193313729	10.9286650742
H95	-1.4981815014	-1.5532231921	12.9518652899
H96	-0.4957161750	-3.0297493859	13.0141621913
H97	-1.8354030389	-2.8099401974	14.1753709929
H98	-5.7607345150	-4.6405122485	9.5466955807
H99	-4.7956195066	-6.1363267453	9.6763425829
H100	-5.9031794185	-5.6723810572	10.9982364595

H101	0.4787908887	1.7505771002	11.1706153324
H102	2.1895154749	3.2297404368	11.7491955681
H103	1.8627159411	2.0459360156	13.0479222882
H104	3.4617269393	2.8291895227	12.9343196772
H105	5.0764908957	1.2117296617	9.9101553975
H106	6.1416640318	-0.2131011624	9.7581019815
H107	4.9873759522	0.1710031875	8.4523457567
H108	1.6159968109	2.1498793221	2.1780354379
H109	2.8454524816	3.9076373944	1.3358394519
H110	1.0891837004	4.1110749429	1.0776208401
H111	2.1553829273	5.5430499694	1.1338694476
H112	1.3627106998	6.6365750658	6.8712839133
H113	0.2481889520	5.2680518017	7.1444890151
H114	1.9956756232	5.0749072430	7.4628513008
H115	-1.0398925989	-0.8055087489	-0.4119748264
H116	3.0728841859	0.7897524050	-2.2556993186
H117	4.7921563812	0.4330591908	-1.9292506395

H118	3.8945450902	1.5241281503	-0.8411130643
H119	0.2811378720	-1.2022804214	-3.7693452337
H120	-0.5036407775	-1.9891419772	-2.3730019468
H121	-0.7202345653	-0.2363584260	-2.6522442734
H122	0.9473053944	3.0438292598	7.0145838997
H123	2.2532578532	-2.4612290106	2.7129820049
H124	-0.9708473471	-0.5182742420	2.0247407330
H125	0.4181270178	0.7431814590	7.3698758423
H126	-0.8849545412	0.3495093339	9.6860921936

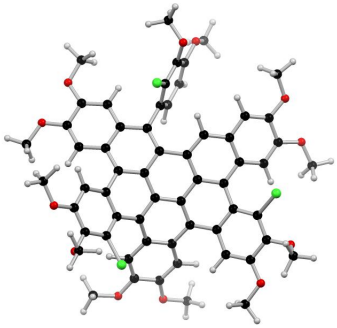

1_3peak_open_1

total energy: -4597.919647985846 hartrees

angstroms

atom	x	y	z
C1	-0.1147778196	0.5489083209	0.1044442014
C2	-0.0713693828	0.2336556337	1.4964555385

C3	1.1986342935	-0.0175406900	2.0907438006
C4	2.3689674293	0.1848593620	1.2989261283
C5	2.3044987919	0.5579808841	-0.0217660394
C6	1.0264322229	0.7015246711	-0.6472941225
C7	-1.2532178493	0.0200980795	2.2772907258
C8	-1.1453920534	-0.6458024540	3.5143190460
C9	0.1300074316	-0.8204005505	4.1614656680
C10	1.2899942879	-0.5071340018	3.4372497864
C11	2.6737563951	-0.8454243838	3.9132288407
C12	3.1214114481	-2.1664530345	3.8236321309
C13	1.2084148512	-1.2682165729	6.3898545145
C14	0.1218865261	-1.3665144672	5.5382070626
C15	4.4069653742	-2.5446600711	4.2111905383
C16	5.2956667319	-1.5908183564	4.7075770132
C17	4.8895072692	-0.2402660358	4.7952559004
C18	3.5962327481	0.1079958536	4.3862507224
C19	-1.0513721849	-2.0362917766	6.0415418642

C20	-1.0529256391	-2.6414489473	7.3221447422
C21	0.2035338783	-2.8192606283	7.9988669521
C22	1.3062771970	-2.0303059810	7.5737461486
C23	-2.2246783463	-2.1239339243	5.2159281121
C24	-2.3121478871	-1.3260098201	4.0276724921
C25	-2.5839061091	0.4747450364	1.8747569224
C26	-3.7331531401	-0.1779377154	2.4110479502
C27	-3.5165199004	-1.3073096339	3.3027108880
C28	-4.3820355164	-2.4533676751	3.4275059956
C29	-4.2343598871	-3.3230594739	4.5430615151
C30	-3.2840828376	-2.9734033968	5.5760842509
C31	-3.4085562613	-3.3588825145	6.9722818085
C32	-2.3358858807	-3.0672218672	7.8730528778
C33	-4.9515284432	-4.5506033914	4.5415252405
C34	-5.8026800111	-4.8965369564	3.5117277162
C35	-5.9847822628	-3.9992958405	2.4163070673
C36	-5.2678978912	-2.8238700937	2.3822598782

C37	-4.6512598700	-3.8130245156	7.4763270631
C38	-4.8632546719	-3.9932780510	8.8282546884
C39	-3.8648840986	-3.5949904238	9.7499896900
C40	-2.6653092424	-3.0851959153	9.2637633661
C41	-4.9955085258	0.4375266007	2.1692177790
C42	-5.1445385112	1.5533813902	1.3509539006
C43	-3.9890422369	2.1583595781	0.8018295502
C44	-2.7396556495	1.6410613920	1.0929046887
C45	0.4303026264	-3.7750297502	9.0253623124
C46	1.6430735372	-3.8651105281	9.6729813722
C47	2.7130116405	-2.9756794095	9.3224555615
C48	2.5367290351	-2.0909355252	8.2861900304
Cl49	3.1196762878	1.7900535992	4.5340480918
O50	6.5651942725	-1.8481501675	5.1349403134
C51	7.0274502951	-3.1912480157	5.0849123632
O52	5.7143466046	0.6991363258	5.3484728235
C53	6.8054144452	1.1283387718	4.5270278200

O54	-6.8463933417	-4.4246545447	1.4532882723
C55	-7.0976527318	-3.5528995364	0.3609735307
O56	-6.4846452364	-6.0710568812	3.4151638166
C57	-6.2711702193	-7.0495589745	4.4168905906
O58	-6.0192216290	-4.4550224452	9.3867697373
C59	-7.0897791056	-4.7947567489	8.5187672349
O60	-4.0835383007	-3.6997506740	11.0942350406
C61	-4.9969689094	-2.7513997586	11.6617211344
Cl62	-1.6852286098	-2.2628451253	10.4746452384
Cl63	-6.4466660968	-0.0457247153	3.0388935375
O64	-6.3831151158	2.0622067868	1.0848041469
C65	-6.7153223431	3.2865290120	1.7537825559
O66	-4.2189037348	3.2773896639	0.0554549064
C67	-3.0985913371	3.9960739093	-0.4386136656
O68	1.9437469735	-4.7539122453	10.6573058666
C69	0.9153696751	-5.6258926639	11.1020507948
O70	3.8515519923	-3.1224565245	10.0532078993

C71	4.9298007593	-2.2446142186	9.7710342930
O72	3.3718783240	0.7778476893	-0.8353457050
C73	4.6689273471	0.6623100958	-0.2727743490
O74	1.0661029456	0.9634239886	-1.9819168726
C75	-0.1629849414	1.0557377307	-2.6808095905
H76	-5.4692774975	-3.9569852349	6.7887351460
H77	3.3338966468	0.0232945836	1.7542057251
H78	-1.0749420871	0.6047908125	-0.3841825451
H79	-0.3688684237	-4.4495991776	9.2961183494
H80	3.3479555785	-1.4514607534	7.9606590835
H81	-1.8572782107	2.1737563000	0.7738282792
H82	4.7006209984	-3.5835985219	4.1331367678
H83	-5.3436563002	-2.1786481598	1.5192107242
H84	-4.7597300001	-5.2626171707	5.3314680651
H85	-7.8526844412	-4.0495309217	-0.2501313919
H86	-7.4807140898	-2.5827440233	0.7004758895
H87	-6.1951825395	-3.3903450099	-0.2424173610

H88	-6.8872797570	-7.9055220691	4.1372986730
H89	-5.2190563918	-7.3589413829	4.4644087714
H90	-6.5807929669	-6.6909950662	5.4079819429
H91	-7.8924171126	-5.1591502790	9.1615987872
H92	-7.4447880271	-3.9255909657	7.9510122674
H93	-6.8001286681	-5.5864229093	7.8158848021
H94	-5.0364339334	-2.9765950362	12.7291646543
H95	-4.6305858769	-1.7284518765	11.5212050187
H96	-5.9952605210	-2.8561106155	11.2274405842
H97	1.3532392993	-6.2160543684	11.9084417056
H98	0.0521835600	-5.0675547943	11.4835791040
H99	0.5830466752	-6.2989001870	10.3010718702
H100	5.7185066871	-2.4995035972	10.4807765447
H101	5.3054203107	-2.3771080686	8.7478918429
H102	4.6413046173	-1.1946316888	9.9080465517
H103	8.0453720784	-3.1711022180	5.4766985802
H104	6.4123719595	-3.8522041266	5.7077416724

H105	7.0424601591	-3.5761705845	4.0574014661
H106	7.3374732229	1.8871469339	5.1037933398
H107	7.4817588349	0.2983226302	4.3017143699
H108	6.4398702812	1.5757422491	3.5948336056
H109	5.3664509501	0.9064671840	-1.0756355092
H110	4.8103873040	1.3636742082	0.5596499517
H111	4.8666168772	-0.3573652482	0.0822680467
H112	0.0974473156	1.2495868110	-3.7224576694
H113	-0.7375855901	0.1228682054	-2.6168728096
H114	-0.7820760068	1.8809863008	-2.3039716602
H115	-3.5069800603	4.8400583822	-0.9963697874
H116	-2.4648471890	4.3704333042	0.3750453763
H117	-2.4888089610	3.3797247705	-1.1114957294
H118	-7.7312791151	3.5331089495	1.4397985975
H119	-6.6945626019	3.1524742934	2.8410500246
H120	-6.0356200138	4.0922605786	1.4622974532
H121	2.4372022889	-2.9200871763	3.4501172470

H122	2.0564402446	-0.6578486943	6.1289274955

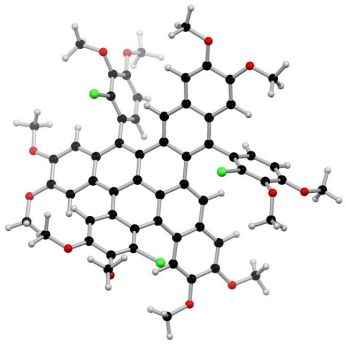

1_3peak_open_2

total energy: -4599.115306022702 hartrees

angstroms

atom	x	y	z
C1	-0.2320695561	0.6697827305	0.0070279412
C2	-0.1115108915	0.2104109852	1.3503562498
C3	1.1446944369	0.2712614987	2.0173538160
C4	2.2552536957	0.8026691611	1.2930001553
C5	2.1207082100	1.2592062919	0.0027256104
C6	0.8458841330	1.1899401280	-0.6635432717
C7	-1.2295095431	-0.2632537234	2.0548084656
C8	-1.1625425410	-0.6514463055	3.3828562868
C9	0.0854667731	-0.5523160966	4.0890416765
C10	1.2276263043	-0.1232892623	3.3890205740

C11	0.0472054434	-0.7759647082	5.5527232635
C12	-1.2035569888	-0.5294478870	6.2215681276
C13	-2.4463655260	-0.6720364898	5.4911036193
C14	-2.3948531024	-1.0292985018	4.1044624222
C15	-3.4986595767	-1.6490015742	3.5182114784
C16	-4.6902432722	-1.8664476982	4.2868178712
C17	-4.7844213572	-1.3785954302	5.6246067713
C18	-3.6624230220	-0.6901559561	6.1947166361
C19	-5.7865073930	-2.6052820097	3.7510185820
C20	-6.9105720968	-2.8863180401	4.4897088463
C21	-6.9699346426	-2.4726334635	5.8583780822
C22	-5.9362416349	-1.7369505301	6.3891204814
C23	-1.2493639625	-0.3994014235	7.6258012966
C24	-2.4634633786	0.2054939467	8.1809237285
C25	-3.6880552984	0.0188774087	7.4747929696
C26	1.1241471761	-1.1639907384	6.3284831810
C27	3.5189615545	-1.0457112488	3.8008597586

C28	2.5871160151	-0.0246756109	4.0137442682
C29	1.0240302612	-1.3187166899	7.7312281003
C30	-0.1683182963	-0.9292658423	8.4045790440
C31	-2.4941888494	1.1059648735	9.2823022705
C32	-3.6745361521	1.6695224326	9.7635617877
C33	-4.8818248512	1.4267367666	9.0701615826
C34	-4.8672896579	0.6540519118	7.9220580600
C35	2.0985264485	-1.8836335951	8.4750084200
C36	1.9908802711	-2.1110536758	9.8261347290
C37	0.7636913425	-1.7857364375	10.4973770189
C38	-0.2731001202	-1.2143836188	9.7956255012
C39	3.0159476726	1.0869330249	4.7621529069
C40	4.3033069300	1.1638035803	5.3061182294
C41	5.2090435487	0.1021676030	5.0872024635
C42	4.8109532471	-0.9988932090	4.3277192856
O43	-7.9987226529	-3.5729159255	4.0484295987
C44	-8.0090057220	-4.0010084685	2.6968842999

O45	-8.0756133031	-2.8866636143	6.5356780296
C46	-8.1624549423	-2.5862524961	7.9176542168
C47	-3.4197875690	-2.2972457296	2.1675812766
C48	-2.6892694789	-3.4818887843	2.0327205314
C49	-2.6184263050	-4.1875228127	0.8316028816
C50	-3.2940303391	-3.7111489136	-0.2925540962
C51	-4.0426220115	-2.5167480214	-0.2004997830
C52	-4.0998051634	-1.8408608563	1.0226339143
O53	-3.3020226617	-4.3081613642	-1.5179714942
C54	-2.5329794975	-5.4900054093	-1.6881146455
O55	-4.6382474140	-1.9877196200	-1.3122833827
C56	-5.8671720073	-2.6086689661	-1.7018172667
Cl57	-5.0213301557	-0.3459250202	1.0830004941
O58	2.9537071995	-2.6547977610	10.6197576676
C59	4.1785533159	-3.0222860617	10.0102533143
O60	0.7409247577	-2.0989793782	11.8208750073
C61	-0.4206882594	-1.7599248019	12.5633405154

O62	6.4388379908	0.2593954942	5.6555898214
C63	7.4127780031	-0.7465218243	5.4242417756
O64	4.7071265104	2.2788190715	5.9837870326
C65	4.7098660412	2.1511079854	7.4119337443
Cl66	1.9317051019	2.4336334059	5.0377415407
Cl67	-1.0222165105	1.7370484142	10.0129710221
O68	-3.6658886495	2.4393245529	10.8916254126
C69	-3.8315882352	3.8501993345	10.6988515363
O70	-5.9809117574	2.0519772686	9.5842823473
C71	-7.2186311568	1.8980040810	8.9076183000
O72	3.1160135520	1.8093033640	-0.7428920289
C73	4.3805410788	1.9936187961	-0.1269483981
O74	0.8330691183	1.6750809727	-1.9332630331
C75	-0.4131111984	1.7002428336	-2.6124537722
H76	5.4942780956	-1.8179639150	4.1383366081
H77	-5.7193952251	-2.9624648992	2.7339498739
H78	-5.9607268568	-1.4849018314	7.4376281629

H79	3.2139491877	0.8711513328	1.7852960444
H80	-1.2054360913	0.6120820878	-0.4657722487
H81	-5.7609035088	0.5757020035	7.3222816636
H82	-2.0361207815	-5.0994044923	0.7829384504
H83	-1.2033204369	-1.0031204264	10.3028806853
H84	3.0035258549	-2.1491058305	7.9421808329
H85	-0.2121590786	-2.0529679342	13.5934425526
H86	-0.6245348237	-0.6830867089	12.5223210093
H87	-1.3028346515	-2.3057512752	12.2043763047
H88	4.8015639769	-3.4300786223	10.8080405499
H89	4.0318507966	-3.7879601595	9.2369069336
H90	4.6833192274	-2.1562022862	9.5619094043
H91	8.3142997222	-0.4151354811	5.9416225529
H92	7.0993178189	-1.7174241411	5.8295955946
H93	7.6303245661	-0.8589472919	4.3545428744
H94	5.0012056570	3.1280180751	7.8020575538
H95	3.7118457058	1.8934410303	7.7840048195

H96	5.4344826750	1.3970336994	7.7365675335
H97	5.0106944949	2.4755874874	-0.8760560915
H98	4.3063356951	2.6382911800	0.7579640536
H99	4.8312768939	1.0365650185	0.1660777689
H100	-0.2144066157	2.1471191601	-3.5877834042
H101	-0.8197198031	0.6902326868	-2.7507466559
H102	-1.1508000424	2.3100857463	-2.0752345012
H103	-2.6618234826	-5.7823577867	-2.7311685135
H104	-1.4691835433	-5.3090131567	-1.4911414341
H105	-2.8870292851	-6.3005434473	-1.0382996853
H106	-6.2193237450	-2.0623408331	-2.5788770837
H107	-5.7128400519	-3.6602922170	-1.9629287420
H108	-6.6158671455	-2.5284276573	-0.9040478571
H109	-8.9706696453	-4.4944465788	2.5465303148
H110	-7.9219510267	-3.1526940917	2.0056668102
H111	-7.1995066106	-4.7135169444	2.4917747234
H112	-9.0991785464	-3.0264745113	8.2631544636

H113	-7.3269056160	-3.0209238377	8.4813648758
H114	-8.1859112315	-1.5027014234	8.0965396836
H115	-7.9518175754	2.4530063775	9.4949698286
H116	-7.1817062256	2.3094773048	7.8911666140
H117	-7.5203639747	0.8438837103	8.8557568009
H118	-3.7799454363	4.2952534142	11.6944126903
H119	-3.0237037088	4.2551762920	10.0793768413
H120	-4.8012944837	4.0758936482	10.2461601012
H121	-2.1624412201	-3.8611991689	2.9022384728
H122	-2.1822334733	-0.2520819793	1.5467097461
H123	2.0642429890	-1.4230487413	5.8656914152
H124	3.2167220559	-1.9064940501	3.2137162213

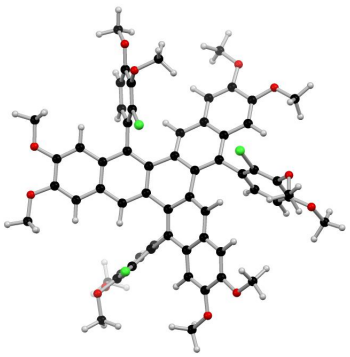

1_3peak_open_3

total energy: -4600.304318896717 hartrees

angstroms

atom	x	y	z
C1	0.2181659094	0.1151918072	-0.0192022234
C2	0.0132679483	-0.0686106878	1.3652085531
C3	1.1325792565	-0.4515544314	2.1122636977
C4	2.3922179676	-0.6355750866	1.5425842687
C5	2.5724886362	-0.4357359880	0.1744657319
C6	1.4707428914	-0.0530749532	-0.6214719090
C7	-1.3045769166	0.0595482195	2.0742806248
C8	-1.5167677095	1.0310726735	3.0742159400
C9	-2.6179553810	0.8596626238	3.9899107536
C10	-3.6470574317	0.0106130349	3.6145836739
C11	-3.5395807478	-0.8613009043	2.5155506977
C12	-2.3044044449	-0.9285586350	1.8082516352
C13	-0.7887903336	2.3209220630	3.1486315196
C14	-0.9161068631	3.1605376339	4.3093077835

C15	-1.5948556260	2.5840378006	5.4916875889
C16	-2.5398356640	1.5069270499	5.3216880679
C17	-0.4308153364	4.4838780057	4.2604154053
C18	0.2476375312	4.9757345870	3.1013794108
C19	0.4036594203	4.1154606014	1.9788747181
C20	-0.1485035340	2.8274646327	2.0277633518
C21	0.7480159666	6.3091226578	2.9853368888
C22	1.3870518627	6.7429185310	1.8481360855
C23	1.5618396777	5.8565393687	0.7293456158
C24	1.0667194744	4.5797934592	0.8052920965
C25	-3.2097249185	1.0080995408	6.4574197320
C26	-2.9705831594	1.5588808923	7.7568516905
C27	-1.9767997445	2.5628069809	7.9113977575
C28	-1.3027996149	3.0278163491	6.7708172924
C29	-4.0945053972	-0.2060657318	6.4593550140
C30	-3.5218834926	-1.4786715099	6.5382267970
C31	-4.6012718246	-1.7486599814	2.1786846449

C32	-4.4440465879	-2.7073475664	1.2093035627
C33	-3.1761646934	-2.8317756855	0.5443900245
C34	-2.1479709101	-1.9698714210	0.8462212060
C35	-4.2926852302	-2.6354430248	6.6607718139
C36	-5.6834702801	-2.5432548213	6.7317728227
C37	-6.3016449647	-1.2756332660	6.6618325360
C38	-5.4999004595	-0.1364109134	6.5184671431
C39	-3.6507467792	1.1126867867	8.9308662238
C40	-3.3682079953	1.6348042100	10.1704496613
C41	-2.3472977865	2.6354406245	10.3181921573
C42	-1.6741198233	3.0759834031	9.2064520452
O43	1.8948158657	7.9917157007	1.6626527036
C44	1.7384256387	8.9339708679	2.7109245160
O45	2.2176350436	6.3941739896	-0.3334742890
C46	2.4044619136	5.5698691372	-1.4737253872
C47	-0.6118808349	5.4880705962	5.3626142234
C48	0.4842595225	5.8777905647	6.1404833690

C49	0.3915051772	6.8520925747	7.1352792217
C50	-0.8299536991	7.4848325227	7.3715463527
C51	-1.9558638187	7.1353888230	6.5955994725
C52	-1.8291343649	6.1519327428	5.6060473472
O53	-3.1147614652	-3.8407866768	-0.3677334926
C54	-1.9080178681	-4.0058131788	-1.0927241381
O55	-5.3936340898	-3.5971556830	0.8088335768
C56	-6.6804911712	-3.4893404097	1.3932179822
Cl57	-6.3071303542	1.4177332403	6.4064108553
O58	-7.6545694984	-1.1524363556	6.8176885094
C59	-8.4491545688	-1.5421665516	5.6929975707
O60	-6.5342510421	-3.6008403325	6.8738403004
C61	-5.9707350396	-4.8974228154	7.0094571714
O62	-2.1465960905	3.0647020074	11.5940740229
C63	-1.1454645687	4.0445346570	11.8073988972
O64	-3.9875803931	1.2839920550	11.3297973001
C65	-5.0491160085	0.3445253849	11.2568256310

Cl66	-3.2480880790	5.7781868680	4.6516911727
O67	-3.1339342847	7.8062765601	6.7621622371
C68	-3.9202224106	7.3826679596	7.8834346018
O69	-1.0441949269	8.4487810442	8.3132026609
C70	0.0626253122	8.8782664988	9.0901739735
O71	3.7550620314	-0.5739268191	-0.4906657761
C72	4.9125546146	-0.8955807909	0.2673387970
O73	1.6444861299	0.2397437075	-1.9465401564
C74	1.8003682860	-0.8893119449	-2.8117852807
Cl75	-1.0962970570	0.6646275205	-1.0464170424
H76	1.2716243961	7.1116619678	7.7114743029
H77	-1.2025221107	-2.0689231891	0.3339549231
H78	-5.5328023839	-1.6600680635	2.7252861905
H79	0.6151321472	6.9923733293	3.8098935011
H80	1.1676102326	3.8949730956	-0.0284616849
H81	-3.8007006279	-3.5990700564	6.7143873753
H82	3.2231930102	-0.9270231970	2.1734455722

H83	-4.4125203902	0.3536450490	8.8404510369
H84	-0.9067678382	3.8371414941	9.2875987244
H85	-5.4218104555	0.2349738744	12.2765072186
H86	-5.8585973863	0.7010613844	10.6077252111
H87	-4.7019576040	-0.6301567994	10.8905256492
H88	-1.1423560756	4.2434996715	12.8803671592
H89	-0.1547030278	3.6829305915	11.5017578825
H90	-1.3672303231	4.9737908210	11.2660677716
H91	-0.3203552873	9.6545733251	9.7542514927
H92	0.4792569755	8.0605054434	9.6928694928
H93	0.8578946448	9.3000312392	8.4624693364
H94	-4.8345171414	7.9781317154	7.8530528837
H95	-4.1749301454	6.3198532816	7.8036739923
H96	-3.3937225168	7.5697920692	8.8251101690
H97	2.2063174558	9.8545916728	2.3583273962
H98	0.6797576597	9.1232678637	2.9292865658
H99	2.2369649533	8.6013654683	3.6308143347

H100	2.9435905966	6.1801245857	-2.2000083426
H101	2.9982579065	4.6783679992	-1.2342631460
H102	1.4458023010	5.2530778433	-1.9036293923
H103	5.7374575694	-0.9274663695	-0.4458705108
H104	5.1200110822	-0.1325565418	1.0276520374
H105	4.8187499648	-1.8739295234	0.7557781239
H106	1.8932313717	-0.4862101823	-3.8220451995
H107	2.6997752938	-1.4595406252	-2.5603834803
H108	0.9204394231	-1.5426576661	-2.7645516834
H109	-2.0770930315	-4.8454629168	-1.7689796766
H110	-1.6640988220	-3.1094717181	-1.6774635021
H111	-1.0654096321	-4.2388146867	-0.4284404688
H112	-7.2930704118	-4.2569952550	0.9174893043
H113	-6.6508067661	-3.6690645210	2.4761896133
H114	-7.1249934537	-2.5025393283	1.2091750917
H115	-6.8143163735	-5.5782138954	7.1332700928
H116	-5.3990710357	-5.1873869520	6.1187424394

H117	-5.3204785983	-4.9631523077	7.8907014486
H118	-9.4866004640	-1.3552844453	5.9770707067
H119	-8.2032196520	-0.9367641697	4.8122597866
H120	-8.3181476692	-2.6048077312	5.4656632011
H121	1.0065247712	-0.6062619372	3.1788145698
H122	-0.1046586955	2.2459927505	1.1224882039
H123	-0.5226638433	3.7568435014	6.9202980643
H124	1.4400824674	5.3941341745	5.9621510601
H125	-2.4406255323	-1.5626066315	6.5033909458
H126	-4.5554615466	-0.0297552925	4.1936364197

2.9.3 UV-vis spectroscopy.

General Procedure and Instrumentation: Absorption spectra were taken on a Shimadzu UV-1800 spectrophotometer. Sample solutions were prepared with anhydrous chloroform as solvent. A 1-cm quartz cuvette was charged with blank chloroform and a background spectrum was recorded. The cuvette was charged with appropriate amount of sample solution in chloroform and an absorption spectrum was recorded.

2.9.4 Cyclic Voltammetry

General Procedure and Data Analysis: Cyclic voltammetry (CV) was performed

using a CHI600c potentiostat interfaced to a PC using the Chi600c electrochemical analyzer software package. The cell was a standard three-electrode setup using a glassy carbon working electrode, a Ag/AgCl reference electrode, and a platinum counter electrode. All electrodes were purchased from Bioanalytical Systems, Inc. Measurements were carried out under argon in anhydrous dichloromethane solution with a tetrabutylammonium hexafluorophosphate as supporting electrolyte (0.1 M). All potentials were measured as the midpoint peak oxidation potential with respect to the Fc+/Fc redox couple. The scan rate in was 0.05 V/s. Calculated from the curve Figure S1, the HOMO, LUMO and band gap of trichloro c-HBC **1** are -5.5 eV, -2.6 eV and 2.9 eV, respectively, by using ferrocene as the standard reference.

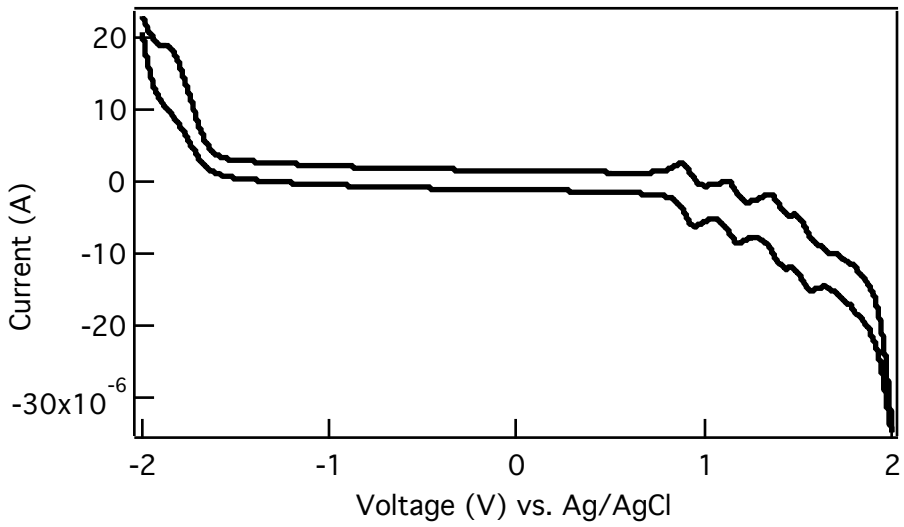

Figure S1. Cyclic voltammetry of trichloro c-HBC **1**

2.10 References

(1) Zhang, Q.; Peng, H.; Zhang, G.; Lu, Q.; Chang, J.; Dong, Y.; Shi, X.; Wei, J. *J. Am. Chem. Soc.* **2014**, *136*, 5057.

(2) Chiu, C. Y.; Kim, B.; Gorodetsky, A. A.; Sattler, W.; Wei, S. J.; Sattler, A.; Steigerwald, M.; Nuckolls, C. *Chem. Sci.* **2011**, *2*, 1480.

(3) Loo, Y. L.; Hiszpanski, A. M.; Kim, B.; Wei, S. J.; Chiu, C. Y.; Steigerwald, M. L.; Nuckolls, C. *Org Lett.* **2010**, *12*, 4840.

(4) Clar, E.; Stephen, J. F. *Tetrahedron* **1965**, *21*, 467.

(5) Xiao, S., PhD thesis, Columbia University, 2007.

(6) Plunkett, K. N.; Godula, K.; Nuckolls, C.; Tremblay, N.; Whalley, A. C.; Xiao, S. X. *Org. Lett.* **2009**, *11*, 2225.

(7) Abbate, S.; Lebon, F.; Longhi, G.; Fontana, F.; Caronna, T.; Lightner, D. A. *Phys. Chem. Chem. Phys.* **2009**, *11*, 9039.

(8) Tremblay, N. J.; Gorodetsky, A. A.; Cox, M. P.; Schiros, T.; Kim, B.; Steiner, R.; Bullard, Z.; Sattler, A.; So, W. Y.; Itoh, Y.; Toney, M. F.; Ogasawara, H.; Ramirez, A. P.; Kymissis, I.; Steigerwald, M. L.; Nuckolls, C. *ChemPhysChem* **2010**, *11*, 799.

(9) Katz et al. *J. Am. Chem. Soc.* **1997**, *119*, 10054.

(10) Martin et al. *Tetrahedron Lett.* **1968**, *9*, 3507.

(11) Waghray, D.; Zhang, J.; Jacobs, J.; Nulens, W.; Basarić, N.; Meervelt, L. V.; Dehaen, W. *J. Org. Chem.* **2012**, *77*, 10176.

(12) Elm, J.; Lykkebo, J.; Sørensen, T. J.; Laursen, B. W.; Mikkelsen, K. V. *J. Phys. Chem. A* **2011**, *115*, 12025.

(13) Grimme, S.; Peyerimhoff, S. D. *Chem. Phys.* **1996**, *204*, 411.

(14) Janke, R. H.; Haufe, G.; Würthwein, E.-U.; Borkent, J. H. *J. Am. Chem. Soc.* **1996**, *118*, 6031.

(15) Lakshman, M. K.; Kole, P. L.; Chaturvedi, S.; Saugier, J. H.; Yeh, H. J. C.; Glusker, J. P.; Carrell, H. L.; Katz, A. K.; Afshar, C. E.; Dashwood, W.-M.; Kenniston, G.; Baird, W. M. *J. Am. Chem. Soc.* **2000**, *122*, 12629.

(16) Liu, J.; Li, B.-W.; Tan, Y.-Z.; Giannakopoulos, A.; Sanchez-Sanchez, C.; Beljonne, D.; Ruffieux, P.; Fasel, R.; Feng, X.; Müllen, K. *J. Am. Chem. Soc.* **2015**, *137*, 6097.

(17) Zhong, Y.; Kumar, B.; Oh, S.; Trinh, M. T.; Wu, Y.; Elbert, K.; Li, P.; Zhu, X.; Xiao, S.; Ng, F.; Steigerwald, M. L.; Nuckolls, C. *J. Am. Chem. Soc.* **2014**, *136*, 8122.

(18) Li, J.-T.; Wang, L.-X.; Wang, D.-X.; Zhao, L.; Wang, M.-X. *J. Org. Chem.* **2014**, *79*, 2178.

(19) Davoren, J. E.; Bundesmann, M. W.; Yan, Q. T.; Collantes, E. M.; Mente, S.; Nason, D. M.; Gray, D. L. *ACS Med. Chem. Lett.* **2012**, *3*, 433.

(20) Guo, X. F.; Xiao, S. X.; Myers, M.; Miao, Q.; Steigerwald, M. L.; Nuckolls, C. *Proc. Natl. Acad. Sci. USA* **2009**, *106*, 691.

(21) Xiao, S. X.; Kang, S. J.; Zhong, Y.; Zhang, S. G.; Scott, A. M.; Moscatelli, A.; Turro, N. J.; Steigerwald, M. L.; Li, H. X.; Nuckolls, C. *Angew. Chem. Int. Ed.* **2013**, *52*, 4558.

(22) Xiao, S. X.; Myers, M.; Miao, Q.; Sanaur, S.; Pang, K. L.; Steigerwald, M. L.; Nuckolls, C. *Angew. Chem. Int. Ed.* **2005**, *44*, 7390.

(23) Xiao, S. X.; Tang, J. Y.; Beetz, T.; Guo, X. F.; Tremblay, N.; Siegrist, T.; Zhu, Y. M.; Steigerwald, M.; Nuckolls, C. *J. Am. Chem. Soc.* **2006**, *128*, 10700.

(24) Cohen, Y. S.; Xiao, S. X.; Steigerwald, M. L.; Nuckolls, C.; Kagan, C. R. *Nano Lett.* **2006**, *6*, 2838.

(25) Mobility calculated from the transfer curve in dark is 2 x 10-5 cm2/V•s

(26) Yang, Y.; da Costa, R. C.; Fuchter, M. J.; Campbell, A. J. *Nat. Photon.* **2013**, *7*, 634.

(27) Jan, C.-M.; Lee, Y.-H.; Wu, K.-C.; Lee, C.-K. *Opt. Express* **2011**, *19*, 5431.

(28) Farshchi, R.; Ramsteiner, M.; Herfort, J.; Tahraoui, A.; Grahn, H. T. *Appl. Phys. Lett.* **2011**, *98*, 162508.

(29) Sherson, J. F.; Krauter, H.; Olsson, R. K.; Julsgaard, B.; Hammerer, K.; Cirac, I.; Polzik, E. S. *Nature* **2006**, *443*, 557.

2.11 Appendix

HPLC traces for the 3-peak

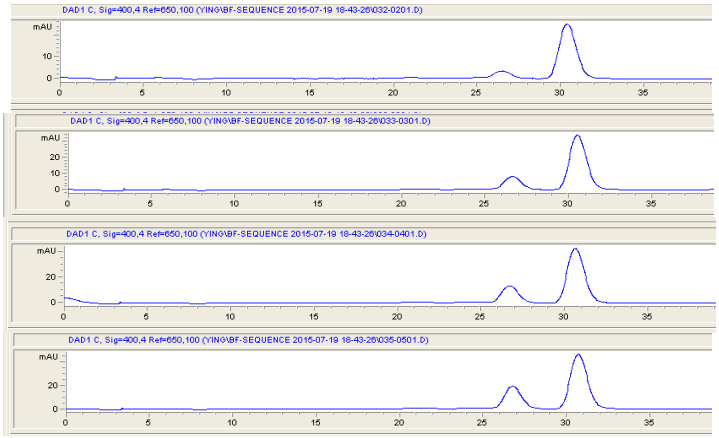

125 ^{0}C 5 min

125 ^{0}C 15 min

125 ^{0}C 25 min

125 ^{0}C 35 min

HPLC traces for the 3-peak

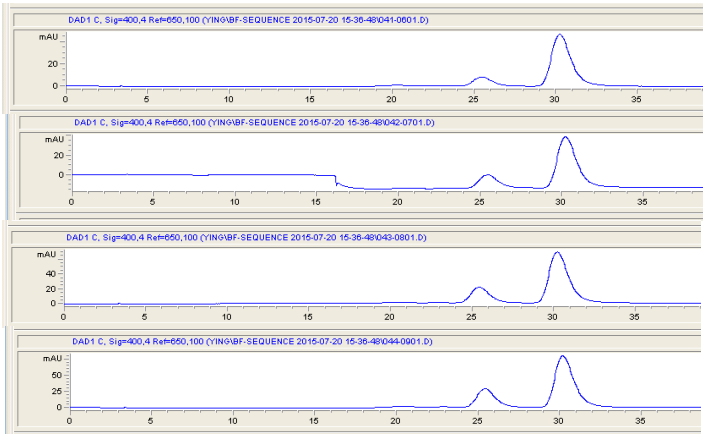

130 ^{0}C 5 min

130 ^{0}C 10 min

130 ^{0}C 15 min

130 ^{0}C 20 min

HPLC traces for the 3-peak

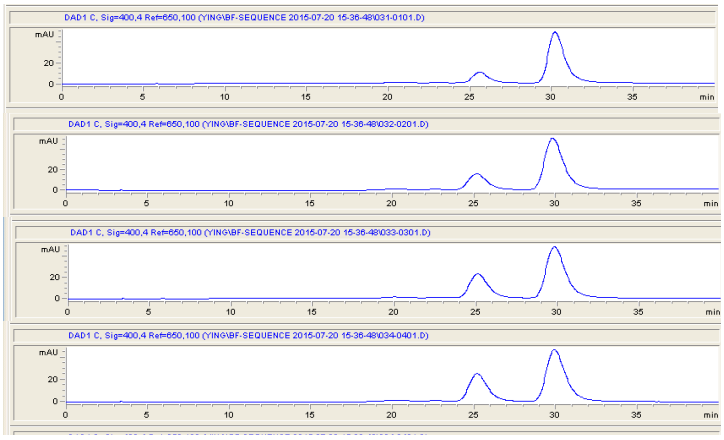

135 ^{0}C 5 min

135 ^{0}C 10 min

135 ^{0}C 15 min

135 ^{0}C 20 min

HPLC traces for the 9-peak

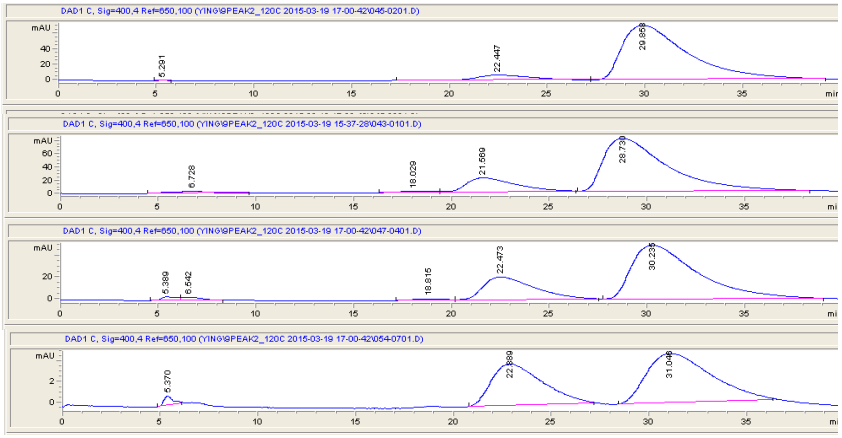

130 ^{0}C 5 min

130 ^{0}C 10 min

130 ^{0}C 15 min

130 ^{0}C 20 min

HPLC traces for the 9-peak

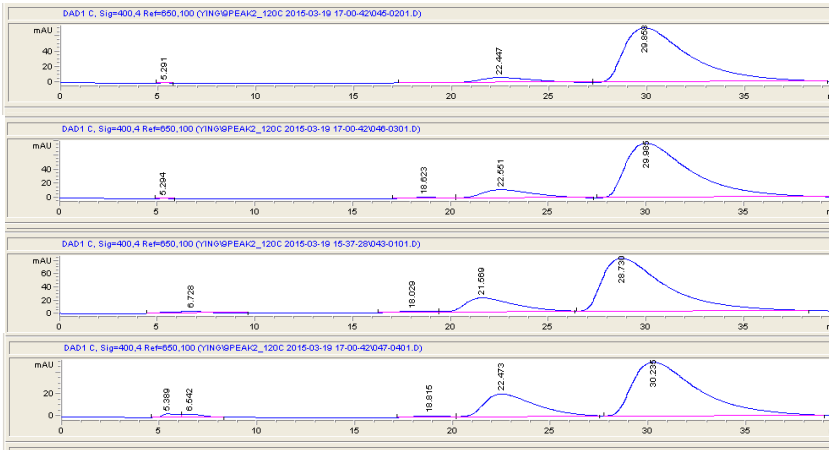

120 ^{0}C 10 min

120 ^{0}C 20 min

120 ^{0}C 35 min

120 ^{0}C 55 min

HPLC traces for the 9-peak

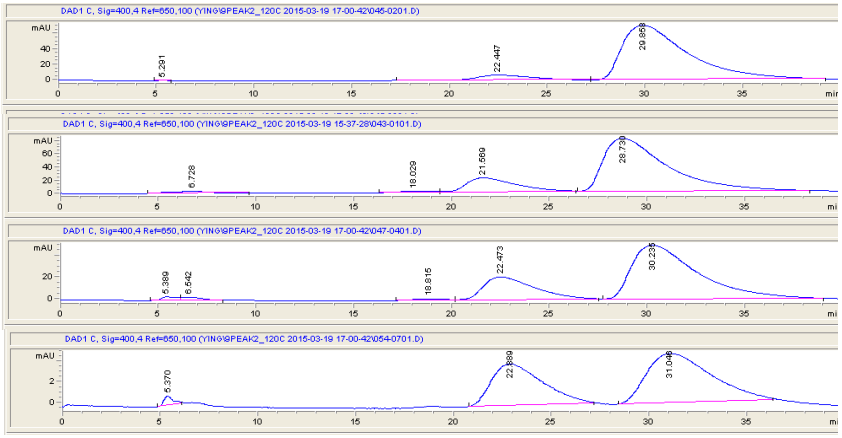

130 ^{0}C 5 min

130 ^{0}C 10 min

130 ^{0}C 15 min

130 ^{0}C 20 min

HPLC traces for the 9-peak

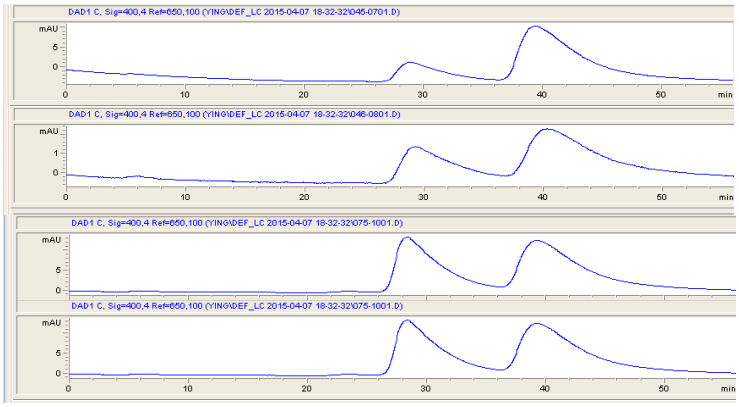

135 ^{0}C 5 min

135 ^{0}C 10 min

135 ^{0}C 15 min

135 ^{0}C 20 min

HPLC traces for the 9-peak

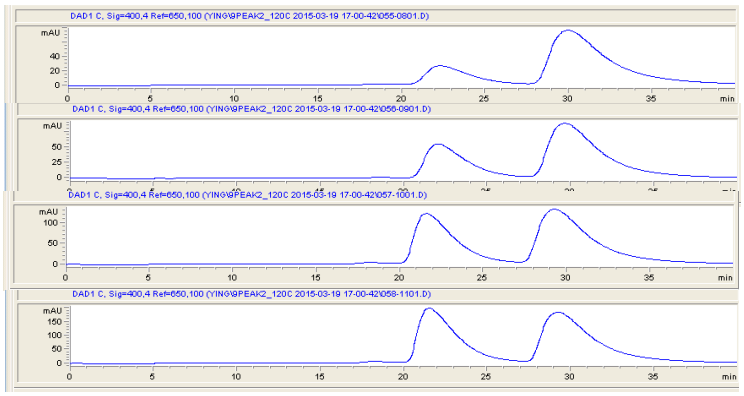

140 ^{0}C 3 min

140 ^{0}C 7 min

140 ^{0}C 10 min

140 ^{0}C 15 min

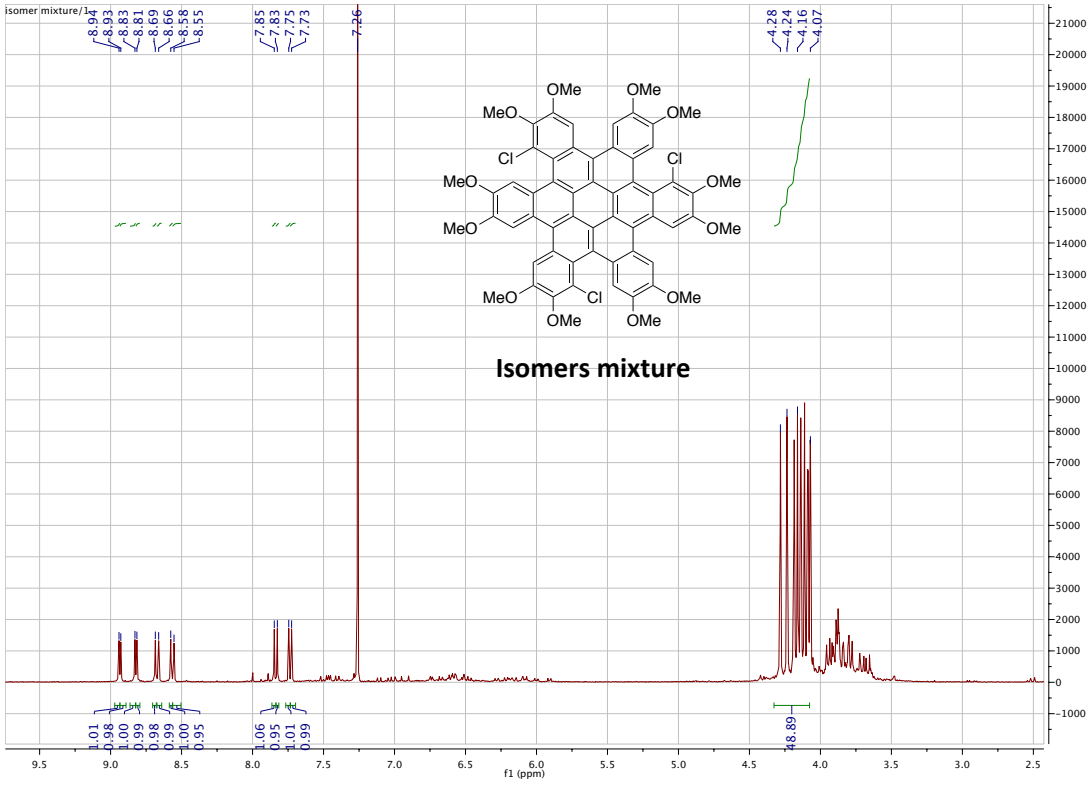

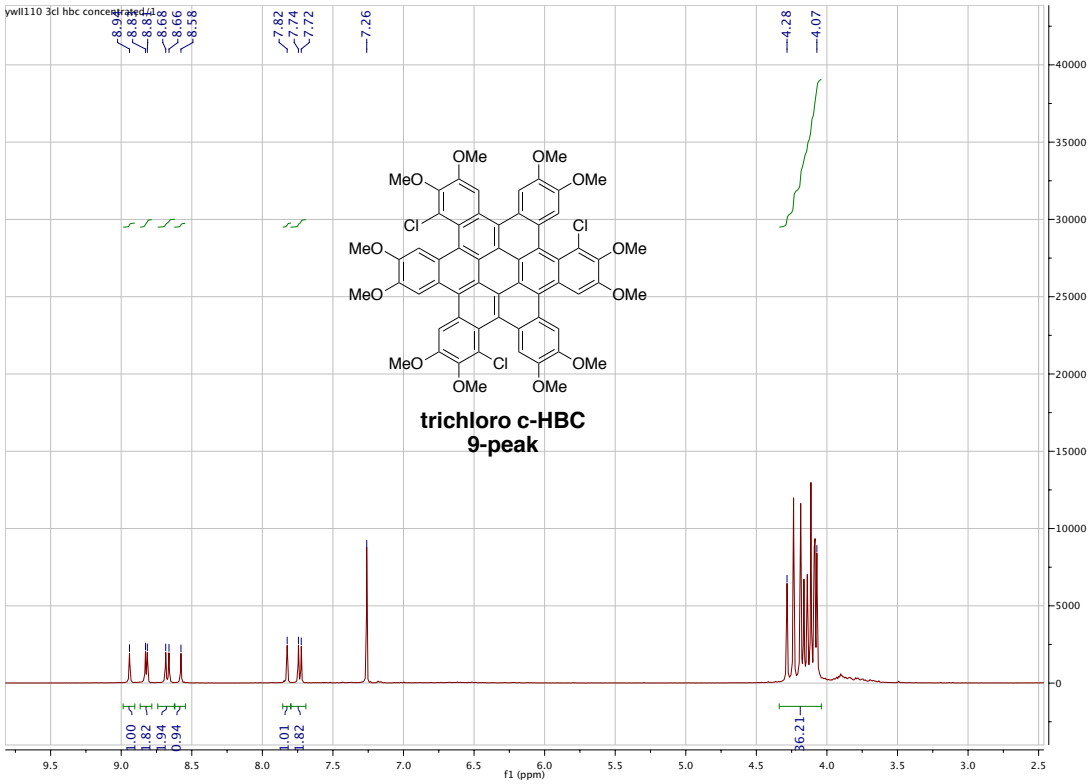
ywll110 3cl hbc concentrated1
8.99
8.84
8.82
8.68
8.66
8.58
7.82
7.74
7.72
7.26
4.28
4.07
OMe
MeO
Cl
trichloro c-HBC
9-peak
1.00
1.82
1.94
0.94
1.01
1.82
36.21
f1 (ppm)

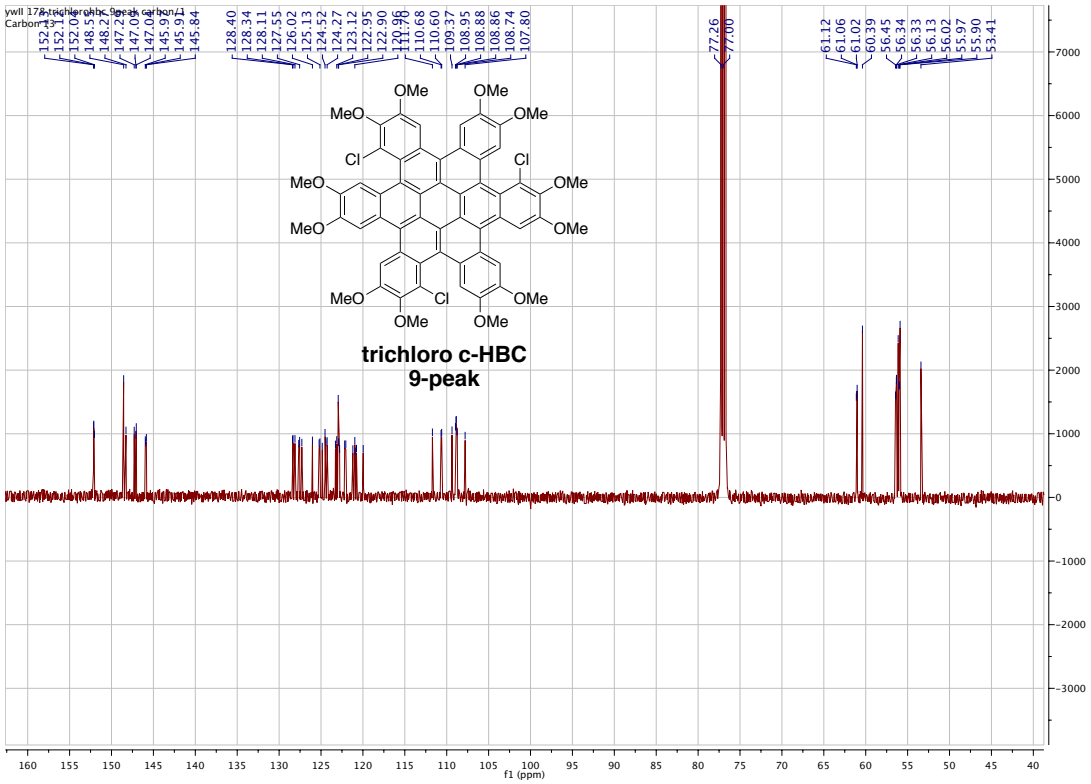
trichloro c-HBC
9-peak
f1 (ppm)

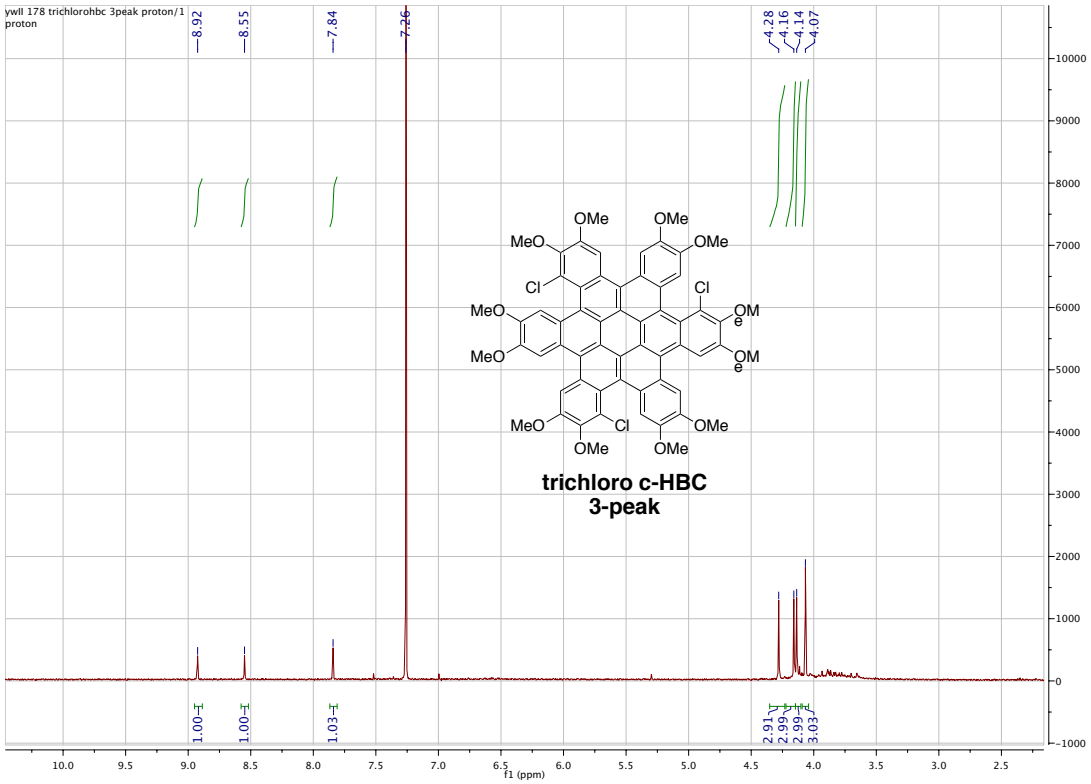
ywll 178 trichlorohbc 3peak proton/1 proton
8.92
8.55
7.84
7.26
4.28
4.16
4.14
4.07
OMe
MeO
Cl
OMe
trichloro c-HBC
3-peak
1.00
1.00
1.03
2.91
2.99
2.99
3.03
f1 (ppm)

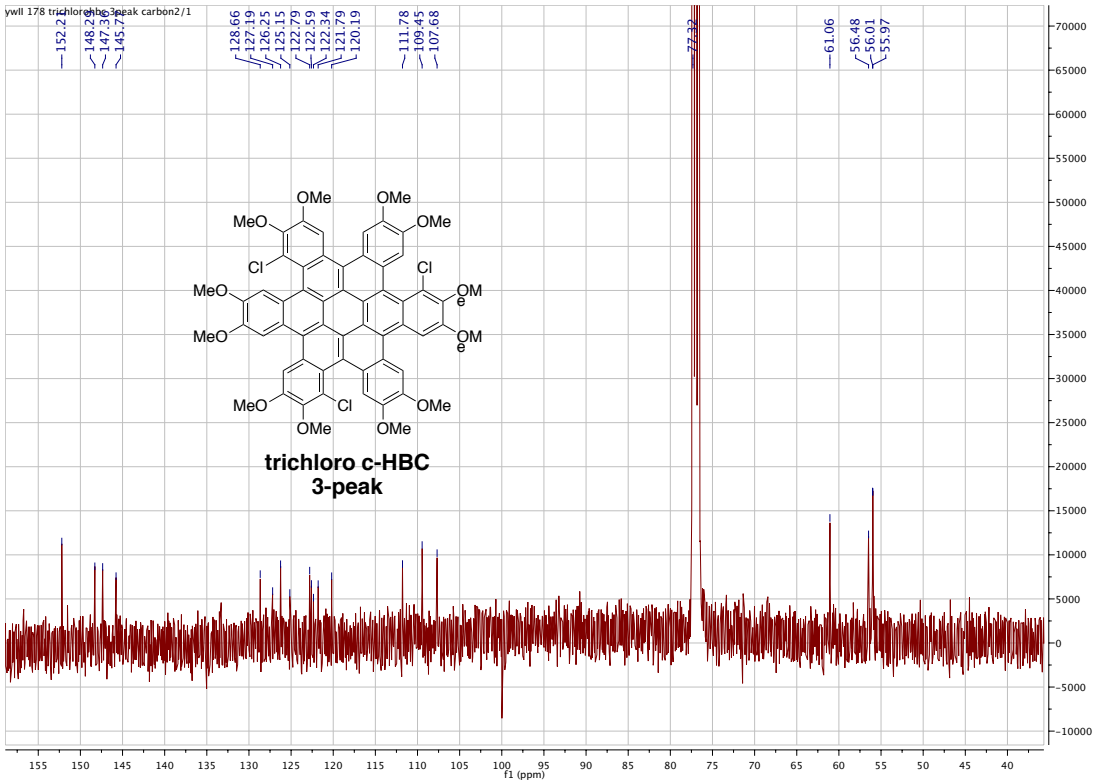
ywll 178 trichloro hbc 3peak carbon2/1
152.2
148.2
147.3
145.7
128.66
127.19
126.25
125.15
122.79
122.59
122.34
121.79
120.19
111.78
109.45
107.68
77.32
61.06
56.48
56.01
55.97
OMe
MeO
Cl
trichloro c-HBC
3-peak
f1 (ppm)

Chapter 3. Expanding the aromatic core: Octabenzocircumbiphenyl[1]

3.1 Design of the expanded aromatics

As we have introduced in Chapter 1, the Nuckolls group has previously synthesized contorted-hexabenzocoronene (c-HBC) **1**, and its derivative **2** c-DBTTC (Figure 1), and has shown that these act as donor materials in organic photovoltaics (OPVs). The contorted conformation introduces some desirable physical properties relative to the flat analog, including increased solubility due to a weaker π-π interaction. The unique 3-D structure of the contorted polycyclic aromatic hydrocarbons (PAHs) results in intriguing intermolecular packing, a complex structure that flat PAHs are unable to adopt. Co-crystal of c-HBC and C_{60} fullerene shows remarkable shape complementarity, similar to a ball-socket structure, which enhances OPV performance. The c-HBC derivative **2** contorted-dibenzotetrathienocoronene(c-DBTTC) also associates with fullerenes, but stacks into columnar arrays while retaining similar electronic properties as c-HBC **1**. Although the efficiency of OPV device is improved by incorporating thiophene motifs, one of the major limitations of these devices is that the absorbance spectra of existing c-HBCs and their derivatives overlap poorly with solar emission spectrum.

We propose that a solution to this problem is to synthesize PAHs with an expanded core. Therefore, octabenzocircumbiphenyl (OBCB) **3** was designed. Figure 2 shows the DFT-optimized structure of the lowest energy conformer of the c-OBCB **3**. The structure is similar to the c-HBC in many aspects but has some important differences. Like the c-HBC, benzo-groups alternate up or down around the exterior of the circumbiphenyl

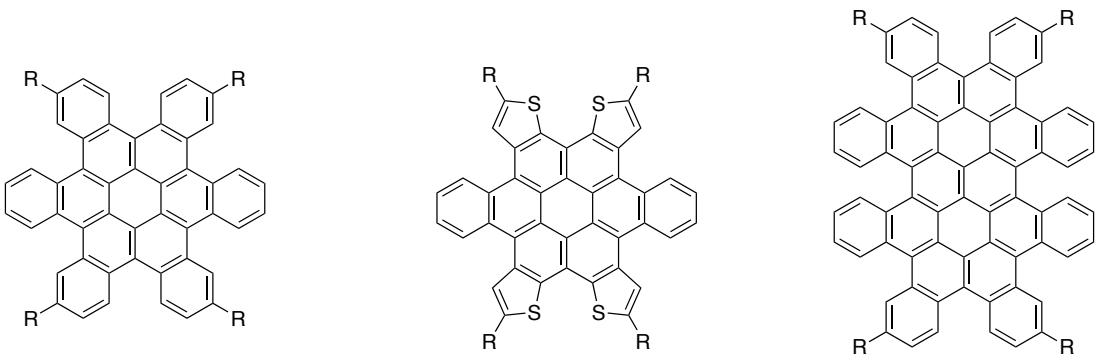

Figure 1. Structures of the contorted disc-shaped molecules c-HBC **1**, c-DBTTC **2**, and c-OBCB **3**.

core. The c-OBCB has two additional [5]-helicenes around its exterior. In this conformation, the additional [5]-helicenes renders the molecule chiral. We found two additional conformations by DFT (Figure S1). These two geometries are essentially isoenergetic, and each is 21 kcal/mol higher in energy than the one shown in Figure 1.

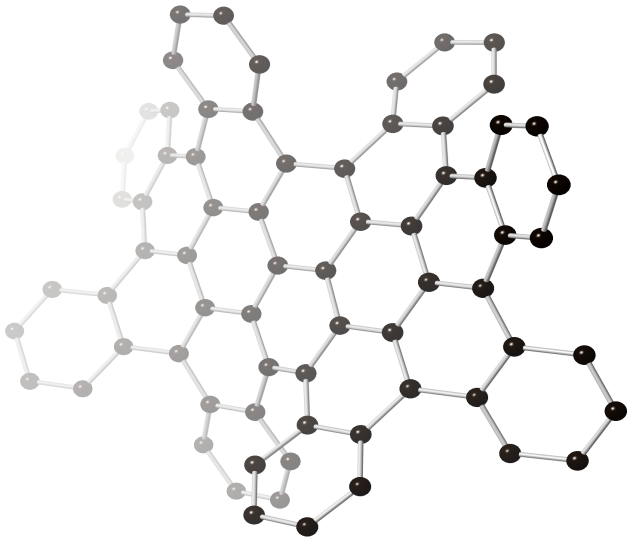

Figure 2. The energy-minimized structure from DFT calculations for c-OBCB **3a**. Hydrogens have been removed to clarify the view.

3.2 Optimized structure and frontier orbitals by DFT calculations

Density functional theory (DFT) calculation showed that c-OBCB adopts a contorted structure as we described above (Figure 2). The calculated HOMO, LUMO, and band gap are -4.90 eV, -2.04 eV, and 2.86 eV, respectively. The calculated band gap of c-OBCB is smaller than that of c-HBC by 0.34 eV, which indicates c-OBCB would red-shift and thus become a more efficient donor material. c-OBCB has more accessible frontier orbitals than its parent c-HBCs. The frontier orbitals of c-OBCB are contained in supporting information.

3.3 Syntheses of c-OBCB

There are no reported syntheses of circumbiphenyls except for the original synthesis of the parent circumbiphenyl by Clar in 1972.[2] The harsh conditions employed in the Clar's synthesis prevent using it to make functionalized derivatives. Our strategy was to synthesize the parent c-OBCB with solubilizing chains and to study its property in thin film devices.

We developed two syntheses for c-OBCB. The first-generation synthesis was developed by Xiao as shown in Scheme 1.[3] The route resembles the first-generation synthesis of c-HBC (see Chapter 2.1) in that it employs the Barton-Kellogg olefination to form the tris-olefin intermediate and subsequently cyclize the tris-olefin to the product under the Katz-modified Mallory photocyclization conditions. The synthesis successfully incorporated solubilizing chains for further solution-based studies. But the overall route is step-intensive as the two starting pieces, thioketone and the diazoalkane, require several steps to be prepared from commercially available compounds.

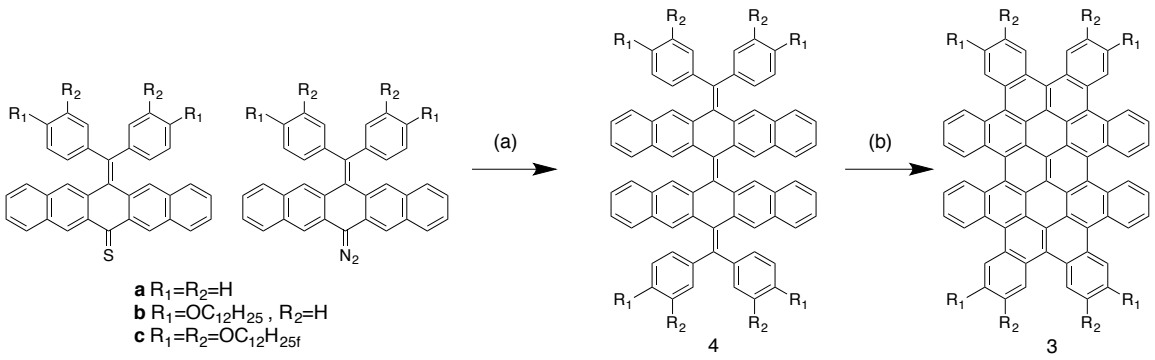

Scheme 1. First-generation synthesis of c-OBCB. (a) dichloromethane in the dark followed by PPh_3, xylenes, reflux; (b) *hv*, I_2, propylene oxide, anhydrous benzene.

In this thesis we developed a more efficient route to yield sufficient c-OBCB for our studies in thin film devices (Chapter 4) and single-wall carbon nanotube sorting (Chapter 5). The alternate synthesis in Scheme 2 obviates the synthesis of either the thioketone or the diazoalkane by utilizing the dione **7**. Dione **7** is prepared in two steps from commercially available reagents.[4,5] Subjecting this dione to Ramirez olefination[6,7] creates the versatile tetrabromide **8**. Compound **8** is a yellow solid that has poor solubility in common organic solvents at room temperature. Fortunately, compound **8** is soluble enough to allow the subsequent reactions to occur. Suzuki coupling of **8** with substituted aryl boronic acid forms tris-olefin **4**.[7,8,9] Finally, Katz-modified Mallory photocyclization conditions were employed to close six rings to provide the final product c-OBCB **3b**.[7,8]

The synthetic challenge laid in the purification of compounds **7** and **8** due to their poor solubility. Fortunately, compound **8** precipitated from reaction mixtures and could be purified by washing with hot toluene. When pure tetrabromide **8** was furnished, the Suzuki coupling and photocyclization went smoothly and the overall yield is 36%.

Moreover, we would be able to cross-couple tetrabromide **8** with other motifs to make more promising donor materials for solar cells.

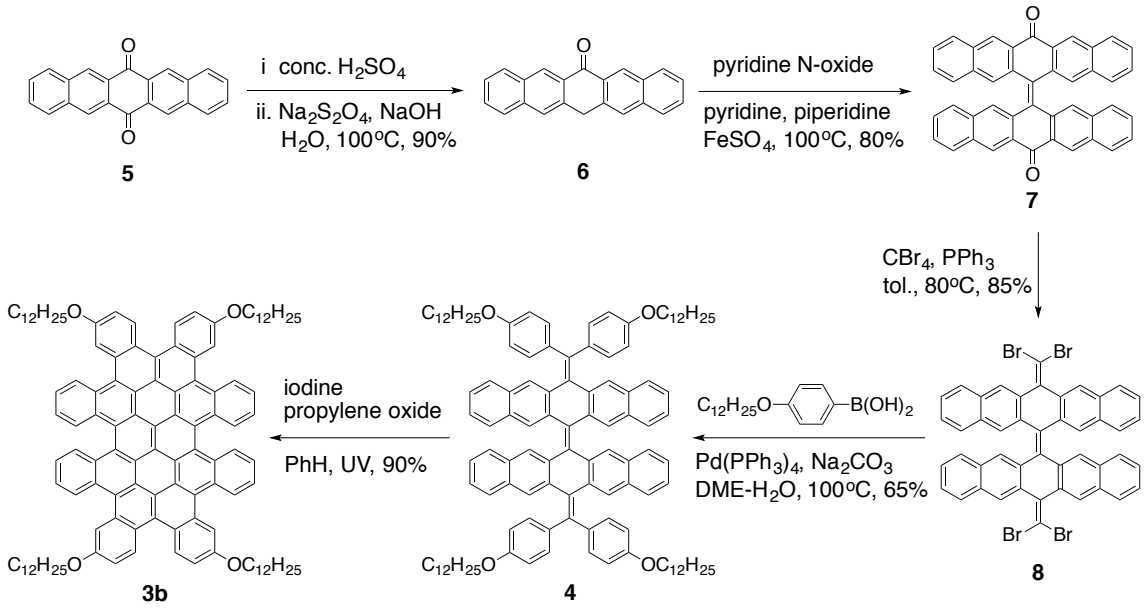

Scheme 2. Second-generation synthesis of c-OBCB.

The key common intermediate in both syntheses is tris-olefin **4**. It consists of three tetrasubstituted double bonds separated by two six-membered rings. Given the crowded structure of this tris-olefin, we grew crystals to investigate its conformational preference. Figure 3 displays the structure obtained crystallographically. The two pentacene-like units along the short axis of the molecule are bent into opposite directions due to steric crowding. The three double bonds along the long axis of the molecule adopt a "zig–zag" conformation.

3.4 Spectroscopic characterizations

The unsubstituted c-OBCB **3a** is a red powder that has limited solubility in common organic solvents (~10 mg/mL in 1,1,2,2-tetrachloroethane). It precipitates from the

benzene solution upon the completion of the photocyclization.[3] As expected, the side chains drastically increase the solubility. Compounds **3b** has a solubility of over 100 mg/mL in chloroform.[3]

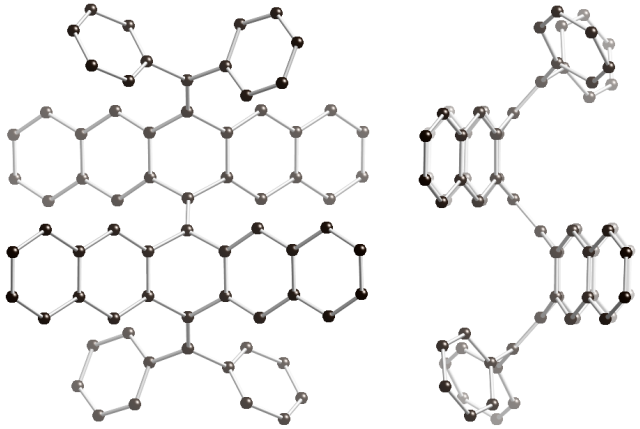

Figure 3. Top and side views of tris-olefin **4** from single-crystal X-ray diffraction. Hydrogen atoms and alkoxy chains have been removed to clarify the view. Crystals were grown by slow diffusion of methanol into a solution of tris-olefin in 1,2,4-trichlorobenzene.

We measured UV-visible (UV-vis) and photoluminescence (PL) spectra of c-OBCB **3b** in o-xylene at 10^{-6} M (Figure 4). The strong absorptions in the UV region, below 350 nm, are due to the pendant phenyl groups. More interestingly, c-OBCB **3b** shows strong absorbance at 411 nm, 433 nm and 493 nm. The peaks at 411 nm and 433 nm are the b-bands of c-OBCB.[1] The peak at 493 nm is the p-band.[1] The weak absorptions at 550 nm are most likely due to (radialene p)–(radialene p*) triplets.[1] The assignment of these transitions to a triplet state is supported by the PL spectrum shown in Figure 4. When excited at 433 nm, the fluorescence spectra showed two strong emission peaks at 549 nm and 593 nm, along with a small peak at 645 nm.

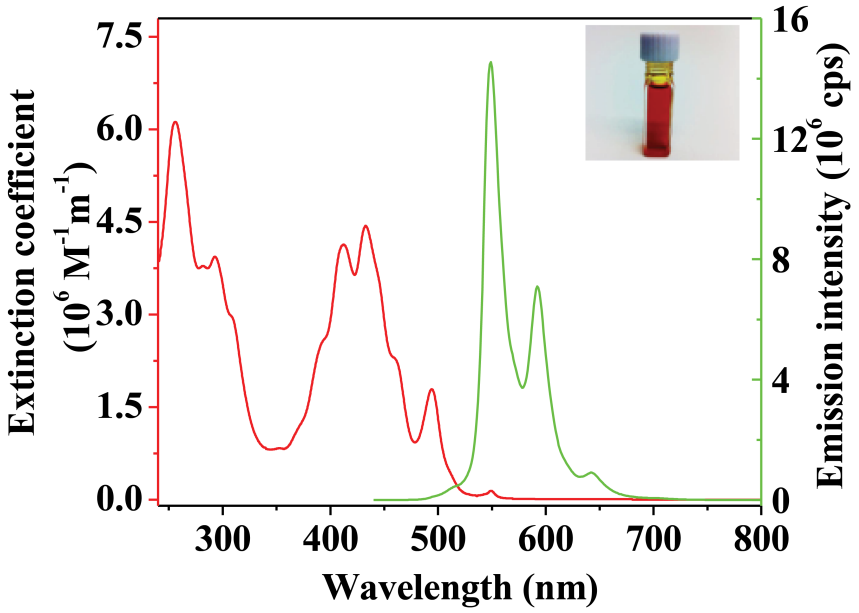

Figure 4. UV-vis (red) and fluorescence (green curve, excited at 433 nm) spectroscopy of c-OBCB **3b** in o-xylene at ~10^{-6} M concentration with a path length of 1 cm. The inset shows a 5 mM solution of **3b** in chloroform.

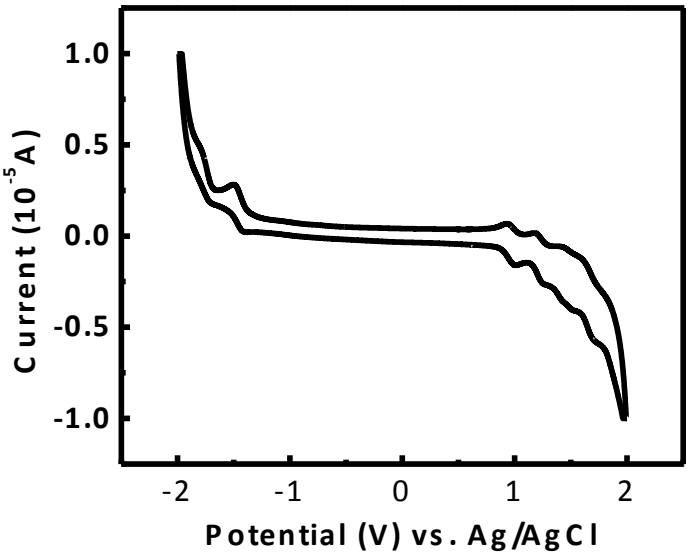

Figure 5. Cyclic voltammetry of c-OBCB **3b** in CH_2Cl_2.

The absorbance peak of the UV-Vis spectrum of c-OBCB is red-shifted by 80 nm relative to c-HBC (Figure S3). The HOMO, LUMO and band gap from cyclic voltammetry are -5.4 eV, -3.0 eV, and 2.4 eV, respectively (Figure 5, ferrocene was used as the standard reference for calculating these values). Both the absorbance spectrum and CV results are in consistence with our previous calculations. Thus, c-OBCB is red-shifted as proposed, which would potentially be a more desirable donor material for solar cell.

3.5 Concentration-dependent NMR spectra of c-OBCB 3b

Serendipitously, we found the ^{1}H NMR spectra c-OBCB 3b are concentration dependent. Figure 6 displays that the chemical shifts of c-OBCB 3b change significantly when the concentration is changed by merely one order of magnitude, from 1.25 mM to 20 mM. Aromatic stacking based on self-association of the molecules through an intermolecular π-stacking interaction is reported to affect the chemical shifts of some aromatic molecules.[10,11] Quinoline and its derivatives is one of the early and well studied systems that exhibit concentration-dependent chemical shifts due to π-interactions.[12] We believe that the chemical shifts variation according to change of concentration in the c-OBCB 3b ^{1}H NMR spectra also arises from the strong intermolecular π - π interactions, although the exact structural arrangement of c-OBCB 3b molecules in solution is difficult to devise from the chemical shifts information. We used the coupling constants from the 1.25 mM and 20 mM ^{1}H NMR spectra to assign the protons (Figure 6).

3.6 NMR titration experiment of c-OBCB 3b/ $PC_{70}BM$

With the observation of self-associated π-interactions of c-OBCB **3b** in solutions from the concentration-dependent ^{1}H NMR study, we hope to use titration experiment

based on ^{1}H NMR spectra to reveal the interactions of electron-donating c- OBCB **3b** and electron-accepting phenyl-C_{70}-butyric acid methyl ester ($PC_{70}BM$) in solution.

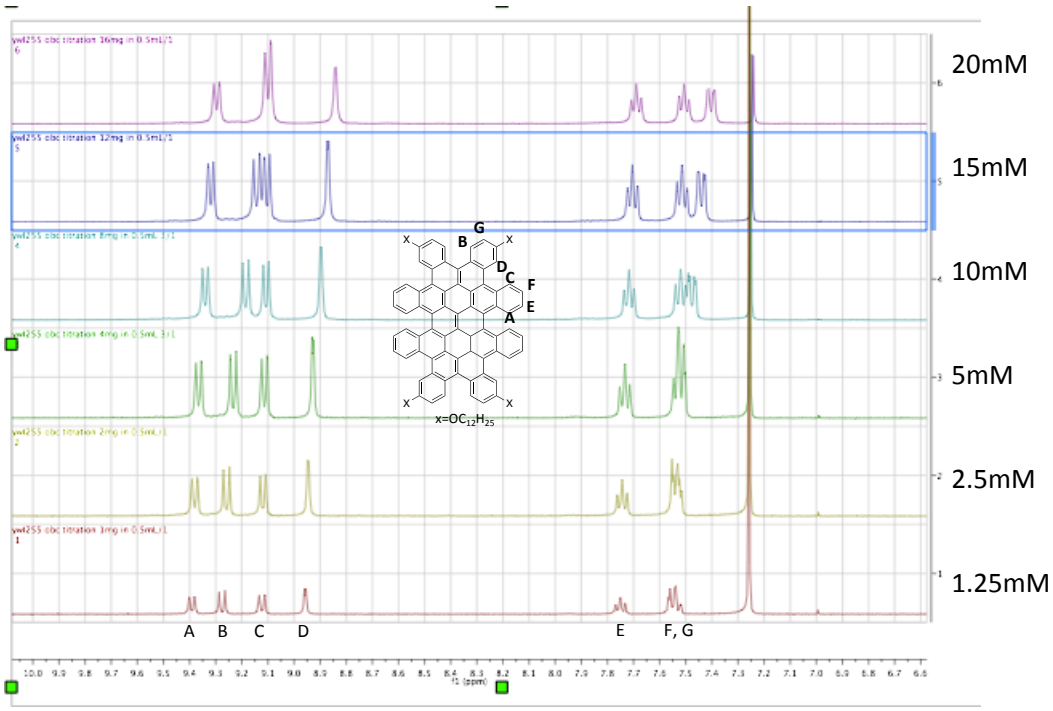

Figure 6. Chemical shifts of c-OBCB **3b** at various concentrations in ^{1}H NMR spectra.

In supramolecular chemistry, the mole ratio method[13] is often used to determine the stoichiometric ratio of host and guest. In our case, we took c-OBCB **3b** as the host, and $PC_{70}BM$ as the guest. We fixed the concentration of $[Host]_0$ or [c-OBCB **3b**]$_0$ and varied the concentration of $[Guest]_0$ or $[PC_{70}BM]_0$, ^{1}H NMR spectra are recorded at various molar ratios of c-OBCB **3b** to $PC_{70}BM$ from 1:0.25 to 1:8 (Figures 7 and 8). The change of chemical shifts for both c-OBCB 3b and $PC_{70}BM$ is obvious for the intermolecular interactions, which we suppose originates from π - π stacking between the two kinds of molecules. To extract semi-quantitative information from these spectra, we plot the chemical shifts of c-OBCB against concentration of $PC_{70}BM$ from the titration study in Figure 9. In both curves, the beginning of the curve decreases and the

end of the curve is nearly flat, suggesting the π-interaction reaches saturation after stoichiometric point of c-OBCB **3b** to $PC_{70}BM$. We are interested in the break point corresponding to the point with the most abrupt change, which corresponds to the $[G]_0/[H]_0$ stoichiometric ratio according to the mole ratio method[4,13]. Thus, we concluded the stoichiometric ratio of c-OBCB **3b** to $PC_{70}BM$ in solution to be 1: 2.

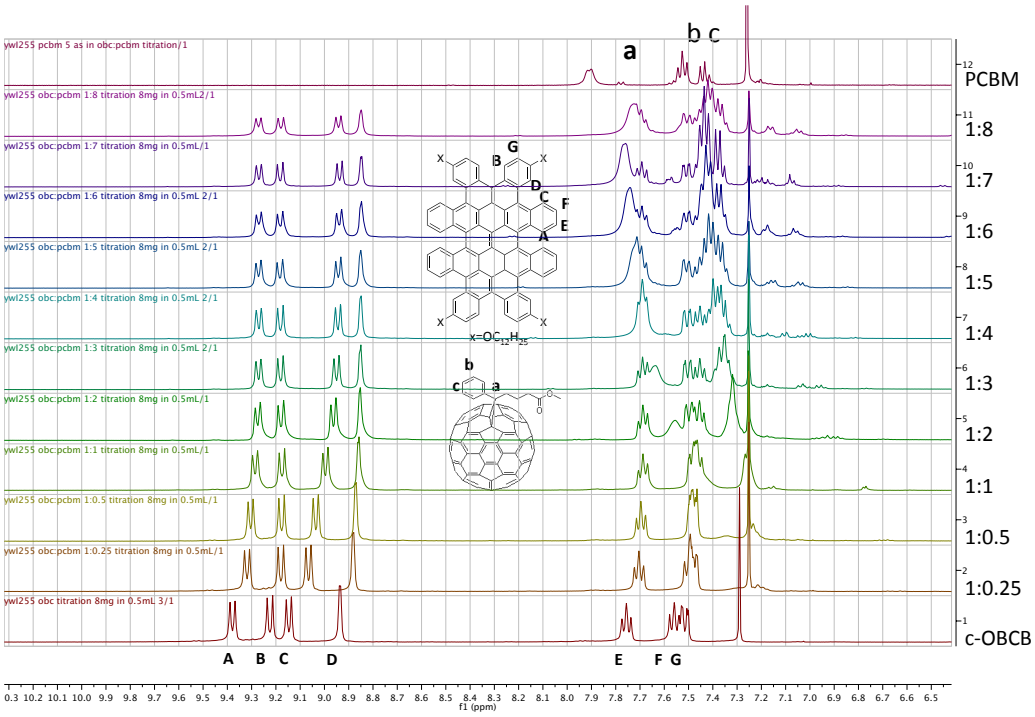

Figure 7. ^{1}H NMR spectra of c-OBCB **3b** and $PC_{70}BM$ mixtures in d-chloroform. The concentration of c-OBCB **3b** is kept constant at 10 mM (8 mg in 0.5 mL $CDCl_3$), and the molar ratio of c-OBCB **3b** to $PC_{70}BM$ varies from 1:0.25 to 1:8.

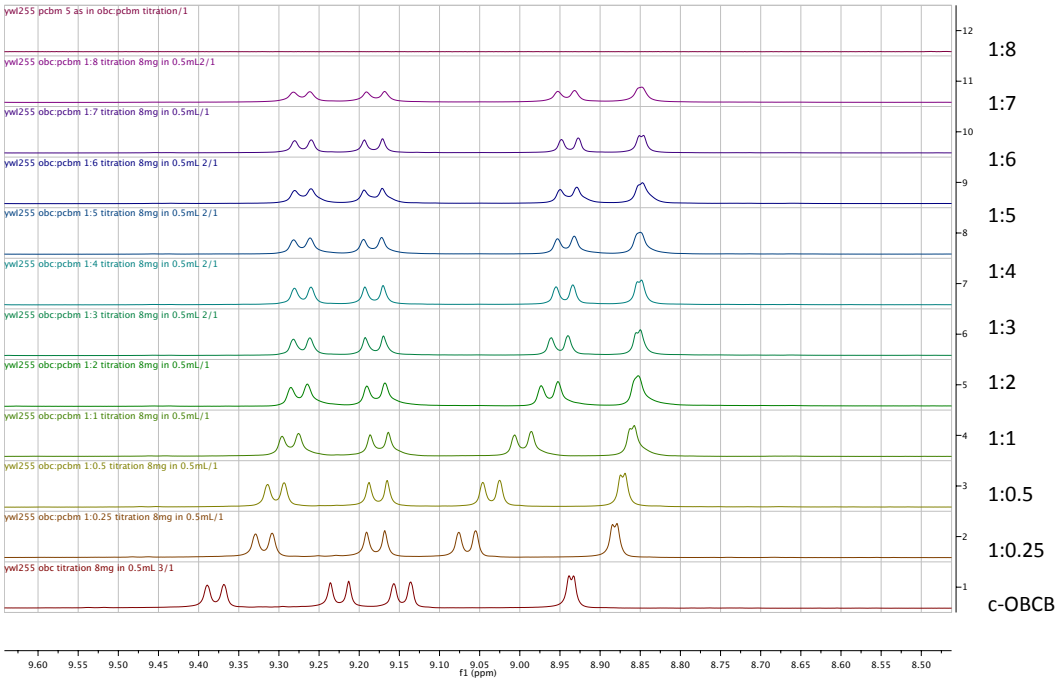

Figure 8. Zoomed in ^{1}H NMR spectra in Figure 7.

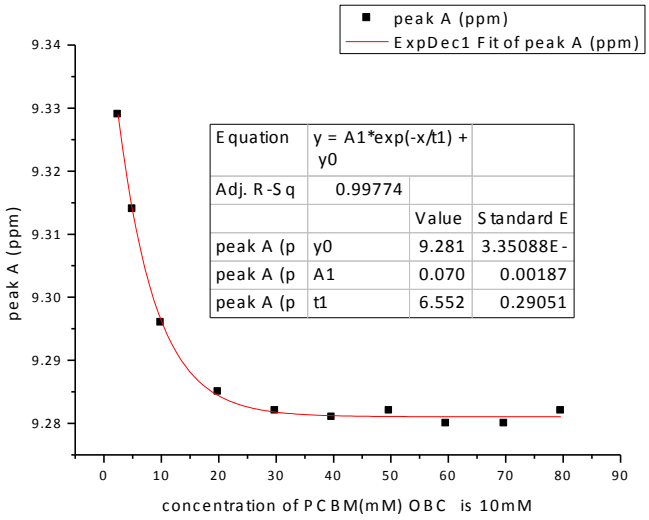

(continue to next page)

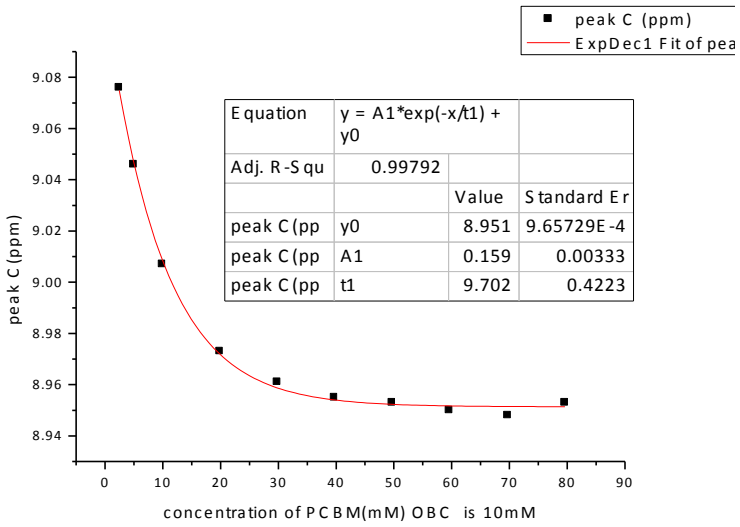

Figure 9. Chemical shifts of peak A (top) and peak B (bottom) from Figures 7 and 8 against the concentration of $PC_{70}BM$.

3.7 Fluorescence quenching titration of c-OBCB 3b/ $PC_{70}BM$

Our previous studies also revealed that the association between the donor and acceptor material plays an important role in solar cell efficiency.[7,8,14] Thus we mixed c-OBCB **3b** and different amount of the n-type phenyl-C_{70}-butyric acid methyl ester ($PC_{70}BM$). Fluorescence quenching studies and Stern-Volmer analysis (Figure 10) give an association constant of 5 x10^4 M^{-1} in chloroform. We believe that the curved structure of the c-OBCB will be able to make a ball-socket interaction with the convex guest $PC_{70}BM$.

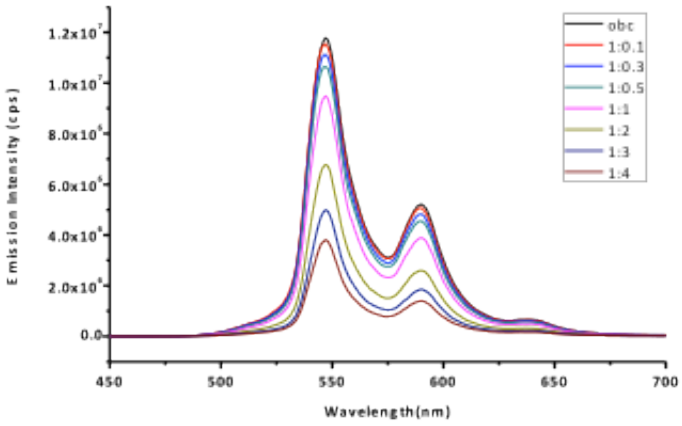

Figure 10. Fluorescence spectra of OBCB **3b** (1 x10^{-3}M in $CHCl_3$) excited at 433nm, with 0, 0.1, 0.3, 0.5, 1, 2, 3, 4 molar equivalents of $PC_{70}BM$ added.

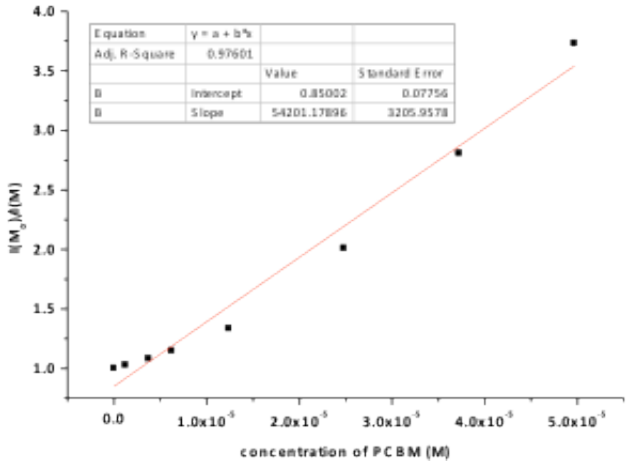

Figure 11. Plot of Stern-Volmer analysis.

3.8 Experimental procedures

3.8.1 Synthesis

General. Reagents employed were either commercially available or prepared according to a known procedure as noted below. Anhydrous and oxygen-free CH_2Cl_2, diethyl ether

and THF were obtained from a Schlenk manifold with purification columns packed with activated alumina and supported copper catalyst (Glass Contour, Irvine, CA). Unless otherwise noted, all reactions were run in oven-dried glassware, and monitored by TLC using silica gel 60 F_{254} precoated plates (EM Science) when necessary. Column chromatography was performed on a CombiFlash® Sg100c system using RediSepTM normal phase silica columns (ISCO, Inc., Lincoln, NE). ^{1}H NMR (400 MHz), and ^{13}C NMR (100 MHz) spectra were recorded on Bruker DRX-300 and Bruker DRX-400 spectrometers at room temperature unless otherwise noted. HRMS were recorded on JEOL JMS-HX110A/110A Tandem mass spectrometer. The photochemistry was carried out according to a reported procedure.[15]

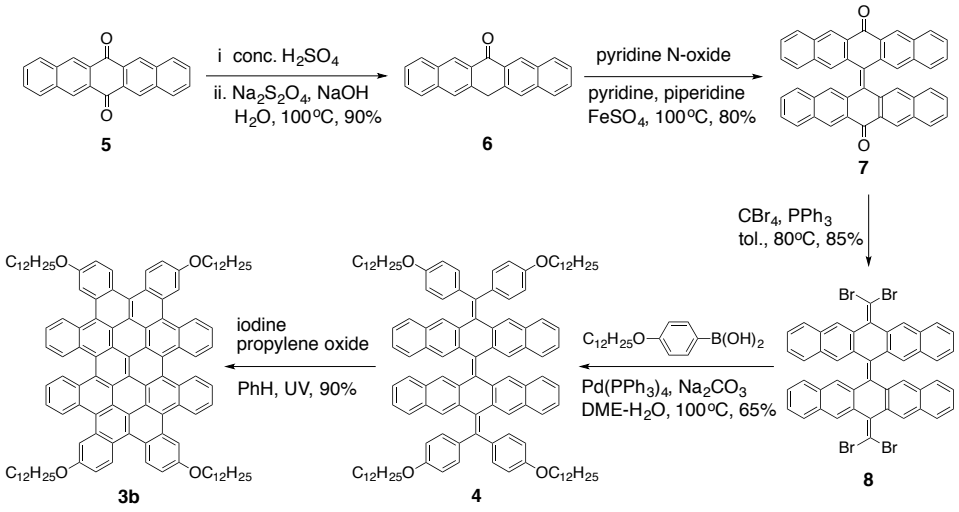

Synthesis of (4-(dodecyloxy)phenyl)boronic acid

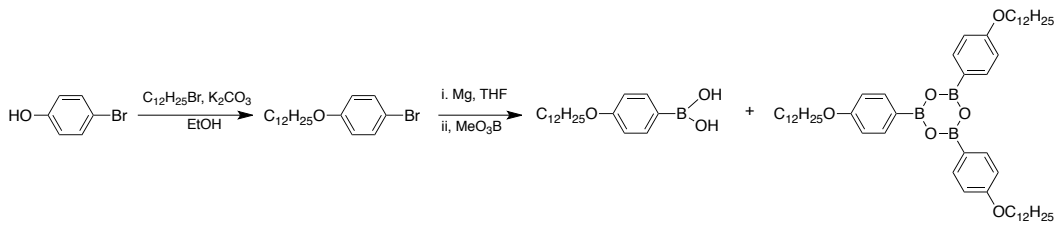

(4-(dodecyloxy)phenyl)boronic acid was prepared according to literature procedure by Cammidge, et al. Boroxine derived from boronic acid exists in the product after purification, which is also reported by Pérez, et al[16],. The mixture of boronic acid and boroxine was used in the Suzuki coupling.

Synthesis of starting materials (6) and (7)

The synthesis of 13,13a-dihydropentacen-6(5a*H*)-one (**6**) was adapted from German literature protocol by Clar et al.[2] Compound **7** was synthesized according to a literature protocol reported by Chen et al.[3] The authors claimed the product contained a small amount of pentacenequinone. However, they mislabeled the 8.97 ppm peak, which belongs to pentacenequione, as a peak in compound **7** in the reported ^{1}H NMR. ^{1}H NMR (400MHz, $CDCl_3$), δ (ppm): 8.76 (s, 4H), 7.99 (d, J=8.4 Hz, 4H), 7.56 (s, 4H), 7.46 (m, 4H), 7.30 (m, 4H), 7.11 (d, J=7.9 Hz, 4H).

Synthesis of 13,13'-bis(dibromomethylene)-13,13a-dihydro-5a*H*,13'*H*-6,6'-bipentacenylidene (8)

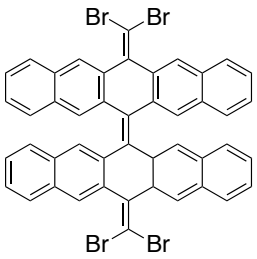

An oven-dried 250 mL two-necked round bottom flask with a condenser were charged with tetrabromomethane (1.66 g, 4 mmol) and triphenylphosphine (2.63 g, 10 mmol), and 50 mL of anhydrous toluene. The mixture was stirred at room temperature for 5 minutes before adding compound **7**. The reaction mixture was stirred under nitrogen at 80 ^{0}C overnight. After cooling down, the reaction mixture was filtered under vacuum. The green solid was collected, dissolved in DCM, and MeOH was added to form yellow precipitate, which was then collected by Millipore to give the titled

compound with 85% yield. ^{1}H NMR (400 MHz, Methylene Chloride-d2) δ (ppm): 8.43 (s, 1H), 7.90 (d, *J* = 8.2 Hz, 1H), 7.63 (s, 1H), 7.48 -7.26 (m, 3H). Compound 8 was not soluble enough to obtain a ^{13}C-NMR spectrum. Molecular Mass (Ion mode:FAB): cald for $C_{46}H_{26}Br_4$ 893.9, found [M+2H] 896.3.

Synsthesis of triolefin 4

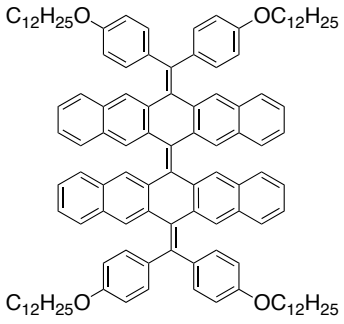

To a 100 mL heavy-walled round bottom flask with a screw thread cap were charged with compound **8** (180 mg, 0.2 mmol), (4-(dodecyloxy)phenyl)boronic acid (612 mg, 2 mmol), sodium carbonate (636 mg, 6 mmol), 15 mL of dimethoxyethane and 5 mL of water, the solution was bubbled for 20 minutes before adding catalyst $Pd(PPh_3)_4$ (46 mg, 0.04 mmol). The reaction mixture was stirred at 100 ^{0}C for 24 hours with the cap closed. The solution was allowed to cool down, extracted with ether and the combined organic layers were dried over $MgSO_4$ and concentrated under vacuum. The crude product was purified by chromatography (1:4 DCM:Hexanes). ^{1}H NMR and ^{13}C NMR are identical as reported in the above synthesis.

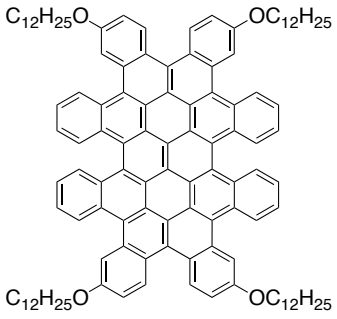

Synthesis of c-OBCB 3b

The photolysis setup has been previously described (Liu, L.; Yang, B.; Katz, T. J.; Poindexter, M. K. *Journal of Organic Chemistry* **1991**, *56*, 3769). ^{1}H NMR and ^{13}C NMR are identical as reported in the methods above. ^{1}H-NMR depends on the concentration.

^{1}H NMR of 0.001 M **c-OBCB 3b** (400 MHz, chloroform-d) δ (ppm): 9.43 – 9.36 (m, 1H), 9.28 (d, *J* = 9.1 Hz, 1H), 9.16 – 9.09 (m, 1H), 8.96 (d, *J* = 2.6 Hz, 1H), 7.75 (ddd, *J* = 8.2, 6.8, 1.3 Hz, 1H), 7.59 – 7.50 (m, 2H), 4.46 (dt, *J* = 9.0, 6.5 Hz, 1H), 4.36 (dt, *J* = 8.9, 6.4 Hz, 1H), 2.04 (p, *J* = 6.5 Hz, 2H), 1.67 (p, *J* = 7.2 Hz, 2H), 1.33 – 1.23 (m, 16H), 0.93 – 0.85 (m, 3H).

^{1}H NMR of 0.02 M **c-OBCB 3b** (400 MHz, chloroform-d) δ (ppm): 9.32 (d, *J* = 8.3 Hz, 1H), 9.12 (d, *J* = 8.7 Hz, 2H), 8.86 (d, *J* = 2.7 Hz, 1H), 7.71 (t, *J* = 7.6 Hz, 1H), 7.53 (t, *J* = 7.6 Hz, 1H), 7.42 (dd, *J* = 9.0, 2.5 Hz, 1H), 4.39 – 4.17 (m, 2H), 1.93 (dt, *J* = 13.0, 6.4 Hz, 2H), 1.48 – 1.27 (m, 18H), 0.90 (t, *J* = 6.6 Hz, 3H).

3.8.2 Theoretical methods of DFT calculations:

The DFT calculations were done with Jaguar (versions 5.0, 6.0 and 6.5) [Schrodinger, L.L.C., Portland, OR, 1991-2005.] Except where specified, complete geometric relaxation was performed. Thermochemistry calculations were performed with hybrid functional of Becke, B3LYP.[17] Selected calculations for **c-OBCB 3a** was done using the generalized gradient approximation (GGA) as formulated by Perdew, Burke and Ernzerhof.[18] These lead to the same conclusions concerning structure and orbital distributions described in the text.

Optimized geometry of **c-OBCB 3a**

angstroms

atom	x	y	z
C1	0.0794666779	0.0934799927	-0.0186909816
C2	0.0426637000	0.0599014049	1.3969246686

C3	1.2785704203	-0.0040468872	2.1107295919
C4	2.4842833987	-0.0255695648	1.3673627295
C5	2.4856966034	-0.0094286853	-0.0120922309
C6	1.2705510353	0.0488440015	-0.7127810586
C7	1.2679887584	0.1006975005	3.5533200189
C8	0.1317501844	0.6627250892	4.1607174947
C9	-1.1123662633	0.7148192464	3.4455339616
C10	-1.1894648608	0.2237826612	2.1329131441
C11	-2.2750774962	1.2845274477	4.0751700916
C12	-2.1727837868	1.8446352106	5.3837177745
C13	-0.9345031028	1.8076921824	6.0952266100
C14	0.2185769488	1.1913037638	5.4935269006
C15	-3.3045623620	2.4459017709	5.9764479150
C16	-4.4857958147	2.6528744820	5.1988660703
C17	-4.5377340337	2.2101289527	3.8587163738
C18	-3.4987459823	1.3406676493	3.3778691434
C19	-5.6400191426	3.2666581624	5.8026331005

C20	-5.5905313935	3.6845157919	7.1785820593
C21	-4.3964552565	3.4761891473	7.9535462554
C22	-3.2540423667	2.8417661473	7.3483955209
C23	-2.0712071453	2.6564211242	8.0948990545
C24	-0.8542381049	2.3366122939	7.3995863869
C25	-6.8127587706	3.4487545320	5.0524245136
C26	-6.7132292080	3.3945190035	3.6073277623
C27	-5.5780804775	2.7744389636	3.0079034078
C28	-2.5009633493	-0.1058264228	1.6139522661
C29	-3.6566899363	0.4225534827	2.2590103927
C30	1.4276934298	1.1138140042	6.2011575703
C31	1.6141186820	2.0148878615	7.3193250653
C32	0.4767128983	2.6404237483	7.9081273559
C33	-4.3427683585	3.8984436645	9.2922296363
C34	-3.3151365342	3.3322201632	10.1429710959
C35	-2.1882202197	2.6954970101	9.5465954707
C36	-7.6446363836	4.0589290445	2.7691792377

C37	-7.4959540174	4.0879190970	1.3980156445
C38	-6.3743514894	3.4813579735	0.8092955670
C39	-5.4331454513	2.8567989835	1.6007435596
C40	-6.7119056564	4.2976666561	7.7671850476
C41	-7.9975896139	4.1234873384	7.1266950051
C42	-8.0477083677	3.6847750649	5.7678487249
C43	-6.5104539403	5.0623725736	8.9786931417
C44	-5.3205421331	4.8623370112	9.7428208050
C45	-1.2877845361	1.9937157603	10.3850834560
C46	-1.4447678435	1.9573601501	11.7548483712
C47	-2.5445723635	2.6013452799	12.3445476725
C48	-3.4626144858	3.2581683102	11.5516480608
C49	2.9056152253	2.4185149714	7.7425739647
C50	3.0810297540	3.3905415723	8.7047280292
C51	1.9611323703	4.0239341217	9.2663466599
C52	0.6931504082	3.6620403947	8.8633852864
C53	2.3480144549	-0.3341125936	4.4123362780

C54	2.4194137232	0.1644790342	5.7489682243
C55	-4.9257430908	-0.0801484159	1.8876335441
C56	-5.0705493195	-1.0157798937	0.8850307891
C57	-3.9359138669	-1.5088944230	0.2217893152
C58	-2.6813879930	-1.0698291705	0.5899152818
C59	-9.2168226909	4.2448269519	7.8401803426
C60	-10.4329043282	3.9673851232	7.2515566778
C61	-10.4803570290	3.5222268739	5.9211407258
C62	-9.3106528846	3.3717152277	5.2062048713
C63	-5.0757380988	5.7172556573	10.8478478544
C64	-5.9616297043	6.7110349114	11.2074715769
C65	-7.1308257148	6.9087432627	10.4560550930
C66	-7.3882001481	6.1084067304	9.3625724836
C67	3.3885954587	-0.3836467337	6.6243623969
C68	4.2749365959	-1.3549585274	6.2071279140
C69	4.2115731880	-1.8384727952	4.8907723214
C70	3.2597240299	-1.3455745869	4.0221596871

H1	-0.8460731933	0.2232578766	-0.5658120488
H2	1.2669139880	0.1024020098	-1.7977046650
H3	3.4285875295	0.0016958780	-0.5514666378
H4	3.4287681189	0.0134681825	1.8946464680
H5	3.1653255189	-1.7896749227	3.0396331758
H6	4.8798313626	-2.6315159712	4.5671692512
H7	4.9909293383	-1.7724156367	6.9095253842
H8	3.3935356725	-0.0762678526	7.6623601486
H9	3.7754911929	2.0047844188	7.2492475257
H10	4.0838853792	3.6957738700	8.9902511934
H11	2.0901570522	4.8236998797	9.9902444828
H12	-0.1572323972	4.1967002871	9.2642915557
H13	-0.4688477056	1.4480073380	9.9364798779
H14	-0.7415519034	1.3997558892	12.3670137419
H15	-2.7013466640	2.5450557756	13.4180141972
H16	-4.3552970838	3.6626748607	12.0106620121
H17	-4.1354615124	5.6374137459	11.3779843512

H18	-5.7288942105	7.3676829172	12.0411183904
H19	-7.8095219867	7.7202457267	10.7037779746
H20	-8.2434164447	6.3352244619	8.7391064054
H21	-9.1900321753	4.4915333797	8.8934630623
H22	-11.3460585388	4.0489802850	7.8343731574
H23	-11.4304896468	3.2550786853	5.4671665647
H24	-9.3532851338	2.9483513137	4.2105977763
H25	-8.4608245624	4.6074868932	3.2206295834
H26	-8.2181063847	4.6193731261	0.7850154581
H27	-6.2237844581	3.5357362760	-0.2653483115
H28	-4.5437819088	2.4526460476	1.1363537219
H29	-5.8022840920	0.2597914042	2.4233388920
H30	-6.0583749438	-1.3923426013	0.6350123119
H31	-4.0386912522	-2.2706252509	-0.5459719488
H32	-1.8123108112	-1.5327843404	0.1417941783

3.8.3 X-ray diffraction.

The X-ray diffraction measurements were performed on an Inel CPS 120 diffractometer using Ni filtered Cu Kα X-rays using a solid sample holder. The instrument was calibrated using an Y_2O_3/Silver Behenate mixture. See reference 1[1].

3.8.4 UV-vis spectroscopy.

General Procedure and Instrumentation: Absorption spectra were taken on a Shimadzu UV-1800 spectrophotometer. Stock solutions of **c-OBCB 3b** were prepared with anhydrous chloroform as solvent. A 1-cm quartz cuvette was charged with appropriate volume of blank chloroform and a background spectrum was recorded. The cuvette was charged with stock solution of **c-OBCB 3b** in chloroform and an absorption spectrum was recorded. The experiment was repeated to record spectra of seven different concentrations of **c-OBCB 3b** (as listed in the graph below). Linear regression of the absorption at peak 433 nm vs. concentration was used to calculate the extinction coefficient according Beer-Lambert law A=εlc, where ε is the extinction coefficient, l is the cuvette width that equals 1cm and c is the molar concentration of the sample. The extinction coefficient of the whole spectrum was proportionate to the value at 433 nm.

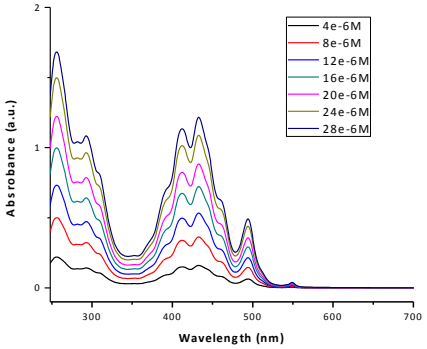

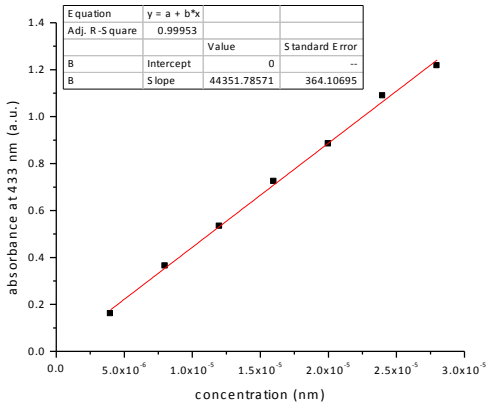

3.8.5 Fluorescence spectroscopy.

Solution photoluminescence spectra were taken with a Jobin Yvon Fluorolog-3 Spectrofluorometer (Model FL-TAU3) from solution of **c-OBCB 3b**. The samples were excited at the wavelength of maximum absorption (433 nm), and the integration time was 2 s. The samples were made from a stock solution of **c-OBCB 3b** and a stock solution of $PC_{70}BM$. The final concentration of **c-OBCB 3b** was kept constant to be 1 $x10^{-3}$ M, and 0, 0.1, 0.3, 0.5. 1, 2, 3, 4 molar equivalents of $PC_{70}BM$ were added to make eight samples. According to Stern-Volmer analysis, the emission intensity at 549 nm was plotted with respect to the concentration of $PC_{70}BM$ and the linear regression gives an association constant of ~5 $x10^4$ M^{-1}.

3.8.6 Cyclic Voltammetry

General Procedure and Data Analysis: Cyclic voltammetry (CV) was performed using a CHI600c potentiostat interfaced to a PC using the Chi600c electrochemical analyzer software package. The cell was a standard three-electrode setup using a glassy carbon working electrode, a Ag/AgCl reference electrode, and a platinum counter electrode**.** All electrodes were purchased from Bioanalytical Systems, Inc. Measurements were carried out under argon in anhydrous dichloromethane solution with a tetrabutylammonium hexafluorophosphate as supporting electrolyte (0.1 M). All potentials were measured as the midpoint peak oxidation potential with respect to the Fc+/Fc redox couple. The scan rate in was 0.01 V/s. Calculated from the curve in Figure 5, the HOMO, LUMO and band gap of **c-OBCB 3b** are -5.4 eV, -3.0 eV and 2.4 eV, respectively, by using ferrocene as the standard reference.

3.9 Supporting information

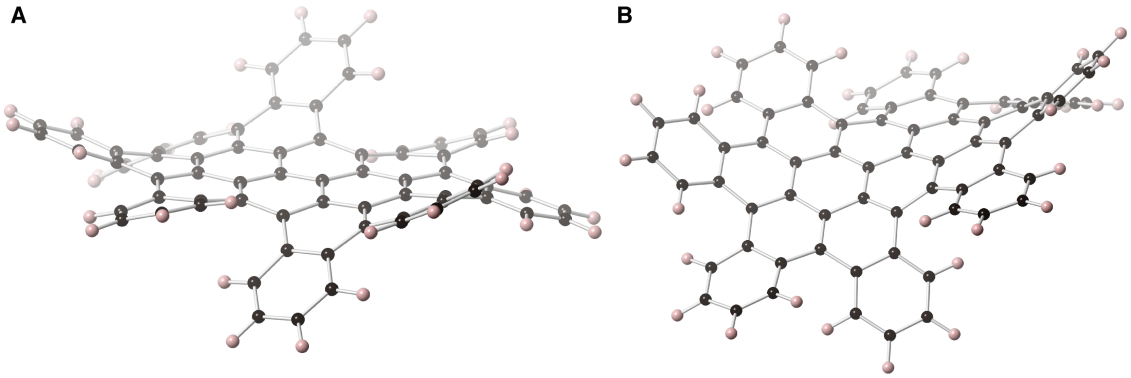

Figure S1. Two higher energy confirmations found for the **c-OBCB 1a** using DFT calculations.

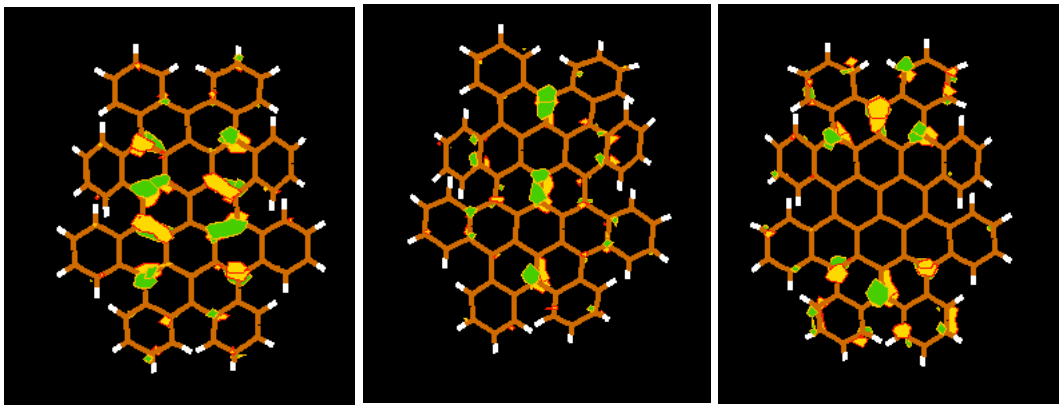

HOMO HOMO+1 HOMO+2

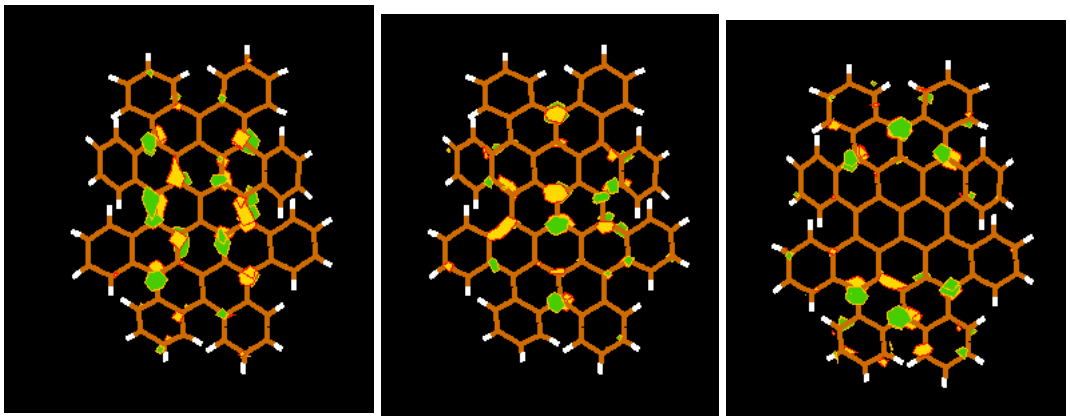

LUMO LUMO-1 LUMO-2

Figure S2. Frontier orbitals of c-OBCB from DFT calculation(6-31G**,B3LYP)

(Software: Molden 5.3)

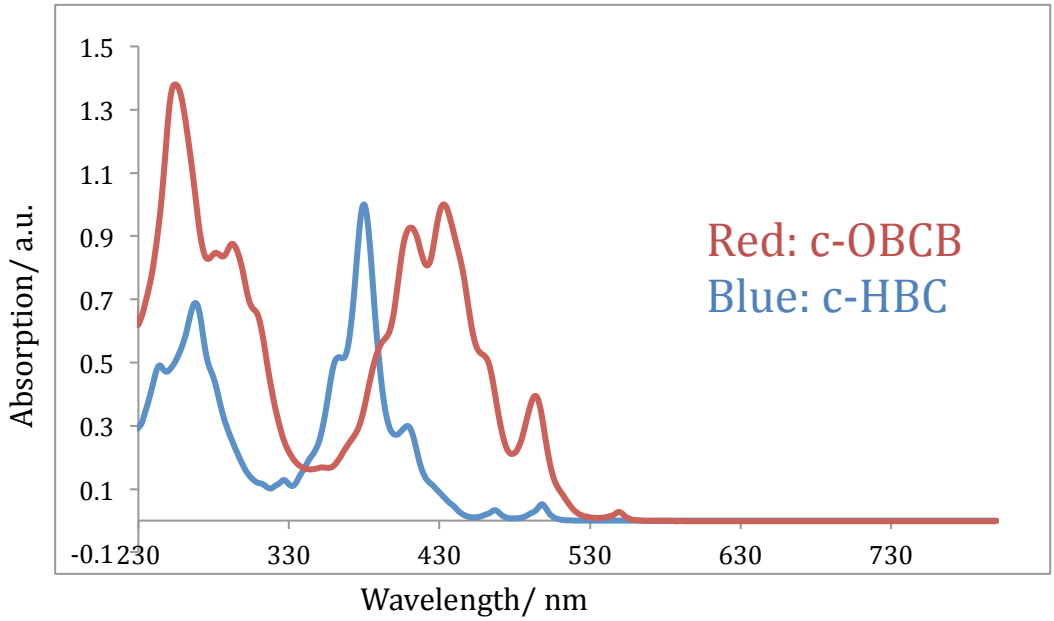

Figure S3. Overlapped absorption spectrao of c-HBC and c-OBCB

3.10 References

(1) This chapter is adapted from our previous publication: Xiao, S. X.; Kang, S. J.; Wu, Y.; Ahn, S.; Kim, J. B.; Loo, Y. L.; Siegrist, T.; Steigerwald, M. L.; Li, H. X.; Nuckolls, C. *Chem. Sci.* **2013**, *4*, 2018.

(2) Clar, E.; Mackay, C. C. *Tetrahedron* **1972**, *28*, 6041.

(3) Xiao, S., Doctoral thesis, Columbia University, 2007.

(4) Clar, E. *Chem. Ber.* **1949**, *82*, 495-514.

(5) Zhang, X.; Jiang, X.; Luo, J.; Chi, C.; Chen, H.; Wu, J. *Chem. Eur. J.* **2010**, *16*, 464.

(6) Desai, N. B.; McKelvie, N.; Ramirez, F. *J. Am. Chem. Soc.* **1962**, *84*, 1745.

(7) Plunkett, K. N.; Godula, K.; Nuckolls, C.; Tremblay, N.; Whalley, A. C.; Xiao, S. X. *Org. Lett.* **2009**, *11*, 2225.

(8) Chiu, C. Y.; Kim, B.; Gorodetsky, A. A.; Sattler, W.; Wei, S. J.; Sattler, A.; Steigerwald, M.; Nuckolls, C. *Chem. Sci.* **2011**, *2*, 1480.

(9) A. Bauer, M. W. Miller, S. F. Vice, S. W. McCombie, *Synlett* **2001**, 254–256

(10) Katsuyama, I.; Khalil, A. A.; Dunbar, C.; Zjawiony, J. K. *Spectrosc. Lett.* **2003**, *36*, 477.

(11) Mitra, A.; Seaton, P. J.; Ali Assarpour, R.; Williamson, T. *Tetrahedron* **1998**, *54*, 15489.

(12) Attimonelli, M.; Sciacovelli, O. *Organic Magnetic Resonance* **1979**, *12*, 17.

(13) Thordarson, P. *Chem. Soc. Rev.* **2011**, *40*, 1305.

(14) Tremblay, N. J.; Gorodetsky, A. A.; Cox, M. P.; Schiros, T.; Kim, B.; Steiner, R.; Bullard, Z.; Sattler, A.; So, W. Y.; Itoh, Y.; Toney, M. F.; Ogasawara, H.; Ramirez, A. P.; Kymissis, I.; Steigerwald, M. L.; Nuckolls, C. *ChemPhysChem* **2010**, *11*, 799.

(15) Liu, L.; Yang, B.; Katz, T. J.; Poindexter, M. K. *J. Org. Chem.* **1991**, *56*, 3769.

(16) Romero, C.; Peña, D.; Pérez, D.; Guitián, E. *Chem. Eur. J.* **2006**, *12*, 5677.

(17) Becke, A. D. *J. Chem. Phys.* **1993**, *98*, 5648.

(18) Perdew, J. P.; Burke, K.; Ernzerhof, M. *Phys. Rev. Lett.* **1996**, *77*, 3865.

3.11 Appendix

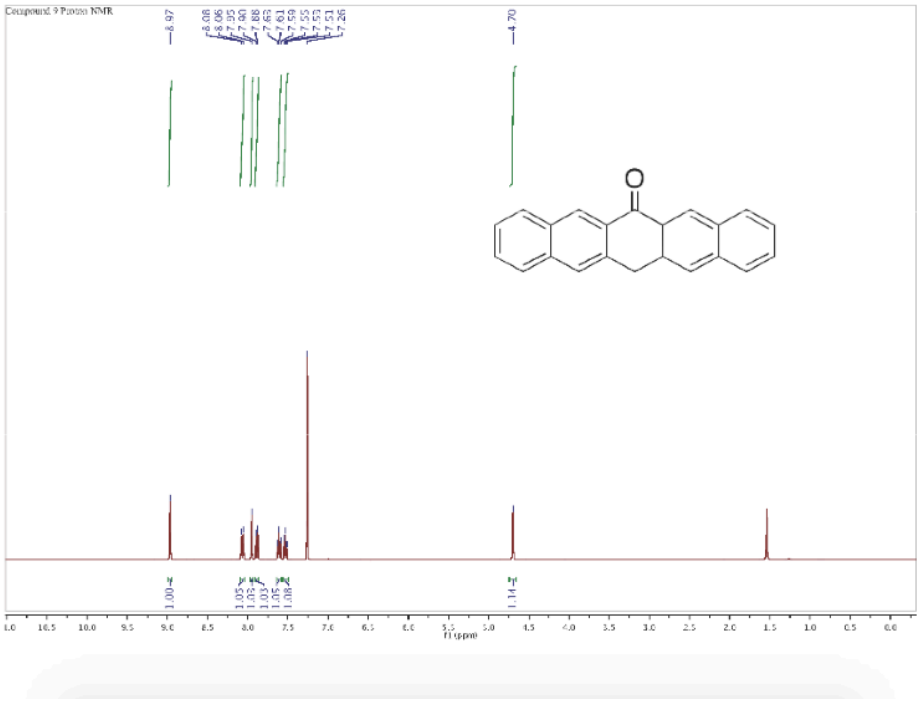

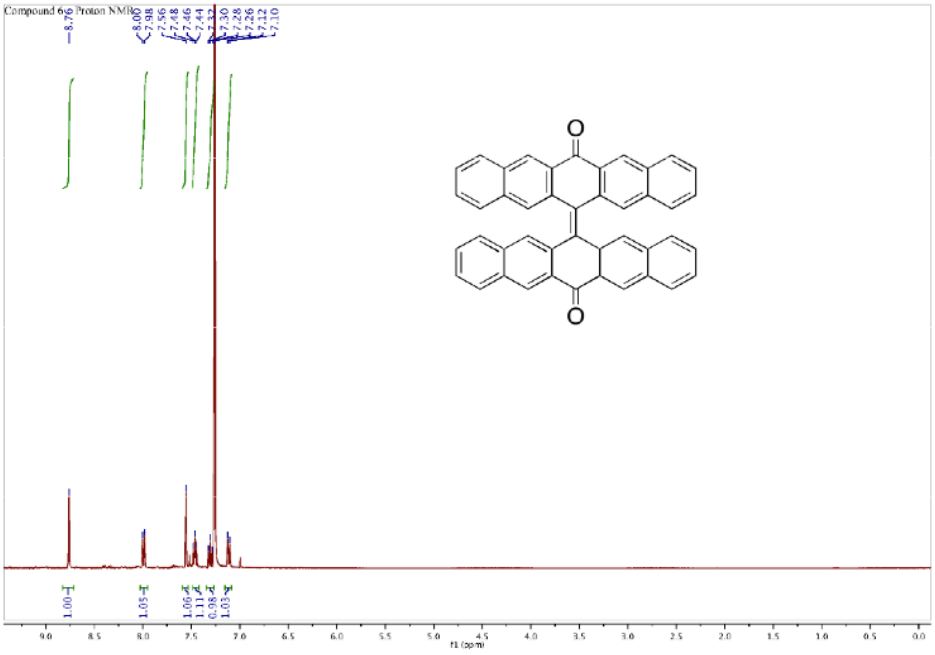
Compound 6 - Proton NMR
8.79
8.08
7.98
7.56
7.48
7.46
7.44
7.30
7.28
7.26
7.12
7.10
O
O
1.00
1.05
1.06
1.11
0.98
1.03
f1 (ppm)

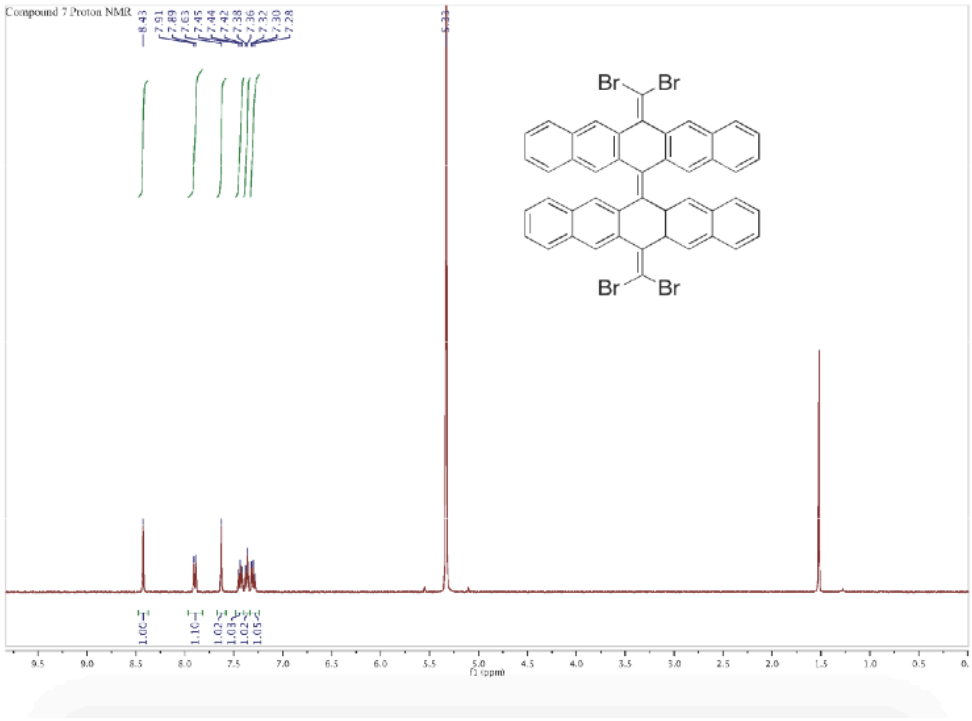
Compound 7 Proton NMR
8.43
7.91
7.89
7.65
7.45
7.44
7.42
7.38
7.36
7.32
7.30
7.28
5.33
Br
Br
Br
Br
1.00
1.10
1.02
1.03
1.02
1.05
f1 (ppm)

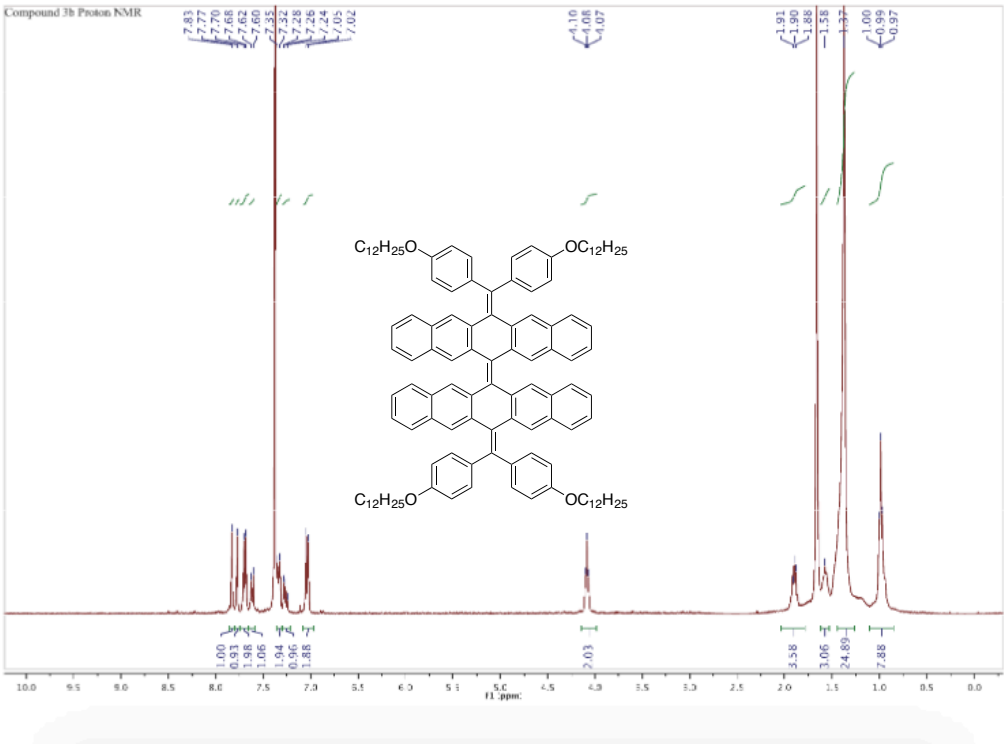
Compound 3h Proton NMR
$C_{12}H_{25}O$
$OC_{12}H_{25}$
$C_{12}H_{25}O$
$OC_{12}H_{25}$

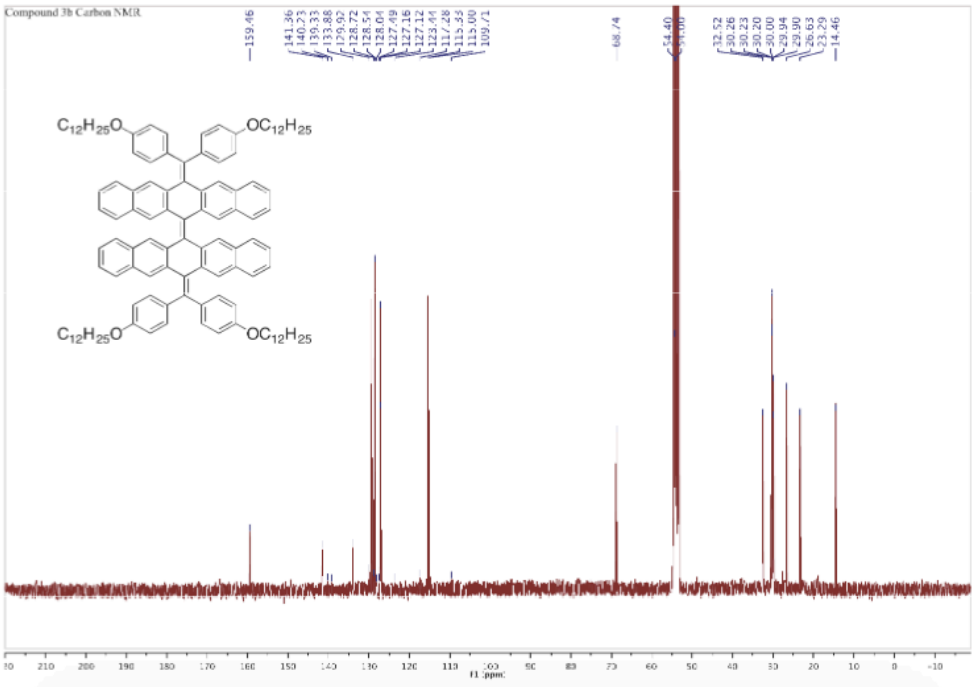
Compound 3b Carbon NMR
159.46
141.36
140.23
139.33
133.88
129.92
128.72
128.54
128.04
127.49
127.16
127.12
123.64
123.28
115.35
115.00
109.71
68.74
54.40
54.08
32.52
30.26
30.23
30.20
30.00
29.94
29.90
29.85
26.55
23.29
14.46
C12H25O
OC12H25
C12H25O
OC12H25
f1 (ppm)

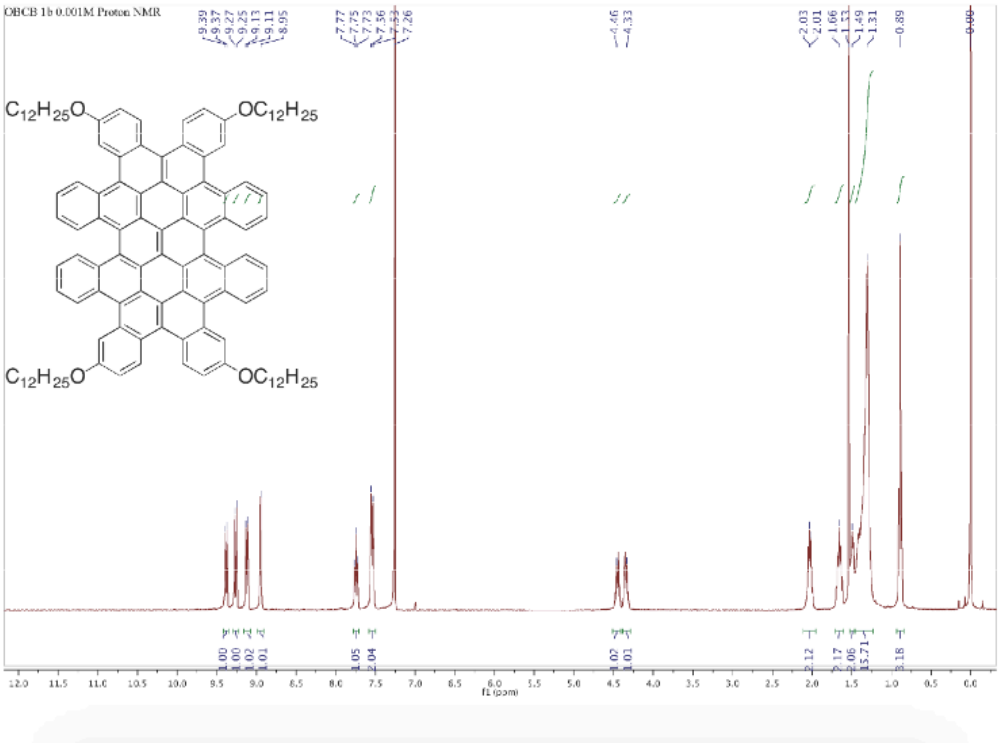
OBCB 1b 0.001M Proton NMR
C12H25O
OC12H25
C12H25O
OC12H25
f1 (ppm)

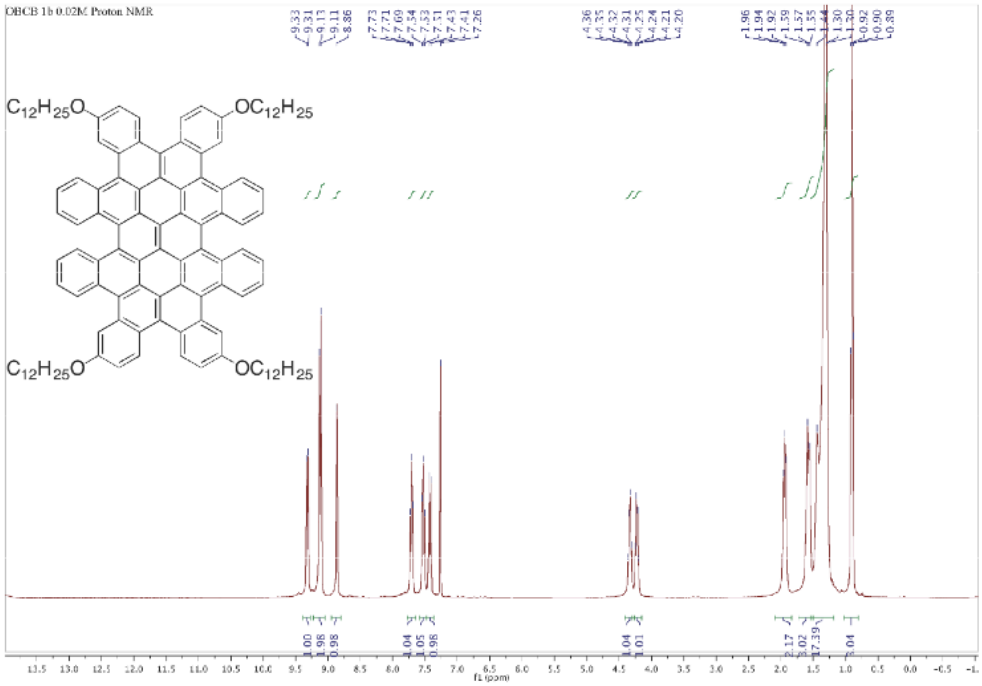
OBCB 1b 0.02M Proton NMR
$C_{12}H_{25}O$
$OC_{12}H_{25}$
$C_{12}H_{25}O$
$OC_{12}H_{25}$
f1 (ppm)

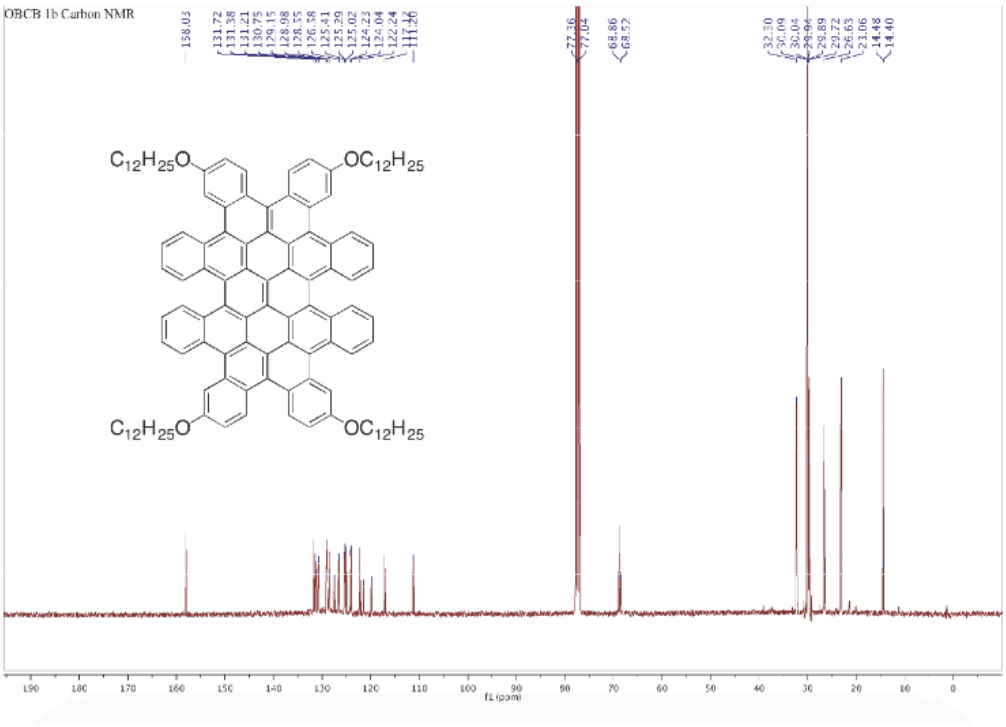
OBCB 1b Carbon NMR
158.03
131.72
131.38
131.21
130.75
129.15
128.98
128.55
126.58
125.41
125.29
125.02
124.23
124.04
122.24
77.36
77.04
68.86
68.52
32.30
30.09
30.04
29.89
29.72
29.65
23.06
14.48
14.40
C12H25O
OC12H25
C12H25O
OC12H25
f1 (ppm)

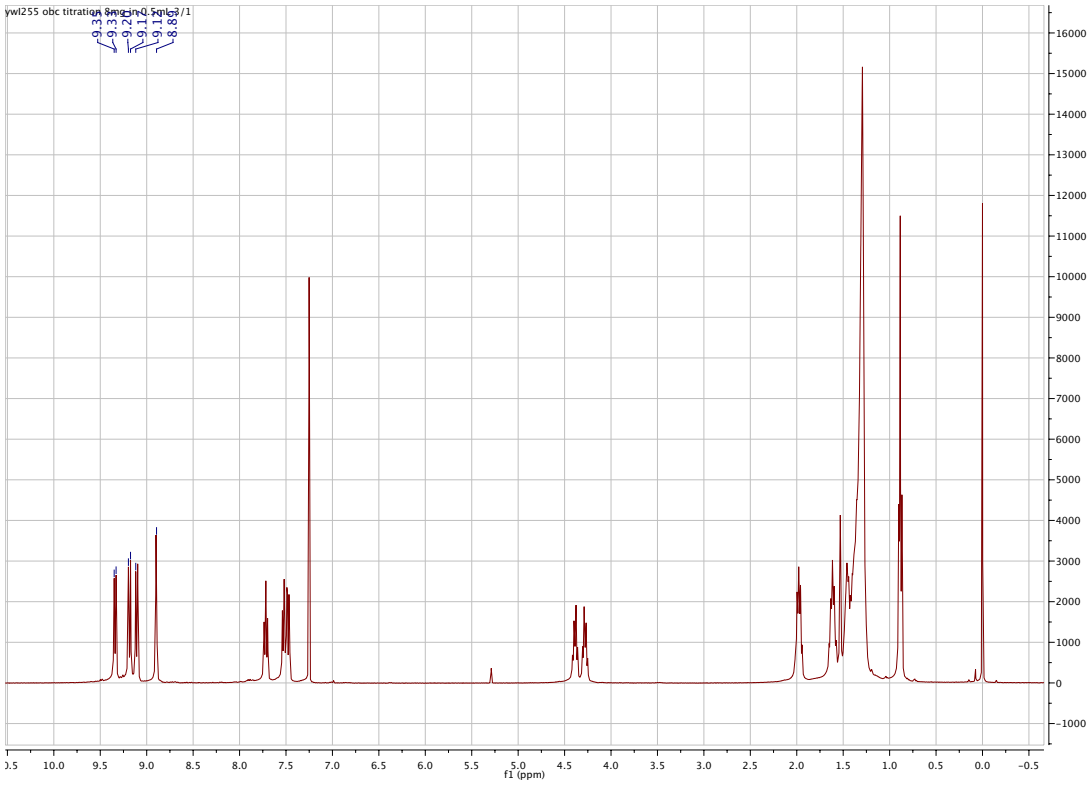

c-OBCB only 16 mg/mL

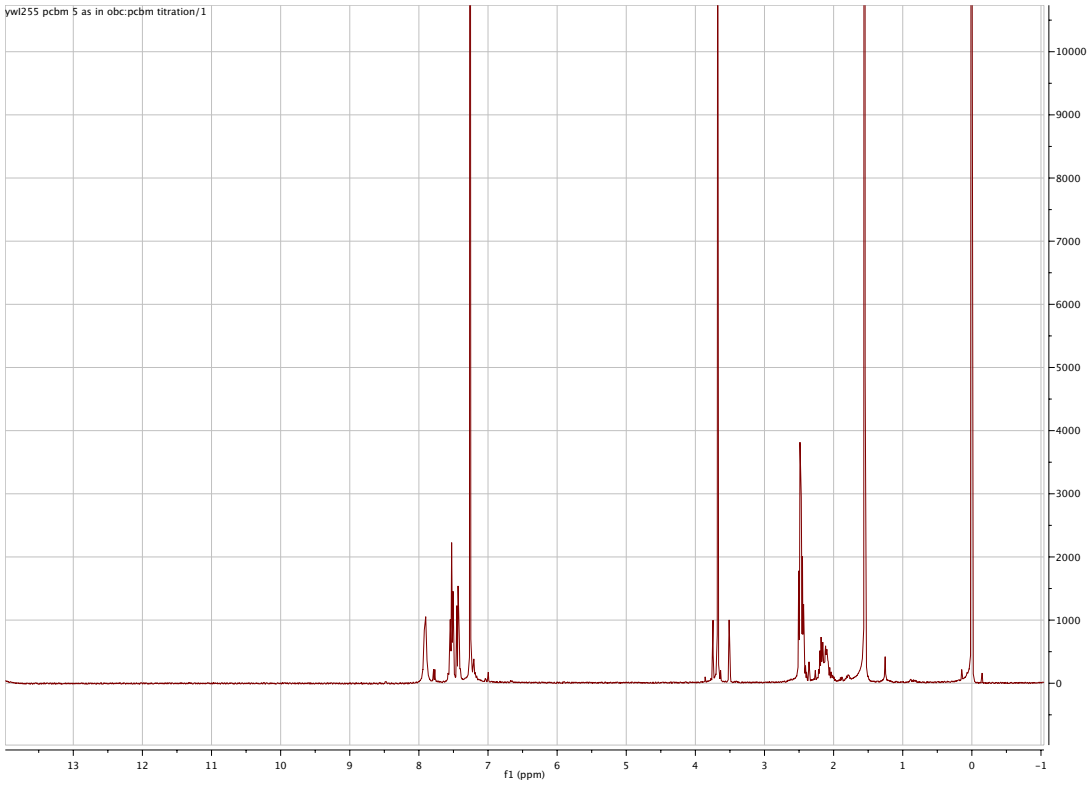
ywl255 pcbm 5 as in obc:pcbm titration/1
10000
9000
8000
7000
6000
5000
4000
3000
2000
1000
0
13
12
11
10
9
8
7
6
5
4
3
2
1
0
−1
f1 (ppm)

PCBM only

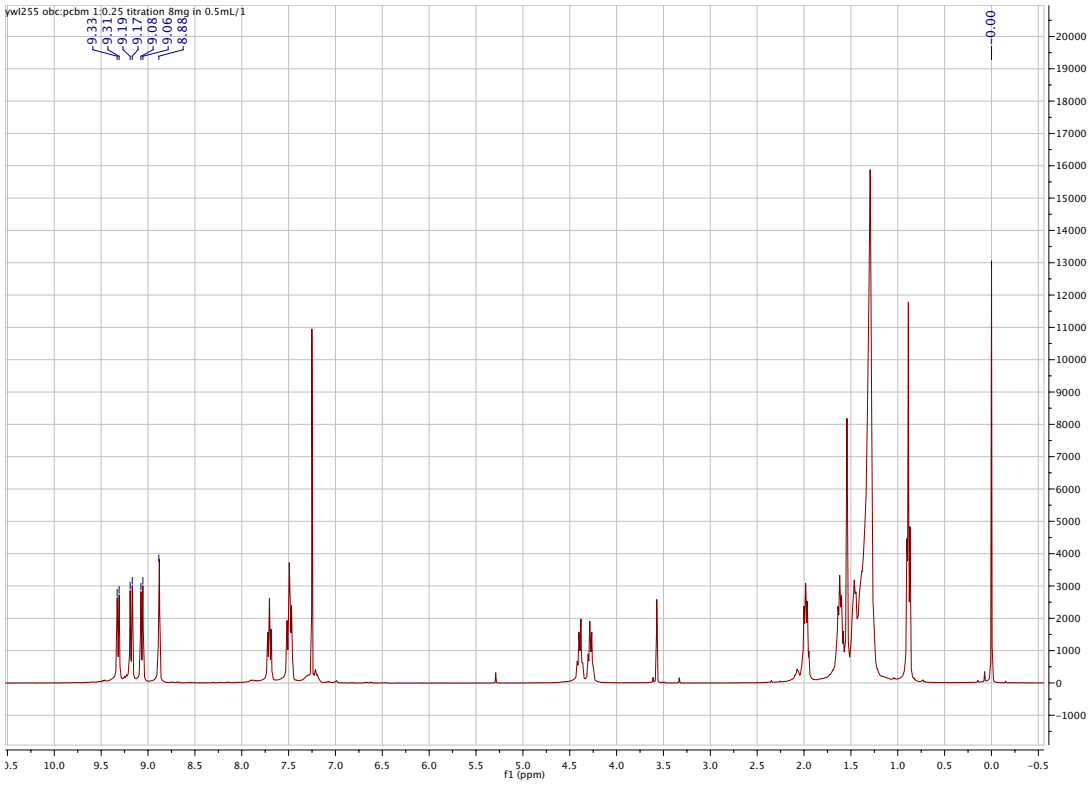

c-OBCB:PCBM=1:0.25

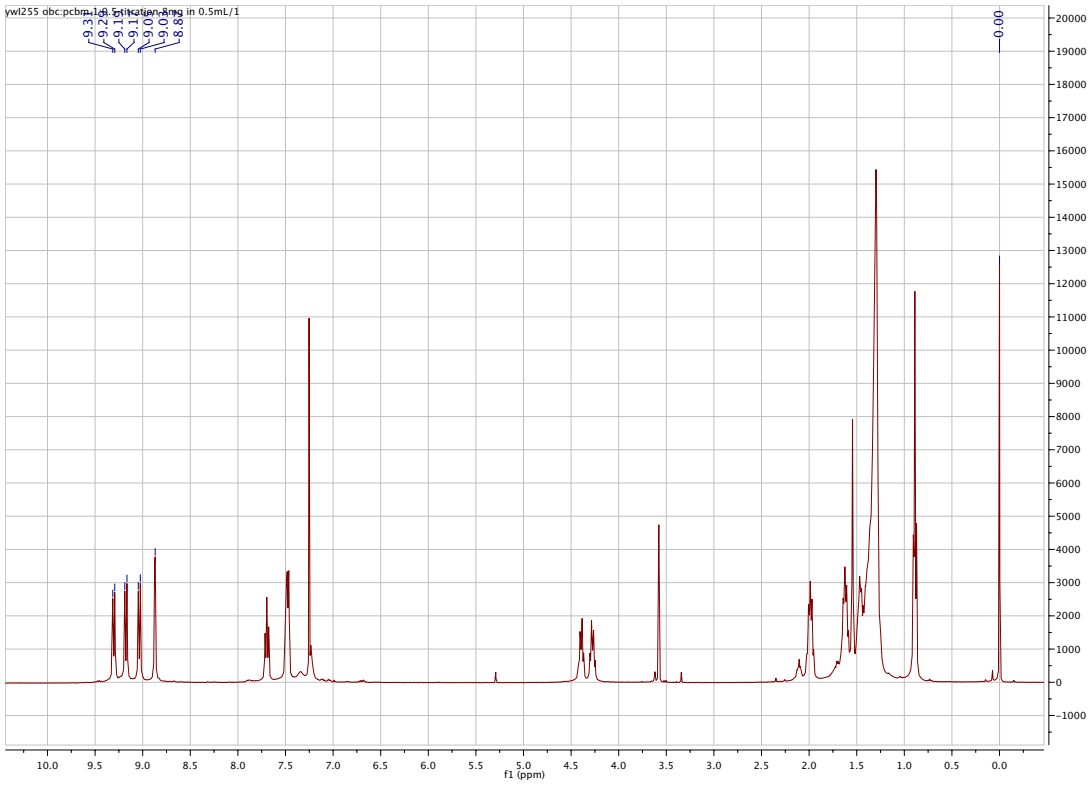

c-OBCB:PCBM=1:0.5

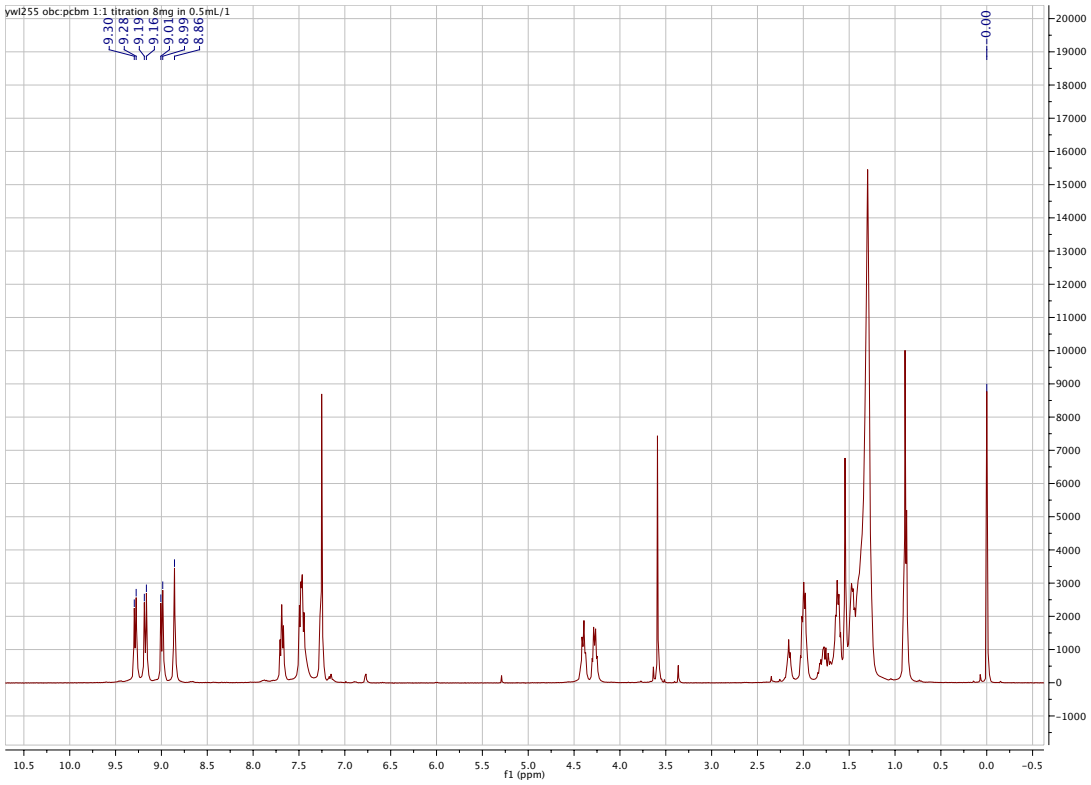

c-OBCB:PCBM=1:1

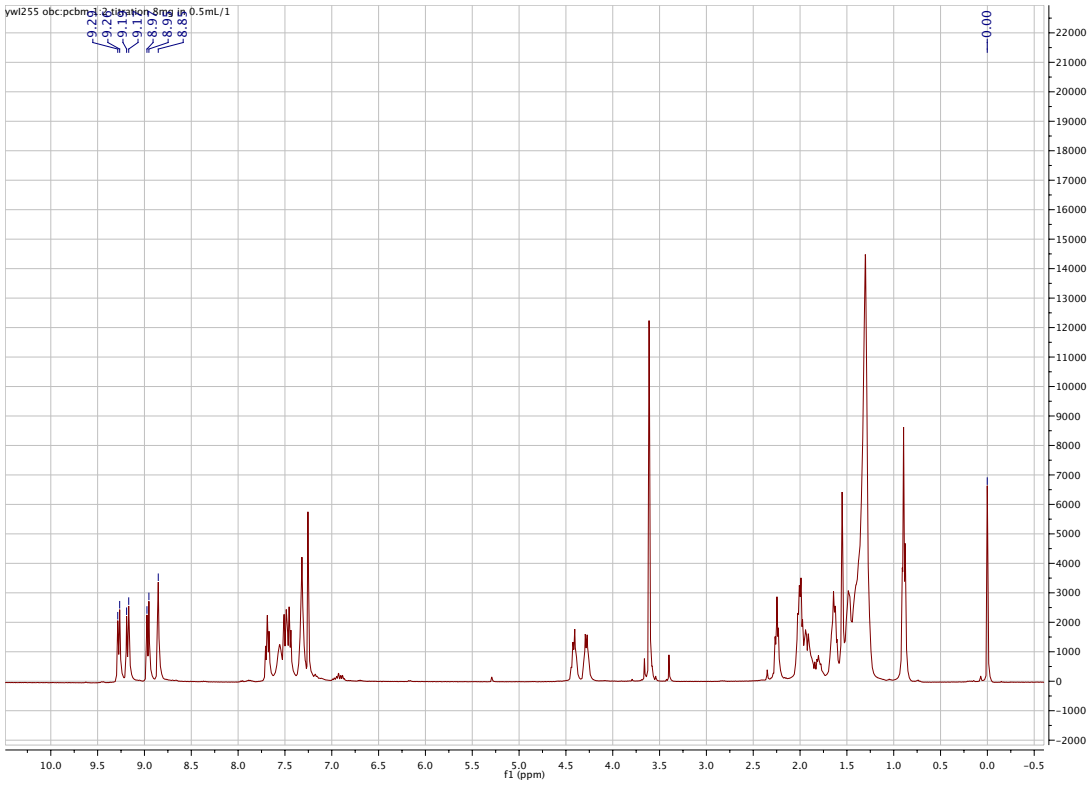

c-OBCB:PCBM=1:2

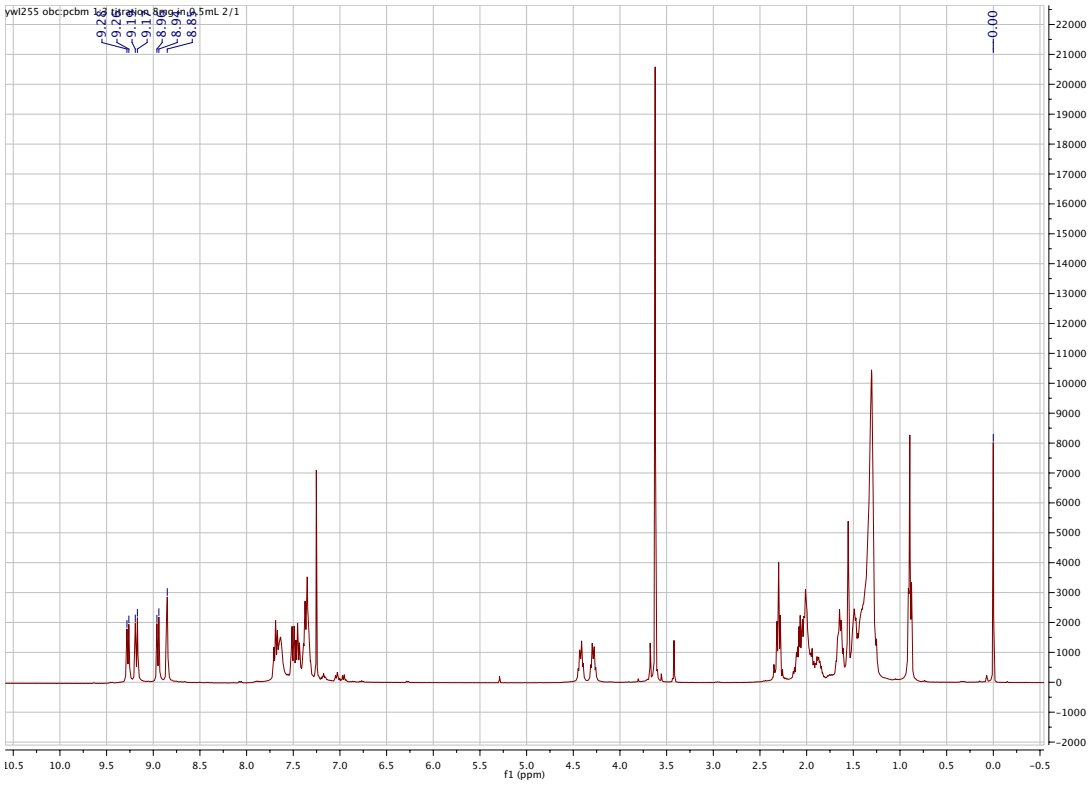

c-OBCB:PCBM=1:3

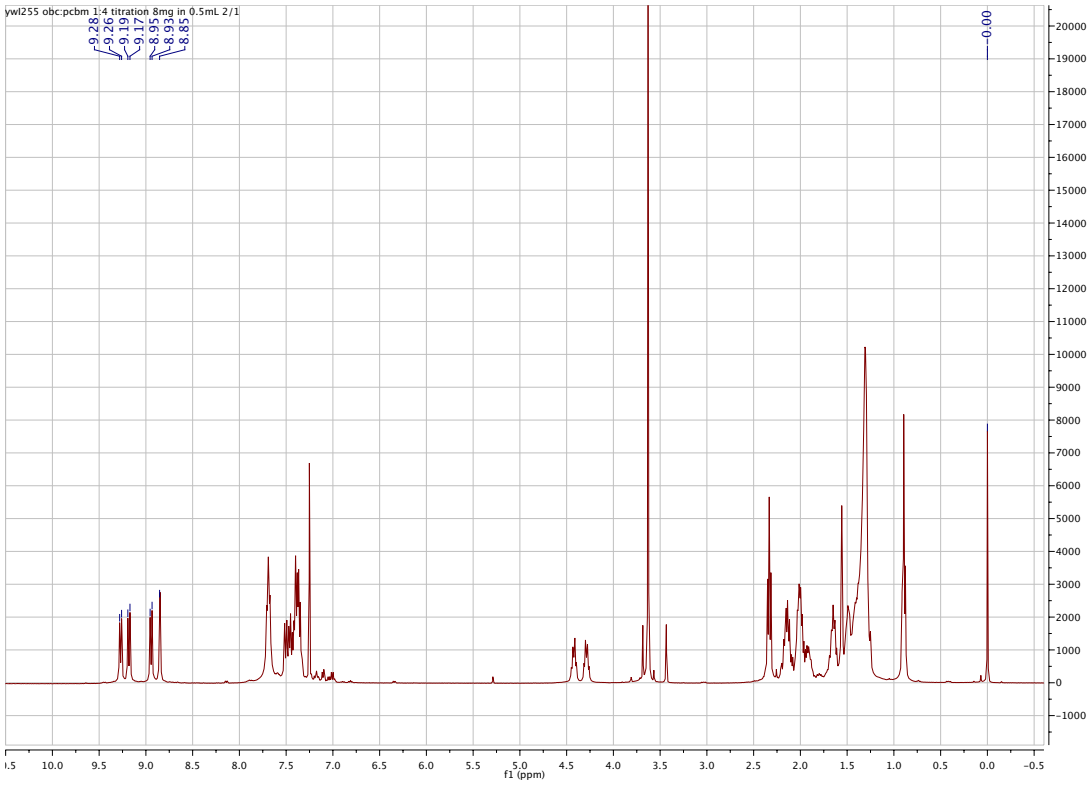

c-OBCB:PCBM=1:4

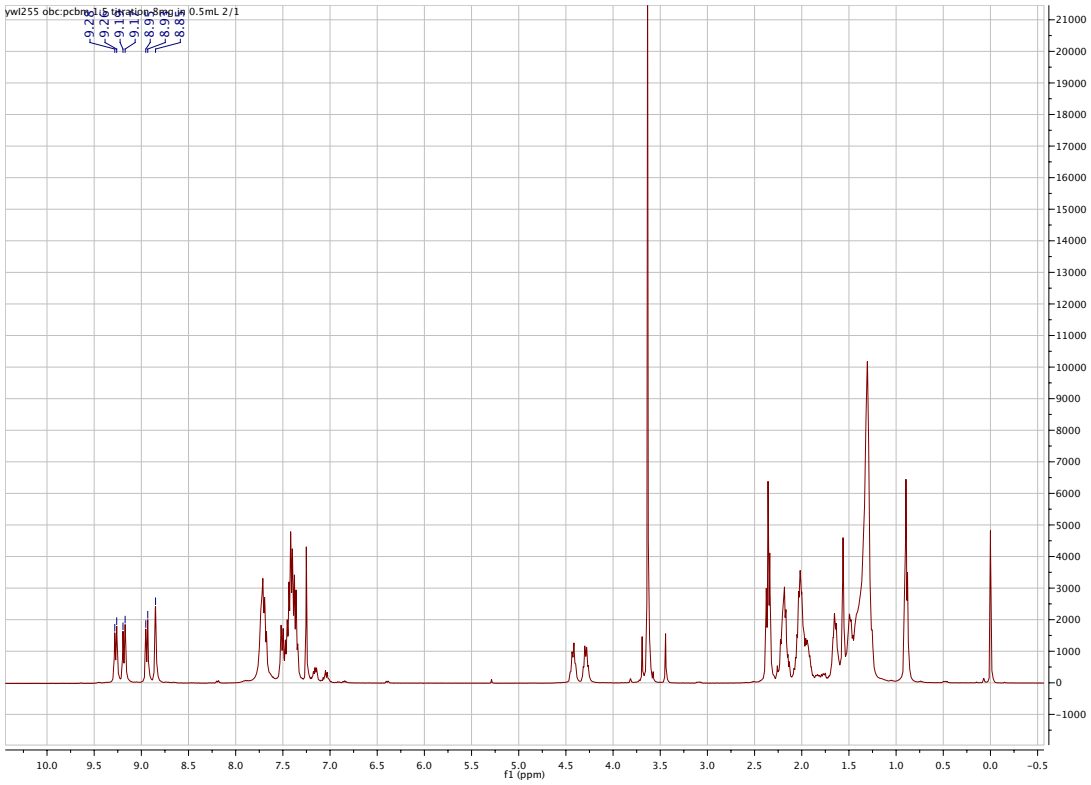

c-OBCB:PCBM=1:5

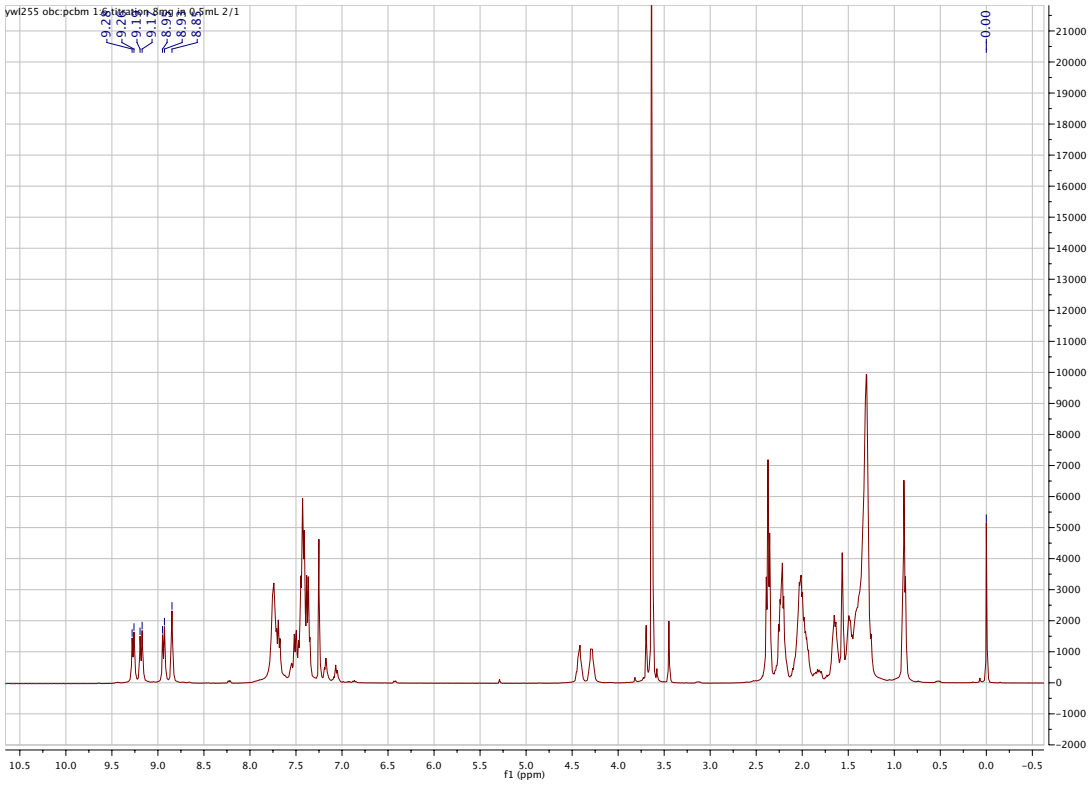

c-OBCB:PCBM=1:6

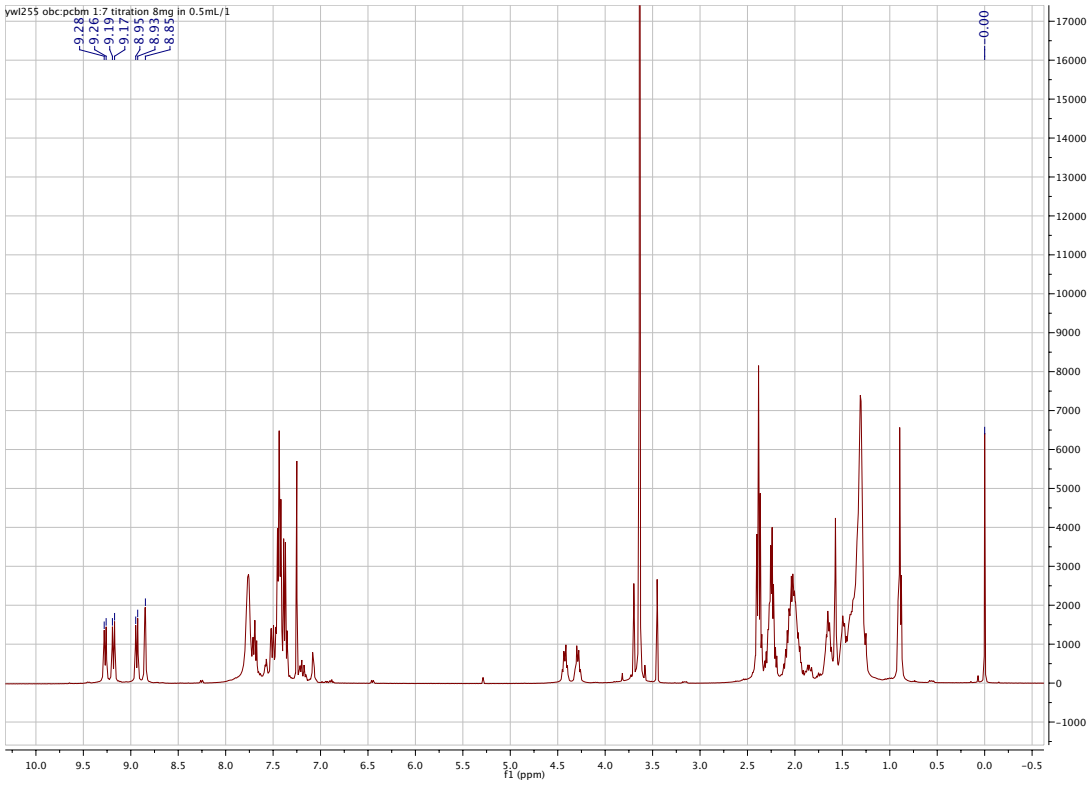

c-OBCB:PCBM=1:7

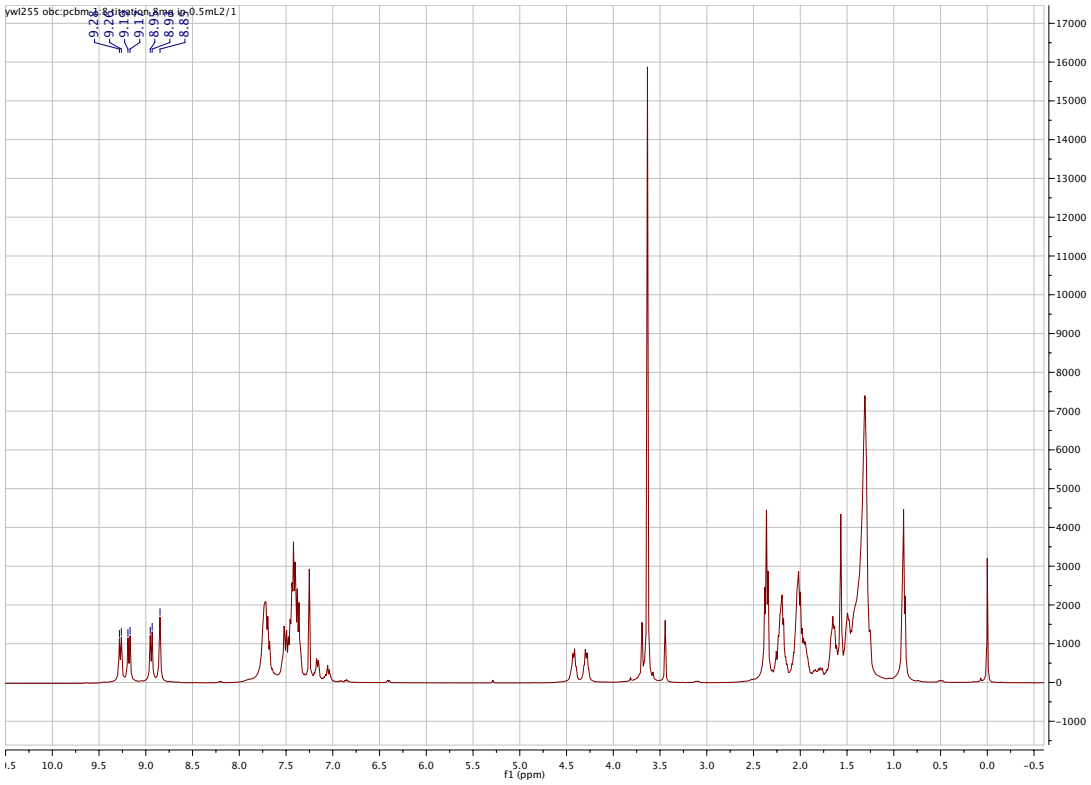

c-OBCB:PCBM=1:8

Chapter 4. Thin film studies of c-OBCB: OFET and solar cells[1]

4.1 Introduction to bulk heterojunction (BHJ) organic solar cells

Solution processed bulk-heterojunction (BHJ) organic solar cells are widely investigated due to their promises in fabricating clean, flexible, economic and light-weight devices for solar power conversion (Figure 1). The active layer of organic BHJs is comprised of at least two organic semiconductors with different electron affinities, namely electron donor and electron acceptor, forming nano-scale interfaces from solution-based spin casting. Upon light irradiation, the tightly bound photoexcited excitons at the interfaces between donor and acceptor materials separate into free carriers.[2] The free electrons flow to the cathode and the free holes flow to the anode, thus generating electricity in the circuit.

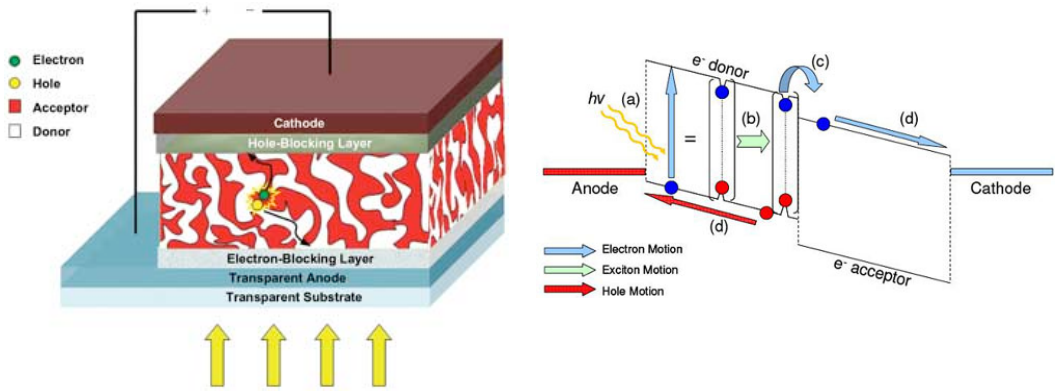

Figure 1. (left) Illustration of a BHJ organic solar cell with cathode, hole-blocking layer, active layer comprising of electron donor and electron acceptor, electron-blocking layer, transparent anode on the transparent substrate. (right) Schematic presentation of charge separation at interfaces upon light irradiation and the generation of electricity.

For BHJ organic solar cells, frontier orbitals are actively engaged in charge separation (Figure 2). The proper alignment of the energy levels is essential to achieve high solar power conversion. The absorption bands of both donor and acceptor materials need to effectively cover the solar spectrum, particularly the visible light region, for maximum solar power efficiency. While other engineering factors such as morphology of the active layer, hole or electron-blocking layers and electrodes are also important to improve device performance, it is the synthesis and development of new materials that lead to the improvement for higher-performance organic solar cells.[3-7] A wide range of conjugated polymers were synthesized and studied in literature for enhancing solar power conversion efficiency.[3,5,7,8] The Nuckolls group has designed and studied a class of contorted aromatic molecules as promising electron-donating materials. This chapter will describe the development of c-OBCB/C_{70} fullerene based BHJ solar cells and the OFET devices using c-OBCB as the hole-transporting material.

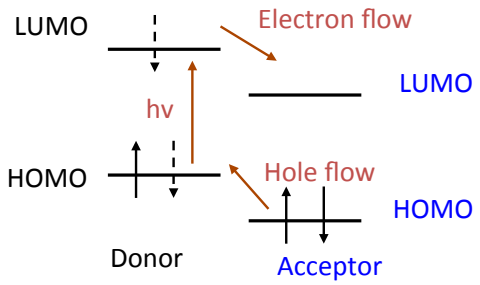

Figure 2. Alignment of energy levels proper for charge separation in the BHJ solar cells.

4.1.1 Self-assembly of contorted-HBC with fullerene-based acceptors in OPVs due to structural complementarity

Self-assembly of the donor and the acceptor at the molecular-scale has been proposed to control morphology and improve device performance in the polymer bulkjunctions.[9-12] In contrast, examples of small molecule self-assembly in solar cells are rare due to lack of favorable interactions between donor and acceptor molecules.[13-15] The contorted disc-like molecules c-HBC **1** and c-DBTTC **2** allow for shape-complementariness with acceptor

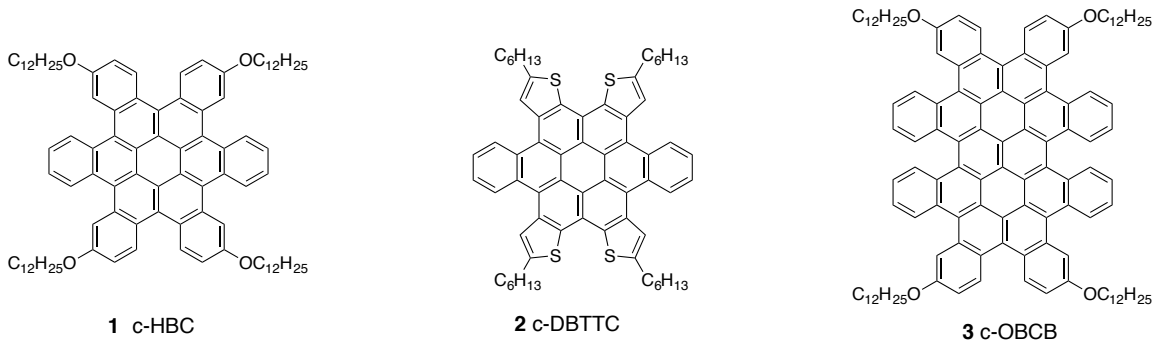

Figure 3. Structures of the contorted disc-shaped molecules.

molecules like fullerenes (Figure 3). c-HBC and its derivatives are complementary in both size and shape to that of ball-shaped fullerene C_{60} and its derivatives, making these two partners perfect candidates for molecular self-assembly or even co-crystallization. Indeed, co-crystallization occurs both from solution and physical vapor transport to form a 'ball-and-socket' ((C_{60})/c-HBC) arrangement.[16] From physical vapor transport, these two molecules form a co-crystal at a 1:1 molar ratio where each C_{60} is centered in the coronene core of the c-HBC and the packing follows the pattern ABABAB. In this structure, the C_{60} fullerenes stack into columns while the c-HBC has close contact with

four other molecules of the same kind in a rectangular array. From solution, C_{60} and c-HBC form a 2:1:1 ternary crystal of C_{60} (A), HBC (B), and chlorobenzene where each c-HBC has two C_{60} neighbors, one sitting into each of the concave aromatic faces of the c-HBC. The crystal packing follows the pattern ABAABA (Figure 4A). We found that c-DBTTC also co-crystallizes with C_{60} to produce a 2:1 ratio of C_{60} to DBTTC with similar ABAABA packing (Figure 4B).[17] This ball-and-socket motif creates a unique system where a 'ball-shaped' n-type semiconductor and 'bowl-shaped' p-type semiconductor are arranged to communicate electronically in crystal, a property that translates into good device properties as will be discussed below.

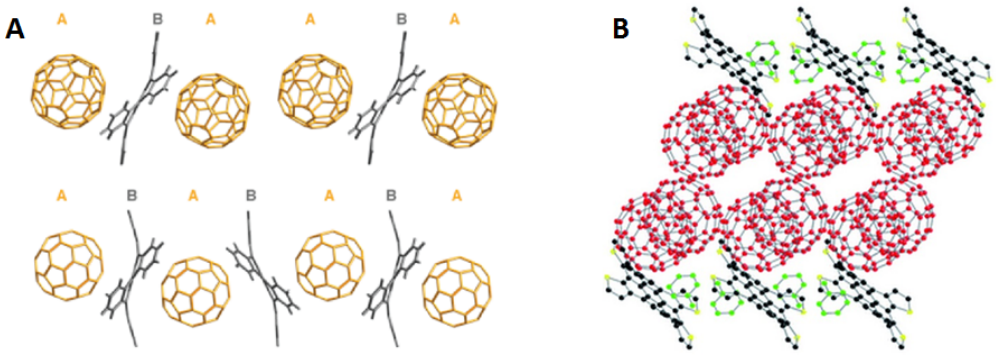

Figure 4. (A) c-HBC and C_{60} co-crystals from vapor deposition (bottom) and solution (top). (B) co-crystals from c-DBTTC and C_{60} grown from toluene, a unit cell viewed from (010) direction shows the sandwich structure. Toluene molecules are shown in green color. Butyl groups and hydrogen atoms have been removed for clarity. Reproduced from ref. 15 and 16. [16,17]

To test whether shape complementarity was important in the devices, we constructed two devices utilizing contorted HBC and, its cousin, a completely planar HBC derivative. Both molecules share similar electronic and physical properties, with the notable shape

difference. We found that devices made from contorted HBC were more efficient relative to the non-contorted derivative by about two orders of magnitude in solar power conversion efficiency (PCE).[16] Notably, under UV-LED irradiation, contorted-HBC device out-performed flat-HBC by more than two orders of magnitude (average efficiencies of 3.36 % versus 0.03 %). We were able to conclude that the c-HBCs form a shape complementary complex with n-type acceptors like fullerenes, yielding a better donor/acceptor interface that results in enhanced electronic properties. Furthermore, the supramolecular complex also exists in both blended films of c-HBC:$PC_{70}BM$[18] and c-DBTTC:$PC_{70}BM$[19]. Grazing Incidence X-ray Diffraction (GIXD results showed a new phase in the blended film which resulted from a supramolecular complex by self-assembly.[18] Formation of the supramolecular complex directly affects charge separation in the active layer (Figure 5), therefore leading to efficient small molecule BHJ organic solar cells. Notably, only 10% of dodecyloxy-substitued c-HBC in the blended film can

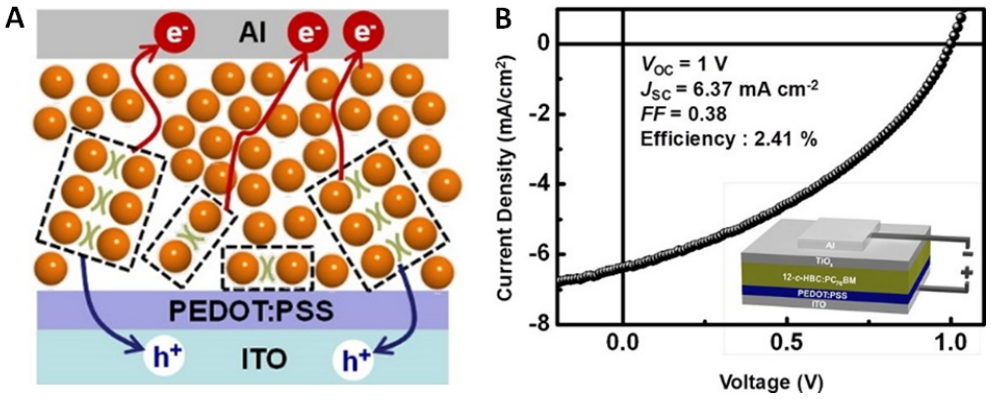

Figure 5. (A) Self-assembled p−n junction of a c-HBC **1**:$PC_{70}BM$ film. (B) J−V characteristics of a 1:9 wt % c-HBC **1**/$PC_{70}BM$ device under illumination. Adapted from ref 17.[18]

achieve the maximum power conversion efficiency of 2.41% (Figure 5B),[18] which is high if we consider that the absorption profile of the c-HBC molecule is largely confined to the UV range. These results suggest a new design strategy for solution-processed solar cells to improve device performance by molecular scale self-assembly via non-covalent interaction between a contorted concave donor and ball-shape acceptor.

4.1.2 Improving solar cell efficiency based on contorted disc-shaped aromatics

In Chapter 3 we have described that the expanded contorted aromatic molecule, c-OBCB **3** (Figure 3), showed a smaller band-gap relative to the c-HBC family. The absorbance edge of c-OBCB red-shifts by ~80 nm relative to c-HBC. The calculated band gap of c-OBCB is smaller than that of c-HBC by 0.34 eV. Stern-Volmer analysis reveals strong association of the c-OBCB **3** and $PC_{70}BM$ with an association constant of 5 $x10^4$ M^{-1} in chloroform. We propose that the curved structure of the c-OBCB will be able to make a ball-socket interaction with the convex guest $PC_{70}BM$. With the more desirable band-gap and shape-complementary interaction with $PC_{70}BM$ acceptors, c-OBCB is a promising p-type material to improve solar cell performance. Before we test c-OBCB in solar cells, we fabricated OFET devices to demonstrate its hole-transporting mobility.

Our micro-patterned c-OBCB film in the OFET operates well with the single layer graphene electrodes and reduces the gate leakage current. In addition, the graphene source/drain electrodes provide very low contact resistance with the c-OBCB film, as seen in the low bias region of transfer curve (Figure 6a). The low contact resistance is due to the large PAH making good contact to graphene electrodes and to the intrinsic work function adjustment of graphene.[20] Figures 7a and 7b display the transfer and output characteristics of the OFET. We calculate the field effect mobility from the transfer

characteristics (Figure 6a) to be 0.002 $cm^2/V•s$. We used the MOSFET standard model in the saturated regime, $I_{DS}=(W/2L)C_i \mu (V_G-V_T)^2$, where W and L are the width and length of channel and C_i, μ, and V_T correspond to the capacitance per unit area of the gate insulator, the field-effect mobility and threshold voltage, respectively. Figure 6b shows the representative output characteristics of the OFET with increasing gate field, which displays characteristics for p-type semiconductors. The film displays an increase of I_{DS} with negative gate bias due to the accumulation of holes in the molecular film; thus c-OBCB **3** transports holes readily.

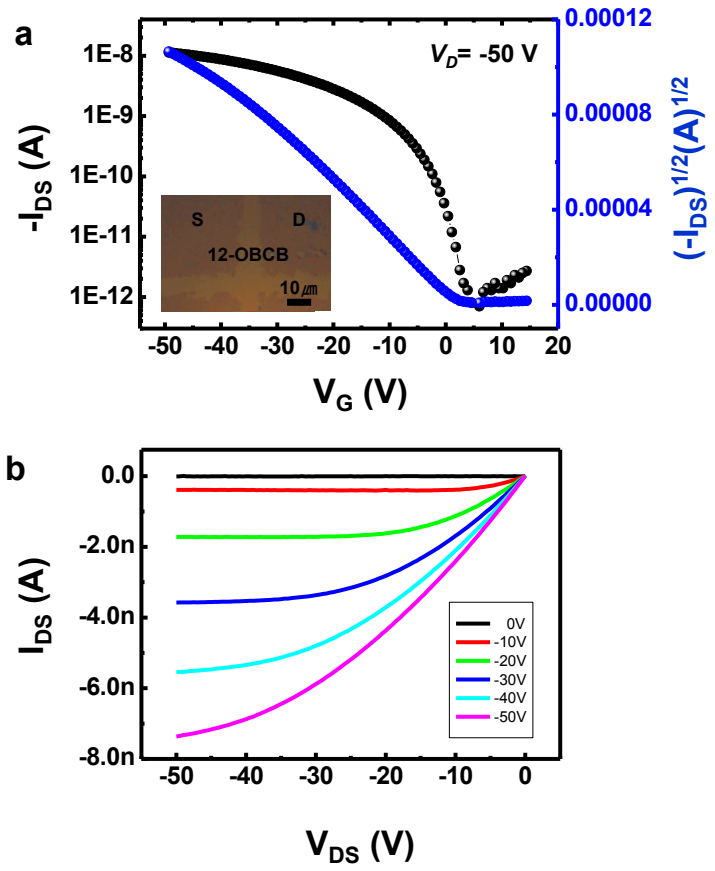

Figure 6. Transfer (a) and output (b) curves of patterned c-OBCB **3** transistor. Inset of (a)

shows an optical microscope image of graphene electrodes with c-OBCB **3.**

4.2 Performance of c-OBCB/C_{70} fullerene BHJ solar cell

Our OFET characteristics demonstrated that c-OBCB **3** is a p-type, hole-transporting material. c-OBCB also associates strongly with the n-type material, $PC_{70}BM$ fullerene, due to its expanded contorted 3-D structure. We believe the red-shifted absorbance of c-OBCB relative to c-HBCs would facilitate the solar power conversion. Therefore, we made bulk heterojunction (BHJ) solar cell devices and tested the power conversion efficiency. The solar cell devices were constructed with an aluminum layer as the cathode, a TiO_x layer as the hole-blocking layer, blended film of c-OBCB 3:$PC_{70}BM$ as the active BHJ layer, a PEDOT:PSS as the electron-blocking layer and ITO substrate as the transparent anode. The electrodes were chosen according to the energy levels of the two molecules, c-OBCB 3:$PC_{70}BM$. Figure 8a shows the energy diagram of each layer in the device architecture. The c-OBCB HOMO and LUMO energies are measured using cyclic voltammetry shown in Figure 7. To make the BHJ solar cell devices, c-OBCB 3 and $PC_{70}BM$ materials with varied weight ratios of 1:9, 2:8 and 3:7 were dissolved in o-xylene. The c-OBCB **3**: $PC_{70}BM$ mixture solution was spin cast on the ~30 nm PEDOT:PSS/ITO substrate. A TiO_x layer was employed on the top of the c-OBCB **3**:$PC_{70}BM$ layer prior to evaporation of ~60 nm aluminum counter electrode.[21]

Of the ratios of the donor and acceptor we tested, we found the optimal performance at 1:4 weight ratio of the donor to acceptor (Figure S2). Figure 8b displaces the J-V curves for the blended films. The open circuit voltage (Voc) is 0.98 V and very close to what would be predicted theoretically from the energy level alignment in Figure 8a. The short-circuit current (J_{sc}) is 7.9 mA/cm^2 and the fill factor is 0.37. These values result in

a 2.88% power conversion efficiency. The average value is 2.86% from twelve devices. The external quantum efficiency (EQE) spectrum in Figure 8c shows the photocurrent response of c-OBCB 3:$PC_{70}BM$ BHJ solar cell devices as a function of wavelengths. We observe that the maximum wavelength in EQE spectra red-shifts ~80 nm compared with the EQE spectra of c-HBC:$PC_{70}BM$ solar cells, which matches the trend of UV-Vis spectra we described in Chapter 3 (Figure S1). The red-shift in absorbance is responsible for the higher PCE for c-OBCB compared to the smaller c-HBC series and charts a clear path to improving the properties of these materials in OPVs by further red-shifting the absorbance.

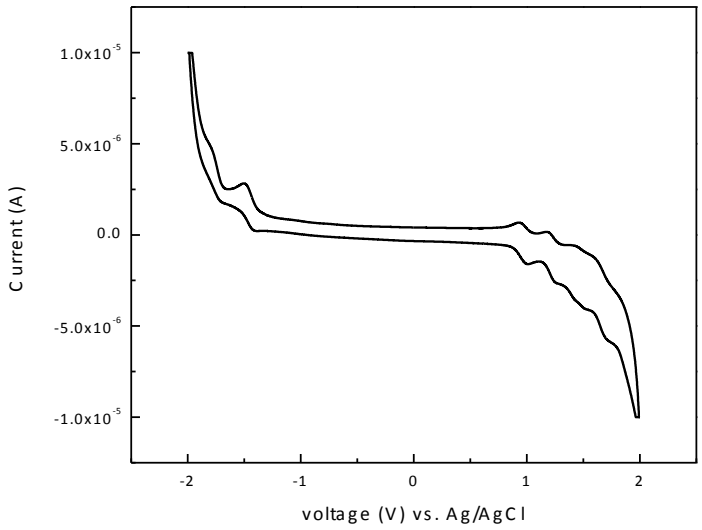

Figure 7. Cyclic voltammetry curve of c-OBCB **3** in chloroform

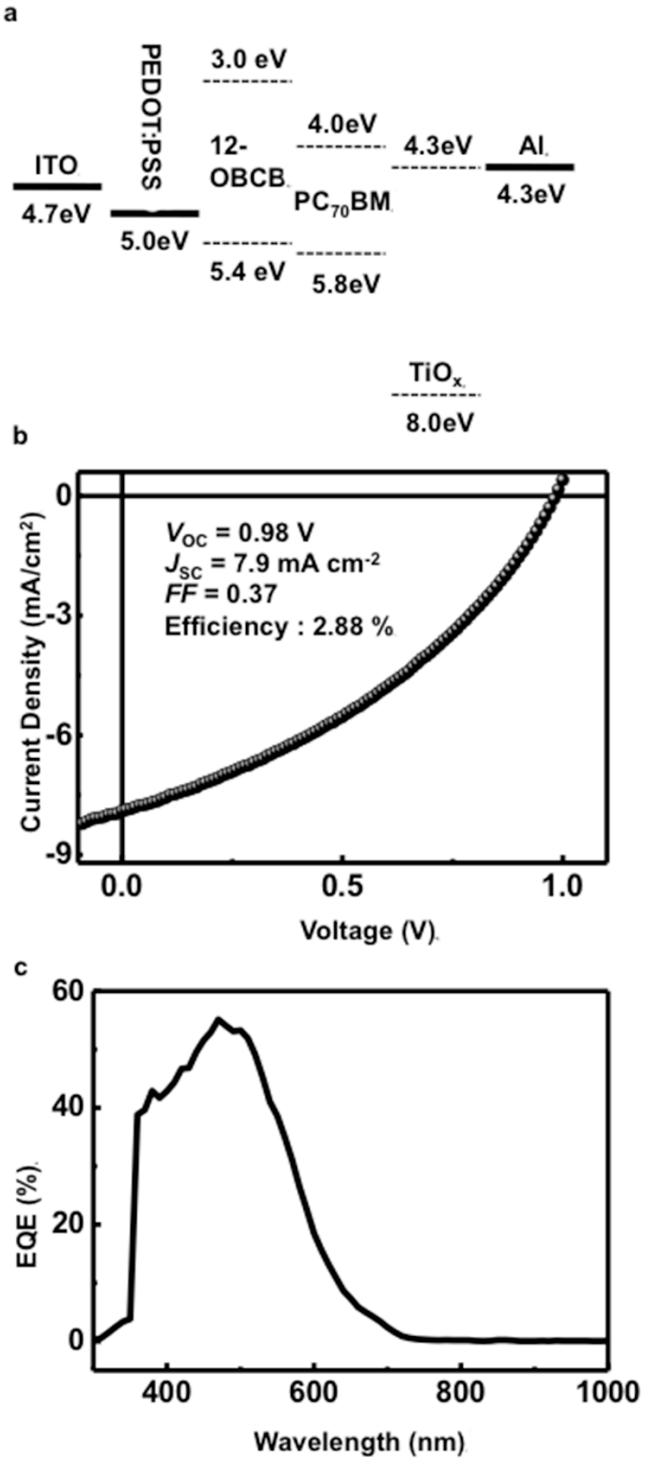

Figure 8. (a) Energy level diagram of the device. (b) Current density-voltage (J-V) characteristics and (c) EQE spectrum of c-OBCB **3**:$PC_{70}BM$ solar cell.

4.3 Supporting information

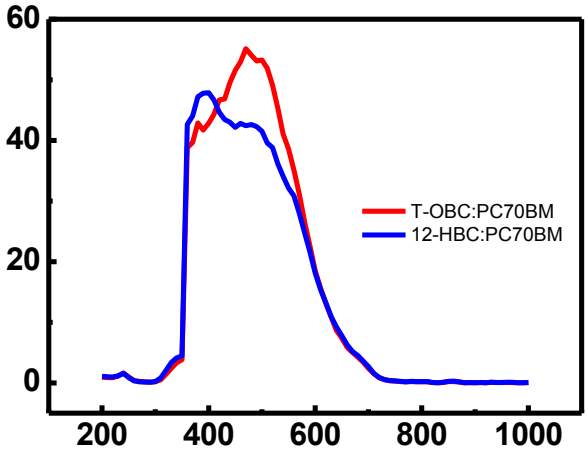

Figure S1. EQE spectra of c-OBCB **3**:$PC_{70}BM$ (red) and c-HBC **1**:$PC_{70}BM$ (blue) solar cells.

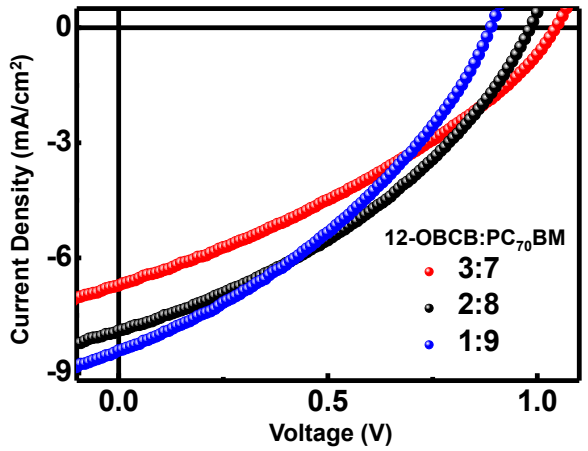

Figure S2. Current density-voltage (J-V) curves of PEDOT:PSS/c-OBCB **3**:$PC_{70}BM/TiO_x$/Al architecture BHJ solar cells with different weight ratios of the electron donor and acceptor in the active layer.

4.4 Reference

(1) This chapter is adapted from our previous publication: Xiao, S. X.; Kang, S. J.; Wu, Y.; Ahn, S.; Kim, J. B.; Loo, Y. L.; Siegrist, T.; Steigerwald, M. L.; Li, H. X.; Nuckolls, C. *Chem Sci* **2013**, *4*, 2018. Dr. Seok Ju Kang fabricated the devices and conducted measurements.

(2) Zhu, X. Y. *J. Phys. Chem. Lett.* **2014**, *5*, 2283.

(3) Guo, X.; Zhou, N.; Lou, S. J.; Smith, J.; Tice, D. B.; Hennek, J. W.; Ortiz, R. P.; Navarrete, J. T. L.; Li, S.; Strzalka, J.; Chen, L. X.; Chang, R. P. H.; Facchetti, A.; Marks, T. J. *Nat. Photon.* **2013**, *7*, 825.

(4) Zhong, Y.; Kumar, B.; Oh, S.; Trinh, M. T.; Wu, Y.; Elbert, K.; Li, P.; Zhu, X.; Xiao, S.; Ng, F.; Steigerwald, M. L.; Nuckolls, C. *J. Am. Chem. Soc.* **2014**, *136*, 8122.

(5) Cheng, Y.-J.; Yang, S.-H.; Hsu, C.-S. *Chem. Rev.* **2009**, *109*, 5868.

(6) Green, M. A.; Emery, K.; Hishikawa, Y.; Warta, W.; Dunlop, E. D. *Progress in Photovoltaics: Research and Applications* **2012**, *20*, 606.

(7) Vohra, V.; Kawashima, K.; Kakara, T.; Koganezawa, T.; Osaka, I.; Takimiya, K.; Murata, H. *Nat. Photon.* **2015**, *9*, 403.

(8) Li, H.; Hwang, Y.-J.; Courtright, B. A. E.; Eberle, F. N.; Subramaniyan, S.; Jenekhe, S. A. *Adv. Mater.* **2015**, *27*, 3266.

(9) Cates, N. C.; Gysel, R.; Beiley, Z.; Miller, C. E.; Toney, M. F.; Heeney, M.; McCulloch, I.; McGehee, M. D. *Nano Lett.* **2009**, *9*, 4153.

(10) Kennedy, R. D.; Ayzner, A. L.; Wanger, D. D.; Day, C. T.; Halim, M.; Khan, S. I.; Tolbert, S. H.; Schwartz, B. J.; Rubin, Y. *J. Am. Chem. Soc.* **2008**, *130*, 17290.

(11) Mayer, A. C.; Toney, M. F.; Scully, S. R.; Rivnay, J.; Brabec, C. J.; Scharber, M.; Koppe, M.; Heeney, M.; McCulloch, I.; McGehee, M. D. *Adv. Funct. Mater.* **2009**, *19*, 1173.

(12) Miller, N. C.; Sweetnam, S.; Hoke, E. T.; Gysel, R.; Miller, C. E.; Bartelt, J. A.; Xie, X.; Toney, M. F.; McGehee, M. D. *Nano Lett.* **2012**, *12*, 1566.

(13) Bürckstümmer, H.; Tulyakova, E. V.; Deppisch, M.; Lenze, M. R.; Kronenberg, N. M.; Gsänger, M.; Stolte, M.; Meerholz, K.; Würthner, F. *Angew. Chem. Int. Ed.* **2011**, *50*, 11628.

(14) Troshin, P. A.; Sariciftci, N. S. In *Supramolecular Chemistry*; John Wiley & Sons, Ltd: 2012.

(15) Loser, S.; Bruns, C. J.; Miyauchi, H.; Ortiz, R. P.; Facchetti, A.; Stupp, S. I.; Marks, T. J. *J. Am. Chem. Soc.* **2011**, *133*, 8142.

(16) Tremblay, N. J.; Gorodetsky, A. A.; Cox, M. P.; Schiros, T.; Kim, B.; Steiner, R.; Bullard, Z.; Sattler, A.; So, W. Y.; Itoh, Y.; Toney, M. F.; Ogasawara, H.; Ramirez, A. P.; Kymissis, I.; Steigerwald, M. L.; Nuckolls, C. *ChemPhysChem* **2010**, *11*, 799.

(17) Chiu, C. Y.; Kim, B.; Gorodetsky, A. A.; Sattler, W.; Wei, S. J.; Sattler, A.; Steigerwald, M.; Nuckolls, C. *Chem. Sci.* **2011**, *2*, 1480.

(18) Kang, S. J.; Ahn, S.; Kim, J. B.; Schenck, C.; Hiszpanski, A. M.; Oh, S.; Schiros, T.; Loo, Y. L.; Nuckolls, C. *J. Am. Chem. Soc.* **2013**, *135*, 2207.

(19) Kang, S. J.; Kim, J. B.; Chiu, C. Y.; Ahn, S.; Schiros, T.; Lee, S. S.; Yager, K. G.; Toney, M. F.; Loo, Y. L.; Nuckolls, C. *Angew. Chem. Int. Ed.* **2013**, *52*, 7063.

(20) Yu, Y.-J.; Zhao, Y.; Ryu, S.; Brus, L. E.; Kim, K. S.; Kim, P. *Nano Lett.* **2009**, *9*, 3430.

(21) The current density–voltage (J–V) characteristic of devices was acquired using a Keithley 2635 source measurement unit under 100 mW cm−2 illumination.

Chapter 5. Molecularly controlled selective dispersion of high purity semiconducting single-walled carbon nanotubes[1]

5.1 Introduction

Single-walled carbon nanotubes (SWCNTs) have a wide range of applications for biological and chemical sensors,[2-6] flexible electronics,[7-9] and transparent electrodes,[10,11] etc. due to their extraordinary mechanical, chemical and electronic properties.[12-14] In particular, the high charge-carrier mobility of semiconducting SWCNTs being able for solution processing is a great candidate for high-performance low-cost transistor application. However, the traditionally chemical vapor deposition (CVD) grown SWCNTs are mixtures of metallic and semiconducting tubes.[15-17] Separating semiconducting SWCNTs from metallic SWCNTs remains a challenge up to date. While great progress has been made to develop synthetic methods to selectively grow carbon nanotubes,[18-21] post-growth separation provides an alternate method to sort and enrich the desired types of SWCNTs.

Conjugated polymers that consist of extensive π-conjugative structures through the backbones, have been reported to interact strongly with SWCNTs.[22-25] The common hypothesis is that the conjugated polymers wrap around selected SWCNTs, forming a "polymer shell' around the carbon nanotubes, thus the polymers enable selective dispersion of certain types of SWCNTs in solution. One example is the regio-regular poly(3-alkylthiophene)s (rr-P3ATs). Bao et al. reported the selective dispersion of semiconducting SWCNTs of several chiralities with rr-P3ATs and fabricated high-performance SWCNT-network transistors from the dispersion.[22] Other dispersants, such

as single-stranded DNA with specific sequences, have also shown selectivity towards SWCNTs[22,26-33]. Recent studies have shown broad application of polymer-sorted SWCNTs in electronic devices, including FETs, light-emitting transistors, photodetectors and photovoltaics.[23-25,34-38]

On the contrary, little attention has been paid to the exploration of small organic molecules to sort semiconducting SWCNTs. Interestingly, it was the non-covalent interactions between SWCNTs and organic small molecules that had attracted broad interest in solubilizing SWCNTs to begin with.[39] Large aromatic molecules, including pyrene, porphyrin, phthalocyanin or perylenediimide, exhibit strong π–interactions with the nanotube surface and have been used in the preparation of SWCNTs dispersion in organic solvents.[40-44] Another family of small molecules, namely organic nanotweezers, in which two aromatic components are bound to a rigid spacer, has also shown promise in sorting and therefore enriching SWCNTs.[45] However, the selectivity of those molecules towards SWCNTs with specific chirality is not as high as that of conjugated polymers. For example, poly(9,9-di-n-octylfluorenyl-2,7-diyl) has been shown to down select for five specific SWCNT species in toluene.

Here we use the contorted aromatic molecule, c-octabenzocircumbiphenyl (*c*-OBCB) to disperse SWCNTs. The Nuckolls group has developed the syntheses of a class of contorted aromatics and found their electronic applications in organic film effect transistors (OFETs), solar cells, and chemical sensors. c-OBCB is by far the largest p-type semiconductor member in this family. In the geometry-optimized structure of c-OBCB by density functional theory (DFT), eight benzo-groups alternate around the circumbiphenyl core up and down, forming the non-planar structure. Two [5]-helicene-

units around the exterior make c-OBCB structurally chiral. c-OBCB is a hole-transporting semiconducting material in OFET devices. In c-OBCB/C_{70} fullerene bulk-heterojunction solar cells, the efficiency is significantly improved relative to the smaller-sized c-hexabenzocorone (c-HBC)/fullerene solar cells. The strong association of c-OBCB with C_{70} fullerene in solution is critical for the high performance of solar cells.

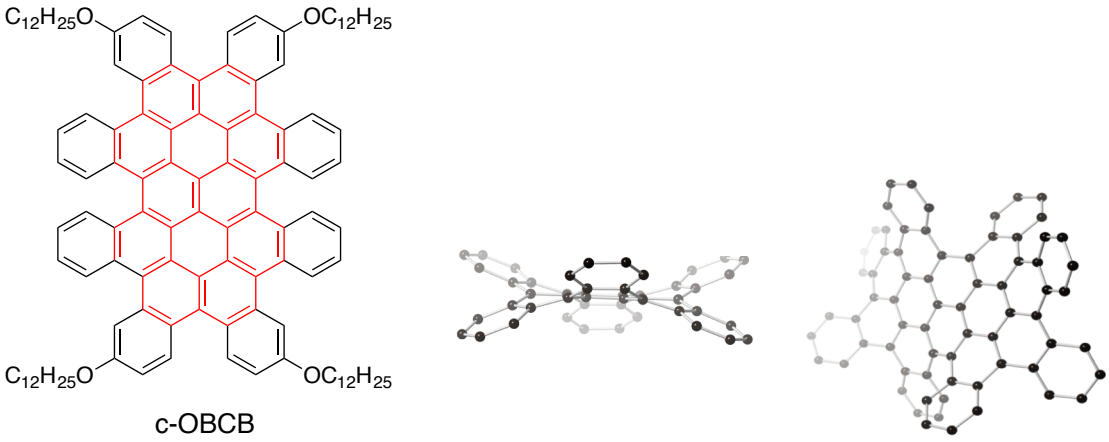

Figure 1. Structure of c-OBCB.

c-OBCB is a good candidate to sort SWCNTs because of its contorted three-dimensional structure, its appropriate size (see Figure S1 in Supporting Information) and the potentially strong π–interaction when in contact with SWCNTs. We envisioned that c-OBCB will interact strongly with SWCNTs due to the strong π–π interaction and hence facilitate the dispersion of SWCNTs. Using tetradodecyloxy-substituted c-OBCB, we achieved highly selective dispersion of semiconducting SWCNTs in toluene and fabricated SWCNT network transistors readily from the sorted SWCNTs.

5.2 Dispersion with c-OBCB

Commercially available High pressure CO (HiPCO) SWCNTs were used for dispersion in this study. We mixed HiPCO SWCNTs and c-OBCB in toluene with varied

weight ratios to optimize the selective dispersion. The suspensions underwent tip sonication (~20w/cm^2) for 1 h before the sonicated suspension was centrifuged at 15 krcf for 30 min at 10 ºC. Then the supernatant was collected and characterized by several spectroscopic characterization tools, including Vis-near IR absorption spectra, photoluminescence excitation and Raman spectroscopy. Comparing with the non-selective SDS-dispersed absorption spectrum using the same HiPCO tubes and dispersion conditions, the c-OBCB-assisted dispersion displays significant selectivity for SWCNTs. In Figure 2, we assigned the 650 nm peak and 1260 nm peak to be the E_{22} and E_{11} transitions of the nanotubes around 1 nm in diameter, respectively. The enriched peaks between 1480 nm to 1700 nm belong to the E_{11} transitions of large SWCNTs with 1.2-1.3 nm diameters, the E_{22} transitions of which are found in the region of 740 nm to 850 nm.

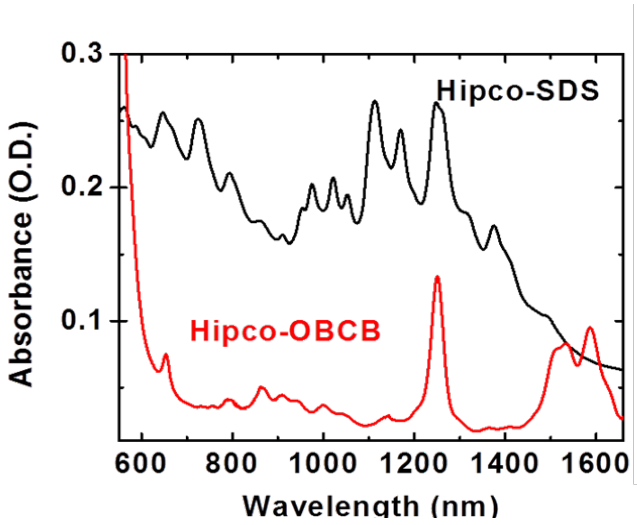

Figure 2. Comparison of the absorption spectra for c-OBCB/HiPCO dispersion and SDS/HiPCO dispersion.

By varying the weight ratio of HiPCO-SWCNTs : c-OBCB, we found that 2 mg HiPCO-SWCNTs and 10 mg c-OBCB in 10 mL toluene gives the most optimal

dispersion for both concentration and selectivity (Figure S2). Less c-OBCB results in a dilute dispersion with low absorption intensity. Too much c-OBCB increases the absorption intensity but sacrifices the selectivity. Solvent is known as an important parameter in dispersing carbon nanotubes. We chose toluene because HiPCO SWCNTs have poor solubility in toluene, thus c-OBCB will assist dispersion. However, chlorinated solvents such as chloroform can disperse SWCNTs under sonication solely, thus they are not effective for selective sorting. We did test HiPCO-SWCNTs /c-OBCB dispersion in another solvent, tetrahydrofuran (THF), but it resulted in a poor dispersion, possibly due to the strong interaction between THF and dodecyloxyl side chains (that prevents the interaction of HiPCO-SWCNTs and c-OBCB, see Figure S3) Therefore, 2 mg HiPCO-SWCNTs and 10 mg c-OBCB in 10 mL toluene was used for further studies.

5.3 Spectroscopic characterization of the selective dispersion

We have discussed that there are mainly two sets of peaks in the Vis-near IR absorption spectrum. For the set of 650 nm and 1250 nm peaks, we can narrow down the selected type(s) of SWCNTs to be (9, 5) and/or (10, 3) according to literature (Figure S4). As for the peaks between 1480 nm to 1700 nm, they are well known to be semiconducting nanotubes with wide diameters. In order to further determine the chiralities in the sorted SWCNTs, we mapped the photoluminescence excitation/emission (PLE) spectra (Figure 3). The sorted SWCNT dispersion was excited from 600 nm to 780 nm with 5 nm intervals, and photoluminescence spectra were recorded. From the PLE map, we can identify the most intense peak to be (10, 3). The peaks between 1480 nm to 1700 nm are beyond the detection range of our photoluminescence set up, but we confirmed that the SWCNTs with absorption in this range are semiconducting in high

purity with the following Raman spectroscopy measurement.

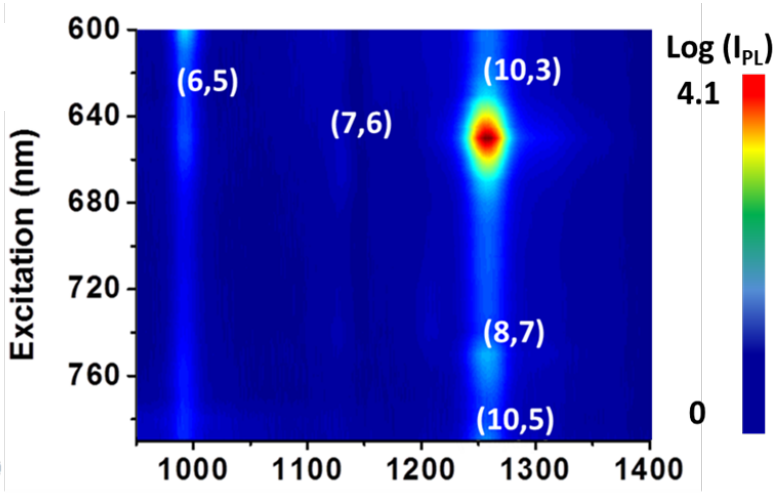

Figure 3. Photoluminescence excitation/emission (PLE) data map for the sorted HiPCO SWCNTs. Intensity increases as the color goes from blue to red.

We performed resonant Raman scattering (RRS) measurement and examined the radial breathing mode (RBM) regions using three excitation wavelengths to characterize the purity of semiconducting tubes in the sorted SWCNTs, namely, 532 nm (2.33 eV), 633 nm (1.96 eV) and 785 nm (1.58 eV). The 532 nm excitation energy is mainly in resonance with metallic SWCNTs. The wavenumber range less than 200 cm^{-1} was ascribed to semiconducting carbon nanotube, and the peaks in the range from 200 to 350 cm^{-1} (grey region) correspond to metallic tubes. The integrated intensity of the latter region can be used to estimate the purity, which is 97% from a quantitative comparison with that of raw HiPCO SWCNTs (Figure 4a). Secondly, with excitation wavelength at 633 nm which is resonant for both metallic (grey shaded) and semiconducting SWCNTs, the metallic (9, 9) and (12, 3) tubes originally present in the SDS dispersed SWCNTs

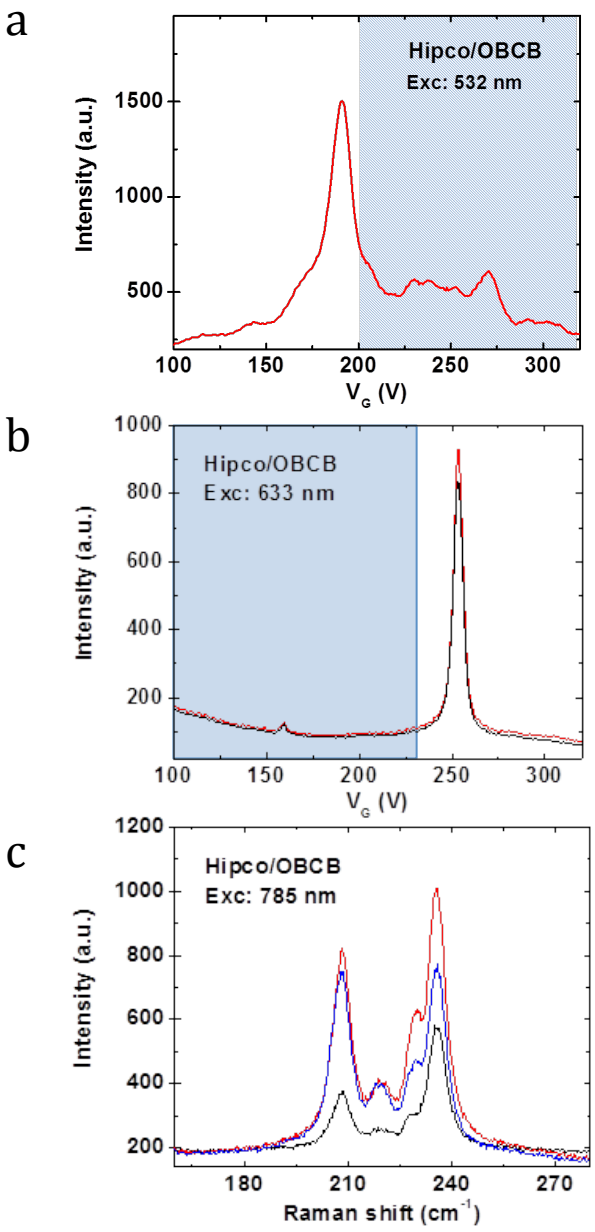

Figure 4. Radial breathing mode (RBM) regions of resonant Raman scattering spectra at three excitation energies. (a) 532 nm (2.33 eV) is mainly resonant with metallic SWCNTs (grey shaded) in the range of 200 to 350 cm^{-1}, (b) 633 nm (1.96 eV) is resonant with metallic (grey shaded) and semiconducting SWCNTs, (c) 785 nm (1.58 eV) is resonant with semiconducting SWCNTs.

disappeared in the c-OBCB sorted SWCNTs.(Figures 4b and S6) The peak at 251 cm-1 is assigned to (10,3), which matches perfectly with PLE measurements (Figures 4b). Finally, only s-SWCNTs were observed using excitation energy of 1.58eV (785 nm), which means that we achieved high purity semiconducting SWCNTs with c-OBCB-controlled sorting.

5.4 Thin film transistor characterization

To further test the property of the sorted SWCNTs, we fabricated SWCNTs network thin film transistors. We removed c-OBCB from SWCNTs by Millipore filtration and rinsing with toluene. The filtrate was spin cast on a silicon substrate with SiO_2 surface, serving as the gate electrode. Source and drain electrodes were defined with lithographic patterns and subsequent thermo-evaporation of gold. AFM image shows that the cast film is a uniform network of SWCNTs (Figure 5). By varying film thickness, we found the optimal performance is 0.6 $cm^2/V•s$ in mobility with 10^4 on/off ratio at 11 nm in film thickness (Figure 6). With these decent values for SWCNTs thin film transistors, we demonstrated that our method to selectively disperse semiconducting SWCNTs with an aromatic molecule, c-OBCB, is a facile approach for solution-based thin film transistor processing.

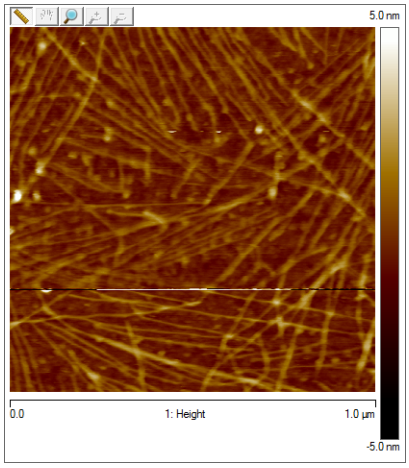

Figure 5. AFM image showing the SWCNT network of the spin-cast film.

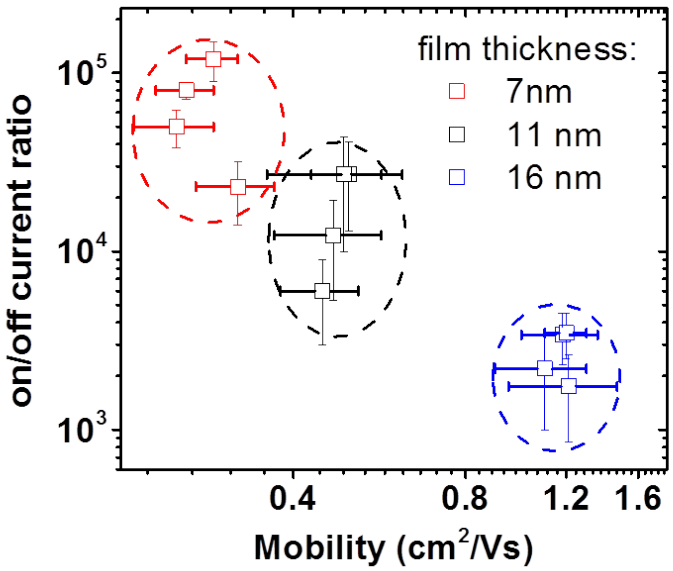

Figure 6. Mobility and on/off ratio performance of sorted-SWCNT network thin film transistor at varied film thickness.

5.5 Discussion and Conclusion

Both of our spectroscopic measurements and transistor data strongly support the successful sorting of semiconduting SWCNTs with c-OBCB from the commercially purchased HiPCO-SWCNTs. We have optimized the recipe for selective dispersion by varing the weight ratio of HiPCO SWCNTs and c-OBCB. c-OBCB on its own is a promising material in organic electronics due to its supersized contorted π-conjugated system. Prior to c-OBCB, we have tested a smaller molecule in our contorted aromatic family, c-HBC, which showed no meaningful dispersion of SWCNTs. The expanded size of c-OBCB, 1.8 nm in length and 1.3 nm in width, is crucial for effective interaction with SWCNTs and subsequent selective dispersion. We believe that two types of SWCNTs/c-OBCB interactions exist in the dispersion, parellel and perpendicular alignments of c-OBCB with carbon nanotubes (Figure S5), which explain the two sets of peaks we

observed in the Vis-near IR absorption spectrum. The parellel c-OBCB adheres to small diameter SWCNTs. Indeed, the (10, 3) SWCNTs, identified by both absoprtion and PLE spectra as one of the main components in the dispersion, has a diamter of 0.92 nm. On the other hand, the perpendicular c-OBCB results in dispersing large diamter SWCNTs, 1.2-1.3 nm, which we observed in the absorption spectrum between 1480 nm to 1700 nm.

Besides the expanded size, the structural contortion of c-OBCB is also beneficial to strongly interact with the selected SWCNTs. The four alternate benzo-groups in the exterior of c-OBCB face the same direction and the other four benzo-groups face the opposite direction. We believe that the four benzo-groups facing the same dierection, together with the circumbiphenyl core, grip the SWCNTs of appropriate sizes and render the selective dispersion as a consequence. Another interesting property of c-OBCB is its intrincsic chirality. It is not farfetched to propose that the two enaniomers of c-OBCB can selectively disperse the diasteromers of SWCNTs and result in chiral semiconductors that could detect polarized light for application in ellipsometry-based tomography,[46] optical communication of spin information,[47,48] and quantum-based optical computing and information processing.[48]

In summary, we achieved the facile sorting of semiconducting SWCNTs using an aromatic molecule, c-OBCB, and demonstrated the fabrication of SWCNTs network transistors directly from our dispersion. Instead of the widely investigated conjugated polymers, our study opens a new avenue for postgrowth sorting of SWCNTs by using contorted aromatic molecules.

5.6 Supporting Information

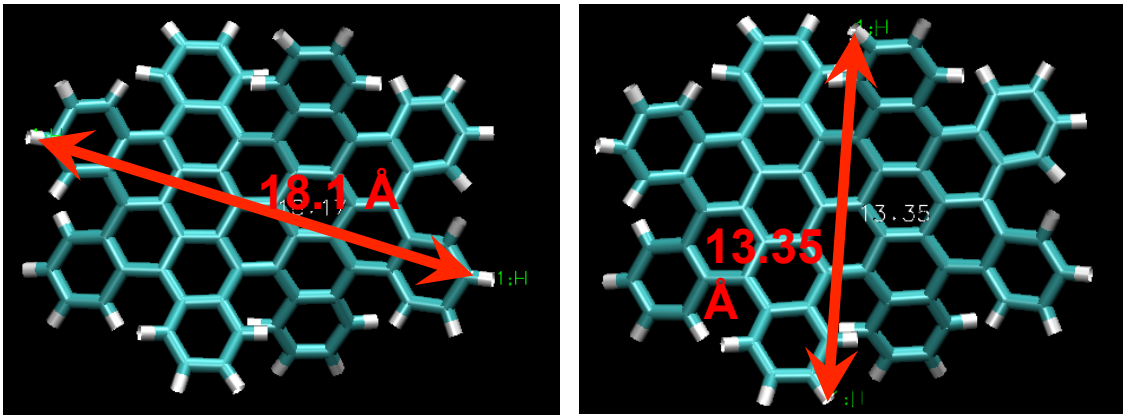

Figure S1. Length and width of c-OBCB from the DFT optimized structure.

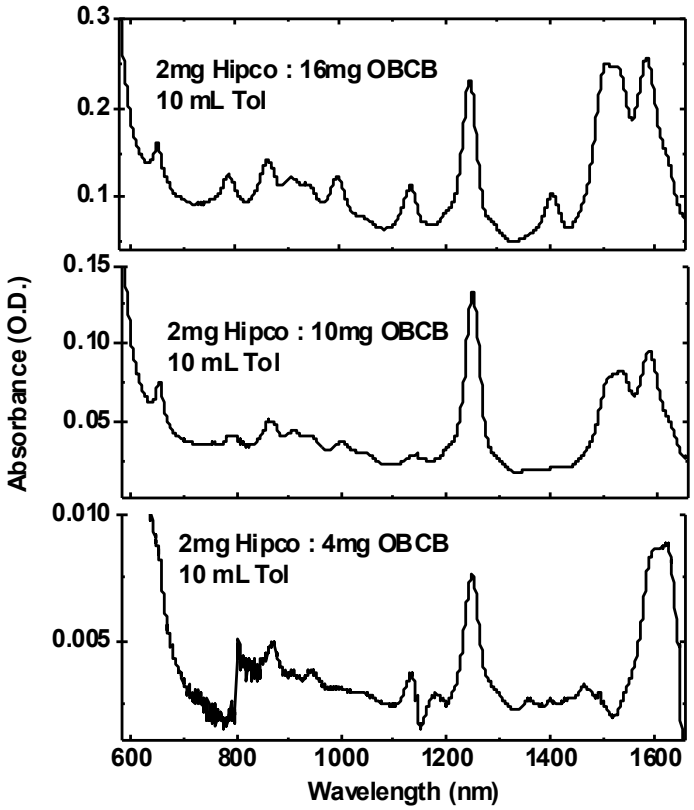

Figure S2. Absorption spectra of c-OBCB-controlled HiPCO dispersions in toluene with varied weight ratios.

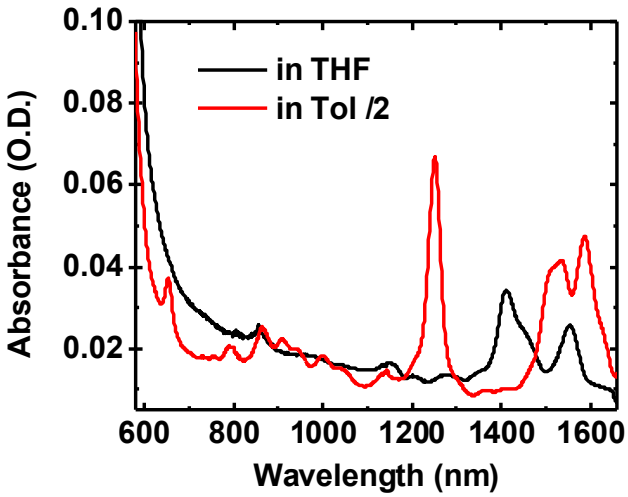

Figure S3. Absorption spectra of c-OBCB-controlled HiPCO dispersions in toluene (intensity cut by half for zooming the peaks in THF) and in THF.

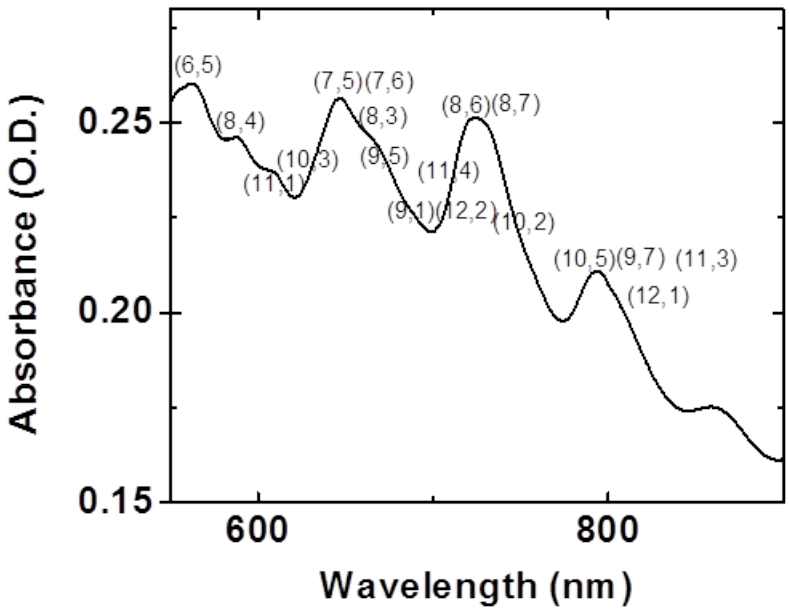

Figure S4. Commonly assigned chiralities in the SDS/HiPCO-SWCNTs absorption spectrum.

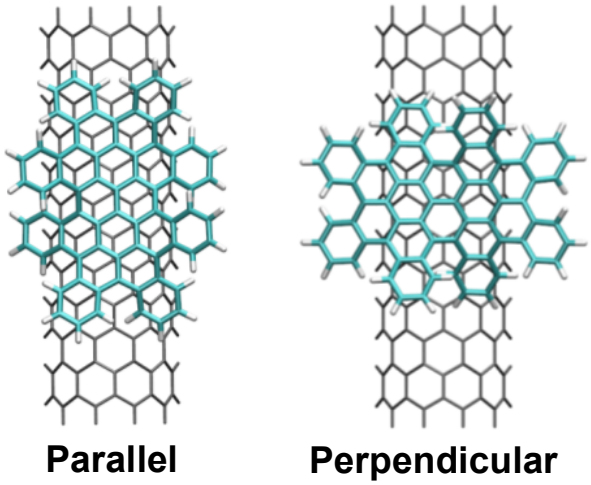

Figure S5. Illustration of parallel and perpendicular alignment of c-OBCB with SWCNTs.

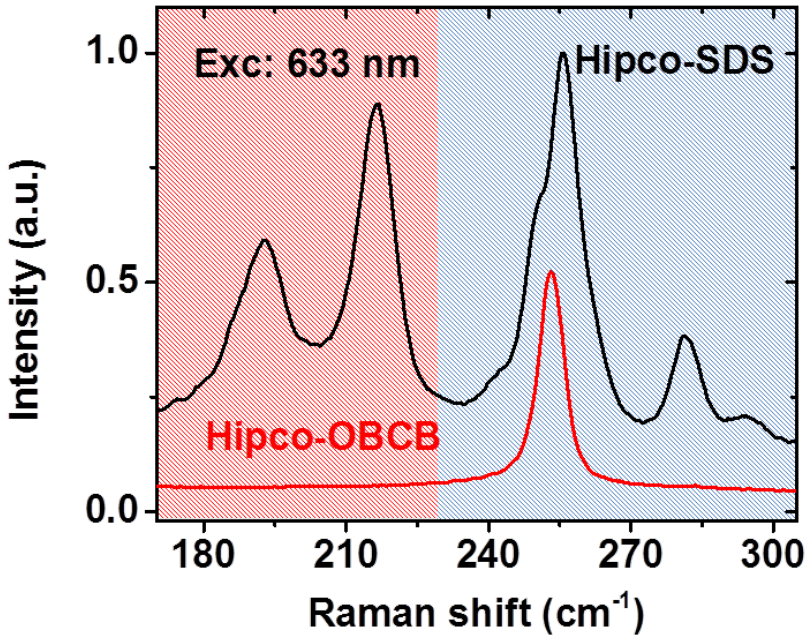

Figure S6. Comparing RBM regions excited at 633 nm for c-OBCB dispersed HipCo CNTs and SDS-dispersed HipCo CNTs.

5.7 References

(1) This chapter is a collabaration with the Dr. Jia Gao in the Loo group at Princeton University.

(2) Guo, X. F.; Gorodetsky, A. A.; Hone, J.; Barton, J. K.; Nuckolls, C. *Nat. Nanotechnol.* **2008**, *3*, 163.

(3) Guo, X. F.; Huang, L. M.; O'Brien, S.; Kim, P.; Nuckolls, C. *J. Am. Chem. Soc.* **2005**, *127*, 15045.

(4) Guo, X. F.; Nuckolls, C. *J. Mater. Chem.* **2009**, *19*, 5470.

(5) Guo, X. F.; Small, J. P.; Klare, J. E.; Wang, Y. L.; Purewal, M. S.; Tam, I. W.; Hong, B. H.; Caldwell, R.; Huang, L. M.; O'Brien, S.; Yan, J. M.; Breslow, R.; Wind, S. J.; Hone, J.; Kim, P.; Nuckolls, C. *Science* **2006**, *311*, 356.

(6) Guo, X. F.; Xiao, S. X.; Myers, M.; Miao, Q.; Steigerwald, M. L.; Nuckolls, C. *Proc. Natl. Acad. Sci. USA* **2009**, *106*, 691.

(7) Hong, S.; Myung, S. *Nat. Nanotechnol.* **2007**, *2*, 207.

(8) Bradley, K.; Gabriel, J.-C. P.; Grüner, G. *Nano Lett.* **2003**, *3*, 1353.

(9) Xiao, L.; Chen, Z.; Feng, C.; Liu, L.; Bai, Z.-Q.; Wang, Y.; Qian, L.; Zhang, Y.; Li, Q.; Jiang, K.; Fan, S. *Nano Lett.* **2008**, *8*, 4539.

(10) Zhang, M.; Fang, S.; Zakhidov, A. A.; Lee, S. B.; Aliev, A. E.; Williams, C. D.; Atkinson, K. R.; Baughman, R. H. *Science* **2005**, *309*, 1215.

(11) Simmons, T. J.; Hashim, D.; Vajtai, R.; Ajayan, P. M. *J. Am. Chem. Soc.* **2007**, *129*, 10088.

(12) Yu, M.-F.; Lourie, O.; Dyer, M. J.; Moloni, K.; Kelly, T. F.; Ruoff, R. S. *Science* **2000**, *287*, 637.

(13) Tang, Z. K.; Zhang, L.; Wang, N.; Zhang, X. X.; Wen, G. H.; Li, G. D.; Wang, J. N.; Chan, C. T.; Sheng, P. *Science* **2001**, *292*, 2462.

(14) Walker, P. L.; Rakszawski, J. F.; Imperial, G. R. *The J. Phys. Chem.* **1959**, *63*, 133.

(15) Eftekhari, A.; Jafarkhani, P.; Moztarzadeh, F. *Carbon* **2006**, *44*, 1343.

(16) Banerjee, S.; Naha, S.; Puri, I. K. *Appl. Phys. Lett.* **2008**, *92*, 233121.

(17) Ren, Z. F.; Huang, Z. P.; Xu, J. W.; Wang, J. H.; Bush, P.; Siegal, M. P.; Provencio, P. N. *Science* **1998**, *282*, 1105.

(18) Yang, F.; Wang, X.; Zhang, D.; Yang, J.; LuoDa; Xu, Z.; Wei, J.; Wang, J.-Q.; Xu, Z.; Peng, F.; Li, X.; Li, R.; Li, Y.; Li, M.; Bai, X.; Ding, F.; Li, Y. *Nature* **2014**, *510*, 522.

(19) Liu, C.; Cheng, H.-M. *Mater. Today* **2013**, *16*, 19.

(20) Ohashi, T.; Shima, T. *Carbon* **2015**, *87*, 453.

(21) Kang, L.; Hu, Y.; Liu, L.; Wu, J.; Zhang, S.; Zhao, Q.; Ding, F.; Li, Q.; Zhang, J. *Nano Lett.* **2015**, *15*, 403.

(22) Lee, H. W.; Yoon, Y.; Park, S.; Oh, J. H.; Hong, S.; Liyanage, L. S.; Wang, H.; Morishita, S.; Patil, N.; Park, Y. J.; Park, J. J.; Spakowitz, A.; Galli, G.; Gygi, F.; Wong, P. H. S.; Tok, J. B. H.; Kim, J. M.; Bao, Z. *Nat. Commun.* **2011**, *2*, 541.

(23) Gomulya, W.; Costanzo, G. D.; de Carvalho, E. J. F.; Bisri, S. Z.; Derenskyi, V.; Fritsch, M.; Fröhlich, N.; Allard, S.; Gordiichuk, P.; Herrmann, A.; Marrink, S. J.; dos Santos, M. C.; Scherf, U.; Loi, M. A. *Adv. Mater.* **2013**, *25*, 2948.

(24) Jakubka, F.; Backes, C.; Gannott, F.; Mundloch, U.; Hauke, F.; Hirsch, A.; Zaumseil, J. *ACS Nano* **2013**, *7*, 7428.

(25) Kwak, M.; Gao, J.; Prusty, D. K.; Musser, A. J.; Markov, V. A.; Tombros, N.; Stuart, M. C. A.; Browne, W. R.; Boekema, E. J.; ten Brinke, G.; Jonkman, H. T.; van Wees, B. J.; Loi, M. A.; Herrmann, A. *Angew. Chem. Int. Ed.* **2011**, *50*, 3206.

(26) Nish, A.; Hwang, J.-Y.; Doig, J.; Nicholas, R. J. *Nat. Nanotechnol.* **2007**, *2*, 640.

(27) Gao, J.; Loi, M. A.; de Carvalho, E. J. F.; dos Santos, M. C. *ACS Nano* **2011**, *5*, 3993.

(28) Gao, J.; Kwak, M.; Wildeman, J.; Herrmann, A.; Loi, M. A. *Carbon* **2011**, *49*, 333.

(29) Berton, N.; Lemasson, F.; Tittmann, J.; Stürzl, N.; Hennrich, F.; Kappes, M. M.; Mayor, M. *Chem. Mater.* **2011**, *23*, 2237.

(30) Tu, X.; Manohar, S.; Jagota, A.; Zheng, M. *Nature* **2009**, *460*, 250.

(31) Samanta, S. K.; Fritsch, M.; Scherf, U.; Gomulya, W.; Bisri, S. Z.; Loi, M. A. *Acc. Chem. Res.* **2014**, *47*, 2446.

(32) Mistry, K. S.; Larsen, B. A.; Blackburn, J. L. *ACS Nano* **2013**, *7*, 2231.

(33) Fagan, J. A.; Khripin, C. Y.; Silvera Batista, C. A.; Simpson, J. R.; Hároz, E. H.; Hight Walker, A. R.; Zheng, M. *Adv. Mater.* **2014**, *26*, 2800.

(34) Bisri, S. Z.; Gao, J.; Derenskyi, V.; Gomulya, W.; Iezhokin, I.; Gordiichuk, P.; Herrmann, A.; Loi, M. A. *Adv. Mater.* **2012**, *24*, 6147.

(35) Brady, G. J.; Joo, Y.; Wu, M.-Y.; Shea, M. J.; Gopalan, P.; Arnold, M. S. *ACS Nano* **2014**, *8*, 11614.

(36) Arnold, M. S.; Blackburn, J. L.; Crochet, J. J.; Doorn, S. K.; Duque, J. G.; Mohite, A.; Telg, H. *Phys. Chem. Chem. Phys.* **2013**, *15*, 14896.

(37) Wang, H.; Koleilat, G. I.; Liu, P.; Jiménez-Osés, G.; Lai, Y.-C.; Vosgueritchian, M.; Fang, Y.; Park, S.; Houk, K. N.; Bao, Z. *ACS Nano* **2014**, *8*, 2609.

(38) Dabera, G. D. M. R.; Jayawardena, K. D. G. I.; Prabhath, M. R. R.; Yahya, I.; Tan, Y. Y.; Nismy, N. A.; Shiozawa, H.; Sauer, M.; Ruiz-Soria, G.; Ayala, P.; Stolojan, V.; Adikaari, A. A. D. T.; Jarowski, P. D.; Pichler, T.; Silva, S. R. P. *ACS Nano* **2013**, *7*, 556.

(39) Britz, D. A.; Khlobystov, A. N. *Chem. Soc. Rev.* **2006**, *35*, 637.

(40) Klare, J. E.; Murray, I. P.; Goldberger, J.; Stupp, S. I. *Chem. Commun.* **2009**, 3705.

(41) Li, H.; Zhou, B.; Lin, Y.; Gu, L.; Wang, W.; Fernando, K. A. S.; Kumar, S.; Allard, L. F.; Sun, Y.-P. *J. Am. Chem. Soc.* **2004**, *126*, 1014.

(42) Cheng, F.; Zhu, J.; Adronov, A. *Chem. Mater.* **2011**, *23*, 3188.

(43) Ma, D.; Liang, L.; Chen, W.; Liu, H.; Song, Y.-F. *Adv. Funct. Mater.* **2013**, *23*, 6100.

(44) Salice, P.; Gambarin, A.; Daldosso, N.; Mancin, F.; Menna, E. *J Phys. Chem. C* **2014**, *118*, 27028.

(45) Liu, G.; Wang, F.; Chaunchaiyakul, S.; Saito, Y.; Bauri, A. K.; Kimura, T.; Kuwahara, Y.; Komatsu, N. *J. Am. Chem. Soc.* **2013**, *135*, 4805.

(46) Jan, C.-M.; Lee, Y.-H.; Wu, K.-C.; Lee, C.-K. *Opt. Express* **2011**, *19*, 5431.

(47) Farshchi, R.; Ramsteiner, M.; Herfort, J.; Tahraoui, A.; Grahn, H. T. *Appl. Phys. Lett.* **2011**, *98*, 162508.

(48) Sherson, J. F.; Krauter, H.; Olsson, R. K.; Julsgaard, B.; Hammerer, K.; Cirac, I.; Polzik, E. S. *Nature* **2006**, *443*, 557.